

Report on the HAARP 2008 Winter Campaign Focusing on Artificial Ionospheric Irregularities

**Edward J. Kennedy
James A. Secan
Arnold Lee Snyder**

**NorthWest Research Associates, Inc.
4118 148th Ave NE
Redmond, WA 98052**

Scientific Report No. 3

31 July 2008

APPROVED FOR PUBLIC RELEASE; DISTRIBUTION UNLIMITED.



**AIR FORCE RESEARCH LABORATORY
Space Vehicles Directorate
29 Randolph Road
AIR FORCE MATERIEL COMMAND
Hanscom AFB, MA 01731-3010**

20100308157


DTIC COPY

AFRL-RV-HA-TR-2009-1024


Using Government drawings, specifications, or other data included in this document for any purpose other than Government procurement does not in any way obligate the U.S. Government. The fact that the Government formulated or supplied the drawings, specifications, or other data, does not license the holder or any other person or corporation; or convey any rights or permission to manufacture, use, or sell any patented invention that may relate to them.

This report is published in the interest of scientific and technical information exchange and its publication does not constitute the Government's approval or disapproval of its ideas or findings.

This technical report has been reviewed and is approved for publication.



James C. Battis
Contract Manager



Dwight T. Decker, Chief
Space Weather Center of Excellence

This report has been reviewed by the ESC Public Affairs Office (PA) and is releasable to the National Technical Information Service (NTIS).

Qualified requestors may obtain additional copies from the Defense Technical Information Center (DTIC). All other requestors should apply to the National Technical Information Service (NTIS).

If your address has changed, if you wish to be removed from the mailing list, or if the addressee is no longer employed by your organization, please notify AFRL/RVIM, 29 Randolph Road, Hanscom AFB, MA 01731-3010. This will assist us in maintaining a current mailing list.

Do not return copies of this report unless contractual obligations or notices on a specific document require that it be returned.

REPORT DOCUMENTATION PAGE

Form Approved
OMB No. 0704-0188

Public reporting burden for this collection of information is estimated to average 1 hour per response, including the time for reviewing instructions, searching existing data sources, gathering and maintaining the data needed, and completing and reviewing this collection of information. Send comments regarding this burden estimate or any other aspect of this collection of information, including suggestions for reducing this burden to Department of Defense, Washington Headquarters Services, Directorate for Information Operations and Reports (0704-0188), 1215 Jefferson Davis Highway, Suite 1204, Arlington, VA 22202-4302. Respondents should be aware that notwithstanding any other provision of law, no person shall be subject to any penalty for failing to comply with a collection of information if it does not display a currently valid OMB control number. **PLEASE DO NOT RETURN YOUR FORM TO THE ABOVE ADDRESS.**

1. REPORT DATE (DD-MM-YYYY) 31-07-2008		2. REPORT TYPE Scientific Report 3		3. DATES COVERED (From - To) 21-02-2008 to 03-03-2008	
4. TITLE AND SUBTITLE Report on the HAARP 2008 Winter Campaign Focusing on Artificial Ionospheric Irregularities and Optical Emissions				5a. CONTRACT NUMBER FA8718-04-C-0001	
				5b. GRANT NUMBER N/A	
				5c. PROGRAM ELEMENT NUMBER N/A	
6. AUTHOR(S) E.J. Kennedy, J.A. Secan, A.L. Snyder				5d. PROJECT NUMBER 4827	
				5e. TASK NUMBER HA	
				5f. WORK UNIT NUMBER R1	
7. PERFORMING ORGANIZATION NAME(S) AND ADDRESS(ES) NorthWest Research Associates, Inc. 4118 148th Ave NE Redmond, WA 98052				8. PERFORMING ORGANIZATION REPORT NUMBER NWRA-BELL-08-R374	
9. SPONSORING / MONITORING AGENCY NAME(S) AND ADDRESS(ES) Air Force Research Laboratory 29 Randolph Road Hanscom AFB, MA 01731-3010				10. SPONSOR/MONITOR'S ACRONYM(S) AFRL/RVBXI	
				11. SPONSOR/MONITOR'S REPORT NUMBER(S) AFRL-RV-HA-TR-2009-1024	
12. DISTRIBUTION / AVAILABILITY STATEMENT Approved for Public Release; Distribution Unlimited.					
13. SUPPLEMENTARY NOTES					
14. ABSTRACT A research campaign was conducted at the joint US joint Air Force, US Navy, and DARPA High-Latitude Active Auroral Research Program (HAARP) site near Gakona, AK, during the period 21 February through 3 March 2008. The focus of the campaign was on generation of plasma-density irregularities in the ionosphere an optical and RF emissions from the ionosphere as a by-product of the interaction between the HAARP HF heater and the atmosphere and ionosphere above HAARP. This report documents the preliminary results obtained from this campaign through short (two to three page) summaries provided by the Principal Investigators for each of the experiments runs.					
15. SUBJECT TERMS Ionosphere, Ionospheric modification, Ionospheric irregularities, Ionospheric optical Emissions, Ionospheric scintillation, HAARP, Stimulated Electromagnetic Emissions (SEE)					
16. SECURITY CLASSIFICATION OF: None			17. LIMITATION OF ABSTRACT SAR	18. NUMBER OF PAGES	19a. NAME OF RESPONSIBLE PERSON Mr. James Battis
a. REPORT U	b. ABSTRACT U	c. THIS PAGE U			19b. TELEPHONE NUMBER (include area code) 781-377-4669

Contents

1. Introduction to Ionospheric Irregularities and Optical Emissions	1
2. Campaign Overview and Organizer's Report	2
3. Preliminary Campaign Results.....	10
4. Campaign Organizers Report	11
5. Concluding Remarks	11

APPENDICES

Appendix A	Geophysical data during the campaign period	13
Appendix B	Generation of large-scale density irregularities and geomagnetic micropulsations.....	30
Appendix C	Observing artificial E region field-aligned irregularities over HAARP	32
Appendix D	Beacon and in-situ observations of IRI-generated plasma-density structures.....	34
Appendix E	Characterization of decameter-scale ionospheric irregularities through imaging of HAARP-induced airglow.....	37
Appendix F	HAARP twisted-beam experiments.....	39
Appendix G	Using the HAARP heating facility to investigate the self-scattering of high power radio waves.....	41
Appendix H	HF power dependence on the cascade spectrum of HF-enhanced plasma lines.....	44
Appendix I	Aspect sensitivity of HF-induced plasma line measured with MUIR	46
Appendix J	HAARP 2008 winter campaign effects of additional X-mode pumping on radio induced optical emissions.....	48
Appendix K	In-situ detection of the ionospheric irregularities due to HF heating	50
Appendix L	Generation of ionospheric ducts by HF-heating	51
Appendix M	Generation of ion outflow by HF-heating.....	53
Appendix N	Detection of super small scale irregularities generated by the HF-heating of triple gyrofrequency	55
Appendix O	3-D determination of artificial optical emission structure	57
Appendix P	Excitation of optical emissions and irregularities in the ionospheric E-region.....	59
Appendix Q	Study of high power nearly vertically incident skywave reflections.....	61
Appendix R	Artificial particle precipitation by VLF cyclotron resonance	64
Appendix S	The temporal evolution of the magnetic zenith self-focusing effect and accelerated electron energy spectrum using VLF waves as a proxy to detect lower-hybrid waves.....	66
Appendix T	A coordinated study of HF-induced irregularities, plasma waves, and ionospheric conditions at HAARP	70

Appendix U	Investigation of large plasma sheets, spatial distribution of Langmuir waves, and whistler wave interactions with ionospheric plasmas	72
Appendix V	Artificial ULF wave generation at HAARP.....	77
Appendix W	Investigating the scintillations of discrete cosmic source radiation due to HAARP-stimulated irregularities using the new imaging riometer at Gakona.....	80
Appendix X	Probing the ELF/VLF source region using dual-beam HAARP experiments	82
Appendix Y	Spectroscopic observations of rrtificially induced airglow and aurora.....	84
Appendix Z	High-speed photometric imaging of HAARP-induced artificial airglow	86
Appendix AA	Optical detection of HAARP-induced particle precipitation from the radiation belts.....	88
Appendix AB	Synergistic auroral enhancements.....	90
Appendix AC	Topside turbulence.....	92
Appendix AD	Two-plasmon decay	94
	List of Symbols, Abbreviations, and Acronyms.....	96

Figures

Figure 1.	Variation of the planetary geomagnetic index (K_p) for four 27-day solar rotation cycles.	2
Figure 2.	Sunrise, sunset, twilight and moon up times during the period covered by the HAARP 2008 Winter Campaign cycles.	3
Figure 3.	Variation in the F-layer critical frequency, f_oF2 as a function of time of day.	4
Figure 4.	Final campaign schedule.	6
Figure A1.	Plot of the K_p “musical diagram” indicating the HAARP campaign interval.	13
Figure A2.	Estimated location of the equatorial boundary of the diffuse aurora as derived from precipitating electron data observed by TIROS and MetOp satellites. Light dashed line indicates the highest boundary latitude (corresponding to lowest activity level) possible; the heavy dashed line indicates the HAARP latitude; and the heavy curve is a three-hour smoothed boundary location. Data from both northern and southern hemisphere are included in these plots.	14
Figure A3.	Data from the University of Alaska Geophysical Institute Magnetometer Array for 21 through 24 February 2008.	15
Figure A4.	Data from the University of Alaska Geophysical Institute Magnetometer Array for 25 through 26 February 2008.	16
Figure A5.	Data from the University of Alaska Geophysical Institute Magnetometer Array for 27 through 29 February 2008.	17
Figure A6.	Data from the University of Alaska Geophysical Institute Magnetometer Array for 01 through 03 March 2008.	18
Figure A7.	Data from the HAARP riometer for 21 through 23 February 2008.	19
Figure A8.	Data from the HAARP riometer for 24 through 26 February 2008.	19
Figure A9.	Data from the HAARP riometer for 27 through 29 February 2008.	20
Figure A10.	Data from the HAARP riometer for 01 through 03 March 2008.	20
Figure A11.	Data from the HAARP Digisonde for 20 through 26 February 2008. The observed f_oF2 is plotted in blue, the observed h_mF2 in red.	21
Figure A12.	Data from the HAARP Digisonde for 26 February through 03 March 2008. The observed f_oF2 is plotted in blue, the observed h_mF2 in red.	21
Figure A13.	Total Electron Content derived from the HAARP GPS receiver for the period 20 February through 26 February 2008. Different colors indicate data from different GPS satellites. The black dashed curve is the vertical TEC obtained from the GPS single-frequency user TEC model.	22
Figure A14.	Total Electron Content derived from the HAARP GPS receiver for the period 20 February through 26 February 2008. Different colors indicate data from	

	different GPS satellites. The black dashed curve is the vertical TEC obtained from the GPS single-frequency user TEC model.	23
Figure A15.	Total backscattered power from the Kodiak SuperDARN radar along Beam 8 on 21 February 2008.	24
Figure A16.	Total backscattered power from the Kodiak SuperDARN radar along Beam 8 on 22 February 2008.	24
Figure A17.	Total backscattered power from the Kodiak SuperDARN radar along Beam 8 on 23 February 2008.	24
Figure A18.	Total backscattered power from the Kodiak SuperDARN radar along Beam 8 on 24 February 2008.	25
Figure A19.	Total backscattered power from the Kodiak SuperDARN radar along Beam 8 on 25 February 2008.	25
Figure A20.	Total backscattered power from the Kodiak SuperDARN radar along Beam 8 on 26 February 2008.	26
Figure A21.	Total backscattered power from the Kodiak SuperDARN radar along Beam 8 on 27 February 2008.	26
Figure A22.	Total backscattered power from the Kodiak SuperDARN radar along Beam 8 on 28 February 2008.	27
Figure A23.	Total backscattered power from the Kodiak SuperDARN radar along Beam 8 on 29 February 2008.	27
Figure A24.	Total backscattered power from the Kodiak SuperDARN radar along Beam 8 on 01 March 2008.	28
Figure A25.	Total backscattered power from the Kodiak SuperDARN radar along Beam 8 on 02 March 2008.	28
Figure A26.	Total backscattered power from the Kodiak SuperDARN radar along Beam 8 on 03 March 2008.	29
Figure B1.	Magnetic field variations recorded by the fluxgate magnetometer.	30
Figure B2.	Composite ionogram showing the variation of the reflection height of the sounding waves from 4.4 to 4.6 MHz in every 15 minutes. The sounding waves appeared to be anomalously absorbed when the x mode HF heater at 4.5 MHz was turned on.	31
Figure B3.	Composite ionogram showing the variation of the reflection height of the sounding waves from 2.5 to 3 MHz in every 15 minutes. The sounding waves appeared to be anomalously absorbed when the x mode HF heater at 2.7 MHz was turned on.	31
Figure C1.	30 MHz radar range time intensity versus universal time and apparent range for Feb. 29, 2008. True range from Homer is apparent range + 370 km. (upper panel) Backscatter signal-to-noise ratio, Doppler shift, and spectral width represented by pixel brightness, hue, and saturation, respectively. Artificial irregularities occupy ranges between 90–130 km, and natural	

	auroral echoes occupy other ranges. (lower panel) Average signal-to-noise ratio in ranges between 90–130 km.	33
Figure D1.	The NWRA ITS30m receiver system deployed near Gakona.	35
Figure D2.	(Left panels) Total ion density data from the DMSP SM sensor (bottom) and detrended density (top). (Right panels) Horizontal (top) and vertical (bottom) ion drift velocity from the DMSP DM sensor. Horizontal bars indicate times the field lines at DMSP altitude were within the IRI heated region (within the beam pattern 3dB points).	36
Figure E1.	The telescopic imaging system and WPI student interns during the HAARP Winter 2008 campaign.	37
Figure E2.	Data from the 2008 campaign. The top panel shows an image from the telescope with fine structured airglow at 557.7 nm (15 seconds exposure). The bottom panel shows an image from the wide field of view imager (also 15 seconds, 557.7 nm). Note that the dome was blocking part of the wide imager’s field of view.	38
Figure F1.	Power pattern of vertical HAARP beam as the field phases turn through 2π while turning once around the array, for a frequency of 4.8 MHz.	39
Figure F2.	The Hewlett-Packard E1437A 20 Msamples/s, analogue-to-digital converter, and laptop computer used sample the electromagnetic emissions.	39
Figure F3.	Two overlaid SEE spectra. The blue spectrum is for a usual pump beam with zero OAM and the red spectrum is for a beam with nonzero OAM. The frequency span shown is 160 kHa wide.	40
Figure G1.	Locations of the receiver sites operated during the Winter 2008 HAARP Campaign. Approximate propagation paths are shown as well. The map is made using OMC tool.	41
Figure G2.	Variations in the signal strength during the OFF (low power) period observed at Millstone Hill (blue) and Kharkov (black) at the operating frequency of 2,755,063 Hz. Signal amplitudes recorded during the full-power heating are considerably larger and are not shown to simplify the graph.	42
Figure H1.	Cascade spectra of HF-enhanced plasma lines for full-power (bottom plot), $\frac{3}{4}$ power, $\frac{1}{2}$ power, and $\frac{1}{4}$ power (top plot) of the HAARP HF transmitter array operated at 5.2 MHz.	44
Figure H1.	Horizontal pattern of relative magnitude of the upshifted HFPL averaged for the first 100 ms after HF turn-on.	46
Figure I2.	Mean PSD (dB) of the upshifted HFPL measured with the MUIR phased-array system. The magnetic zenith is close to (0°, 15°) beam position (red).	46
Figure J1.	During the HF-transmission pulse from 0415 to 0418 UT on February 26th, it appears as if the enhancement in 6300 A was limited to a very narrow region and that the intensity was suppressed during the initial 90 s when there were additional X-mode transmission. For the time period from 0416:30 UT the	

	region with enhanced emissions at 6300 grows and the total intensity increases by a factor of 3.	49
Figure L1.	Density of ionized atomic Oxygen (O^+) as a function of time, and as a function of the respective latitude / longitude of the satellite.....	52
Figure M1.	The measurements made by the F16 ion density meter 02/25 (the top panel), and 02/26 (the lower panel). Zero time corresponds to F16 fly over HAARP.....	54
Figure N1.	The differential carrier phase in arbitrary units measured 02/23/08. The ionospheric heating started at 19.3 UT and lasted for 0.3 h. The left panel shows phase oscillations with the period 20 s, corresponding to the heating pulses. The encircled area in the left panel shows the oscillations. The circled region is zoomed in the right panel where zero time corresponds to 19.3 h.....	56
Figure O1.	630.0 (left) and 557.7 (right) nm wide-field images of HAARP-induced optical emissions from the $\sim 90^\circ$ FOV HAARPOON system at Delta Junction during the experiment on 23 Feb 2008. Note that north is toward the bottom of these quick-look images.	58
Figure O2.	Central spot and partial ring in the vertical as seen at 557.7 nm looking up from the HAARP site on 23 Feb 08 at approximately the same time as the images in Fig.01.....	58
Figure P1.	Possible E-region structure seen during one of the E-region experiments on 3 March 2008.	60
Figure Q1.	Mode calibration sequence showing slowly varying ambient skywave response.....	62
Figure Q2.	Depiction of skywave and groundwave recordings separated into scan groups by color. Scan groups are used to normalize the ambient variation that is not the result of changes in transmission power.	62
Figure Q3.	Comparison of O-mode normalized groundwave and skywave power across multiple scan groups. At lower groundwave power values, the skywave response is weakly non-linear, with increasing reflection efficiency as groundwave power is increased. At higher groundwave power values, a significant roll-off of skywave power is observed at the highest available groundwave power.....	63
Figure Q4.	Comparison of X-mode normalized groundwave and skywave power across multiple scan groups. The X-mode skywave response is strikingly different from the O-mode response across the full range of groundwave power values. In particular, the bifurcation of the response at high power needs to be further analyzed.	63
Figure R1.	VLF signals observed at Chistochina, AK for six successive HF transmitter modulation waveforms.....	65
Figure S1.	Images from the HAARP imager at 557.7 nm (top row), from the ST9 imager at 630 nm (middle) and from the Pike imager at 630 nm (bottom).	

	Images for the HAARP transmit cycles ending at 04:21 on the left and at 04:25 on the right.	67
Figure S2.	Ion line backscatter observations from the HAARP MUIR UHF radar.	68
Figure S3.	HAARP photometer data at 630 nm.	68
Figure T1.	Spectra of HFPL (lower panel) with MUIR at MZ (14o) and HAARP pointed at 7°	
Figure T2.	Spectra of HFPL (lower panel) with MUIR at 22° and HAARP pointed at MZ 14°	71
Figure T2.	Spectra of HFPL (lower panel) with MUIR at 22° and HAARP pointed at MZ 14°	71
Figure U1.	Large plasma sheets are generated by O-mode heater waves within the meridional plane.	72
Figure U2.	Large plasma sheets generated by X-mode heater waves are orthogonal to the meridional plane. Ionosonde signals transmitted near the zenith will be guided by these plasma sheets to propagate away. Those ionosonde signals transmitted at large angles from the zenith can still be reflected by remote plasma blobs and recorded in ionograms.	73
Figure U3.	Arecibo radar detection of HF heater-created large plasma sheets seen on RTI plot as slanted stripes, starting from about 00:50 till 00:50 LT on July 25, 1997 [Lee et al., GRL, 1998].	73
Figure U4.	SuperDarn data recorded during CW O-mode and CW X-mode operation of HAARP heater on 2/27/2008 for the investigation of large plasma sheet generation.	74
Figure U5.	Altitude cross-sections of MUIR data from Winter HAARP Campaign on March 18, 2006.	75
Figure V1.	Dual-axis induction coils were deployed at four sites around HAARP.	77
Figure V2.	ULF-modulated heating was performed using different beam shapes. (Courtesy of Mike McCarrick)	78
Figure V3.	3Hz heating signature in H and D components recorded by the induction coil at Tok Junction.	78
Figure V4.	Chirped ULF wave signal recorded by the induction coil at Tok Junction.	79
Figure V5.	ULF waves at Gakona Junction Trailer (left) and Tok Junction (right).	79
Figure W1.	Antenna pattern of the HAARP Imaging riometer showing trajectories of selected DCS and the locations of ionospheric disturbed regions.	80
Figure W2.	Source scintillations over a two hour period showing the effect of heater ON and OFF intervals.	81
Figure X1.	ELF/VLF receiver located at Sinona Creek in Chistochina, Alaska to detect the ELF/VLF signals generated by the HAARP HF heater.	82

Figure X2.	Split-beam HF heating geometry for the proposed experiment. Power-stepped CW heating is coupled with modulated HF heating using a different HF frequency.	83
Figure X3.	ELF/VLF observations performed at Sinona Creek in Chistochina, AK	83
Figure Y1.	A CCD-equipped 0.5 m grating spectrometer used to obtain spectra of heater-induced aurora and airglow.....	84
Figure Y2.	Sample spectra obtained during the HAARP 2008 optics campaign showing the presence of heater-induced auroral emissions.	85
Figure Z1.	HAARP All Sky Imager images from (from left column to right column) 0400 UTC, 0430 UTC, 0500 UTC, and 0530 UTC on February 29, 2008 (top row) and March 3, 2008 (bottom row). No stars can be seen in the images in the top row due to overcast skies. In the bottom row, the skies are overcast earlier in the observation period (bottom row, left images) but cleared up (i.e., stars appear in the images) later in the period (bottom row, right images).....	87
Figure Z2.	HAARP photometer data from February 29, 2008 from 0400 to 0530 UTC. Only the red line (630 nm) and green line (560 nm) measurements are shown. The decay brightness during twilight is clearly visible, but no 4-minute periodicities can be seen due to the overcast skies.	87
Figure AA1.	Pictures of the PIPER instrument (left) and the HAARP photometer (right) as mounted in the optics shelter in Science Pad 3 at HAARP. PIPER is composed of four multi-anode photomultiplier tubes and a field-of-view camera mounted on top. The HAARP photometer is composed of three photometer: two behind fixed-wavelength optical filters and one behind a rotating filter wheel with six different optical filters.	89
Figure AA2.	HAARP All Sky Imager images from 0900 UTC on, left to right, February 29, 2008, March 1, 2008, March 2, 2008, and March 3, 2008. No stars can be seen in the images on the left due to overcast skies. In the images on the right, stars begin to appear due to clearer skies, but these nights saw weak D-region absorption. None of the four nights presented useful observation conditions, and our experiment was not performed.....	89
Figure AB1.	An example of the type of data sought from the MUIR observations. This example was recorded by the EISCAT VHF radar and shows aurorally-enhanced ion lines between 200 and 500 km altitude and between 23:28 and 23:33 UT. Collaborators: Brett Isham, Vasily Beley, and Mike Rietveld.....	90
Figure AC1.	An example of the type of data sought from the MUIR observations. This example was recorded with the EISCAT VHF radar showing HF-excited topside ion lines between about 12:30 and 12:33 UT. Reference: Isham et al., 1999, Aspect angle dependence of HF-enhanced incoherent backscatter, Adv. Space Res., 24(8), 1003-1006.	92

Figure AC2. Diagram showing the relationship between the MUIR receiver band and the HAARP HF pump frequency used for this observation (exp. 8) and for the two-plasmon observation (exp. 9).....93

Figure AD1. Standard ionosonde (HF radar) ionospheric frequency profile recorded on 31 July 2007 at 00:30 UT showing 6.9-MHz pump frequency (verical red line) and 3.45-MHz observation frequency (verical green line), along with height of anticipated enhancement (horizontal red line). Collaborators: Darlene Maldonado-Nieves, Noel Robles-Arce, Brent Watkins, and Brett Isham.94

Figure AD2. Maximum ionospheric frequency (f_0F_2) for 24 hours on 31 July 2007 as measured by ionosonde (HF radar). The 6.9-MHz pump frequency (horizontal red line) and 3.45-MHz observation frequency (horizontal green line) are shown, as utilized at 00:30 UT (verical red line). Collaborators: Darlene Maldonado-Nieves, Noel Robles-Arce, Brent Watkins, and Brett Isham.95

Figure AD3. Diagram showing the relationship between the MUIR receiver band and the HAARP HF pump frequency used for this observation (exp. 9) and for the topside turbulence observation (exp. 8).95

Tables

Table 1. HAARP 2008 Winter Campaign Schedule as Executed.....7

Table D1. NWRA HAARP campaign experiment times.....34

Table G1. HAARP operation mode summary42

Preface and Acknowledgements

The HAARP 2008 winter irregularities and optical emission campaign was conducted at the HAARP Gakona Facility over the period February 20 through March 3, 2008. The experiments executed during the campaign, exploited the facility's state-of-the-art design. The variety of operational requirements for the experiment suite tested the versatility of the system to uniquely configure transmitter and antenna array parameters. Preliminary results show that many of the creative operating procedures developed by participating scientists resulted in new physical results not seen in previous studies at other ionospheric interaction facilities.

What is not as readily apparent is the dedicated efforts invested by the HAARP facility's staff and the transmitter system operators. The often complex and sophisticated transmitter and antenna beam operations required many hours of software set-up to control the physical transmitting system in the desired manner, consistent with safety and licensing requirements. We recognize the efforts of the following individuals who set up each of the experiments and operated the transmitter and antenna array during the campaign.

Dr. Mike McCarrick Chief of Operations
David Seafolk-Kopp Software engineer and operator

Perhaps even less visible but equally as important to the campaign's success were the contributions by the site support staff who provided support services, transmitter and diagnostic maintenance and assisted individual researchers in equipment set up data retrieval. The 100% availability of the transmitter system during this campaign was a direct result of the work invested by the following staff members and we are grateful for their contributions:

Marty Karjala HAARP Site Manager
Deana Rietveld HAARP Admin Assistant
Jay Scrimshaw HAARP Senior Electrical Engineer
Travis Million HAARP Power Engineer
Tracy Coon HAARP Associate Electrical Engineer
Dave Coon HAARP Associate Electrical Engineer
Stef Scribner HAARP Maintenance Technician
Josh Geldersma HAARP Maintenance Technician

We would also like to thank Dr. Paul Bernhardt for authoring Section 1 of this report.

1. Introduction to Ionospheric Irregularities and Optical Emissions

In a quiescent, uniform ionosphere, high power radio waves from HAARP can propagate until they reach the *reflection* altitude where the plasma frequency is equal to the wave frequency. At this altitude, the wave swells and the electric field amplitude grows. For high power pump waves, the electromagnetic wave decays into an ion-acoustic wave and an electron plasma wave. When the electron plasma wave propagates to lower densities it can Landau damp by accelerating electrons that can produce optical emissions. After a few seconds the originally quiescent plasma will start to field aligned irregularities by thermal and ponderomotive (or radiation) pressures. Self focusing occurs when a small plasma cavity captures Langmuir waves that then enhance the density reductions inside the cavity. Once field aligned irregularities are formed, conversion of electromagnetic waves occurs where the pump wave frequency is equal to the upper-hybrid wave frequency in the plasma; this occurs at a lower altitude than the *reflection* altitude. Electron acceleration can occur by upper-hybrid waves to produce the optical emissions.

The artificial aurora produced by high power radio waves provides a visible signature of electron acceleration. If this acceleration is the result of focusing in field aligned irregularities, then the optical emissions outline these plasma structures. Field aligned irregularities (FAI) are always present in the high latitude ionosphere. These natural FAI are supported by plasma interchange processes driven with large electric fields and by neutral wind velocities across the nearly vertical magnetic field lines. When the ionosphere is illuminated by a high power beam of electromagnetic waves from HAARP, the preexisting FAI structures are intensified by self-focusing processes. Horizontal transport of the F-region plasma brings new, unmodified plasma into the HF beam. The motion of the optical emissions associated with the irregularities is seen with time-lapse images of the artificial aurora produced by the HAARP facility.

2. Campaign Overview

The preliminary announcement for the HAARP 2008 winter campaign was distributed by e-mail on December 31, 2007 to a list of scientists who had previously participated in irregularities or optical research campaigns at the HAARP facility. The formal campaign announcement was posted on a special campaign web site January 4, 2008. The announcement requested submission of proposals and provided detail on proposal requirements, a timetable leading up to the campaign and information on the required post-campaign quick-look reports. Two weeks were allowed for the preparation of proposals with a deadline of January 18, 2008. All proposals submitted by the cutoff date were reviewed by an evaluation committee and successful proposers were notified of acceptance on February 1, 2008.

Determining the dates for the combined campaign required consideration of several factors. Generally, the study of artificial irregularities requires geomagnetically quiet conditions. A review of the planetary geomagnetic K_p index beginning in December 2007 revealed a reasonably repetitive pattern correlating with the 27 day solar rotation period as shown in Figure 1 below.

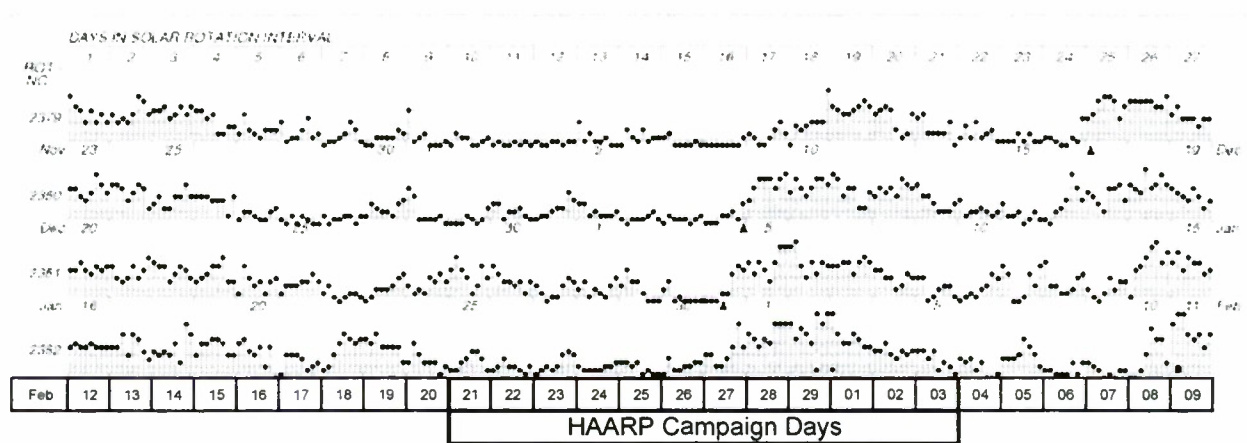


Figure 1. Variation of the planetary geomagnetic (K_p) index for four solar 27 day rotation cycles. The top three plots show the three cycles prior to the campaign. The bottom plot includes the campaign dates of 21 Feb through 3 March 2008.

The inclusion of optical emission research as a second campaign focus required a second set of conditions tied to dark sky conditions. Although some types of optical studies can tolerate a limited amount of twilight, in general, successful experiments depend on the moon being below the horizon and a solar depression angle exceeding -12 degrees. This condition occurs following the end of astronomical twilight in the evening and prior to the beginning of astronomical twilight in the morning. At the latitude of the HAARP Research Station, lengthy periods of complete darkness occur during the winter months of December, January and February.

A chart of sunset, sunrise, twilight and moonrise times is shown in Figure 2 below. In this chart, the shaded area shows dates and times that were suitable for optical emission research during late-February and early-March 2008. From Figure 2, the first day suitable for optical emissions experiments was 21 February, although the darkness period was less than one hour. The number of hours of darkness increases each succeeding day, reaching nearly 9 hours on 28 February

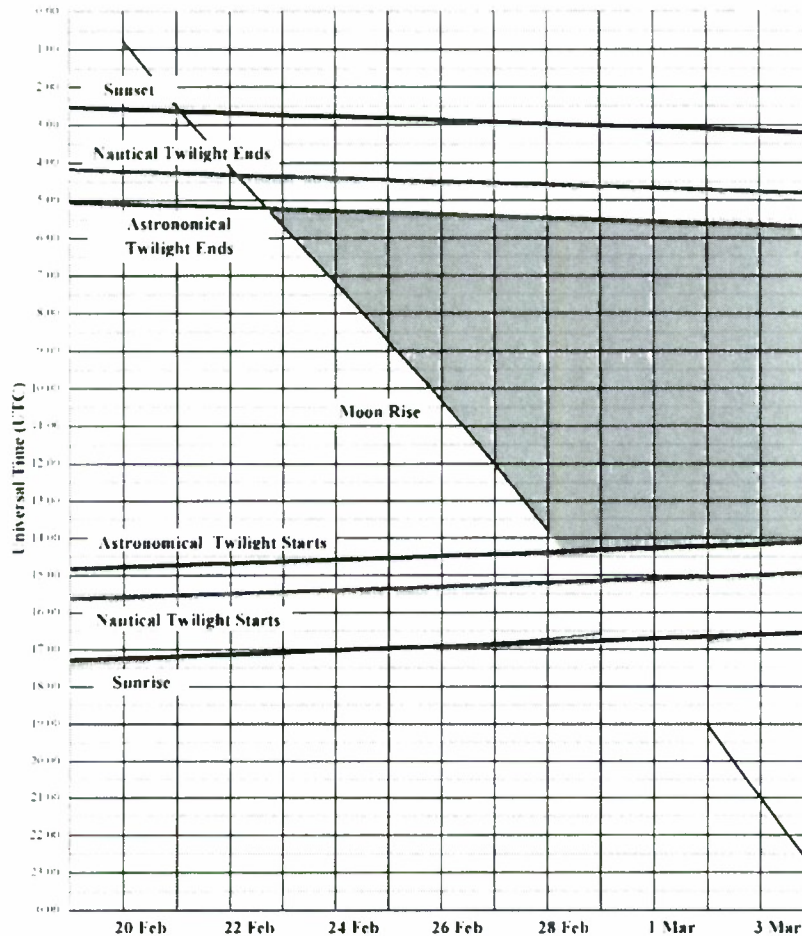


Figure 2. Sunrise, sunset, twilight and moon up times during the period covered by the HAARP 2008 Winter Campaign. Total darkness is indicated by the shaded area..

An additional consideration that affected the development of the campaign schedule was the anticipated variation of ionospheric density as a function of time of day. The ionospheric F-layer critical frequency for vertical incidence, also called f_oF_2 , is a useful measure of ionization density. Figure 3 shows the expected variation of f_oF_2 as a function of time of day, obtained by averaging HAARP digisonde data for the corresponding winter period in 2007. The impact of f_oF_2 variation on irregularities and optical emission experiments is somewhat different. For irregularities research a high level of ionospheric density (high f_oF_2), concurrent with a low K_p is desirable. For many experiments, as high a level of f_oF_2 as possible is very desirable to take advantage of the higher levels of HAARP transmitter Effective Radiated Power (ERP) that is characteristic of higher operating frequency.

For optical emission experiments, where the emission occurs in the F-region, it is only necessary for the f_oF_2 to be greater than or equal to the lowest HAARP authorized frequency (currently, 2.7 MHz). However, recent research at HAARP has successfully studied optical emissions from within the ionospheric E-region. Although Figure 3 indicates that the likelihood of suitable F-region ionospheric density ends after approximately, 2000 AST (0500 UTC), sufficient ionization occasionally occurs in the E-region either as a Sporadic E (Es) event or as a result of electron precipitation effects (Auroral E). These effects can occur at any time during the evening hours and are generally unpredictable.

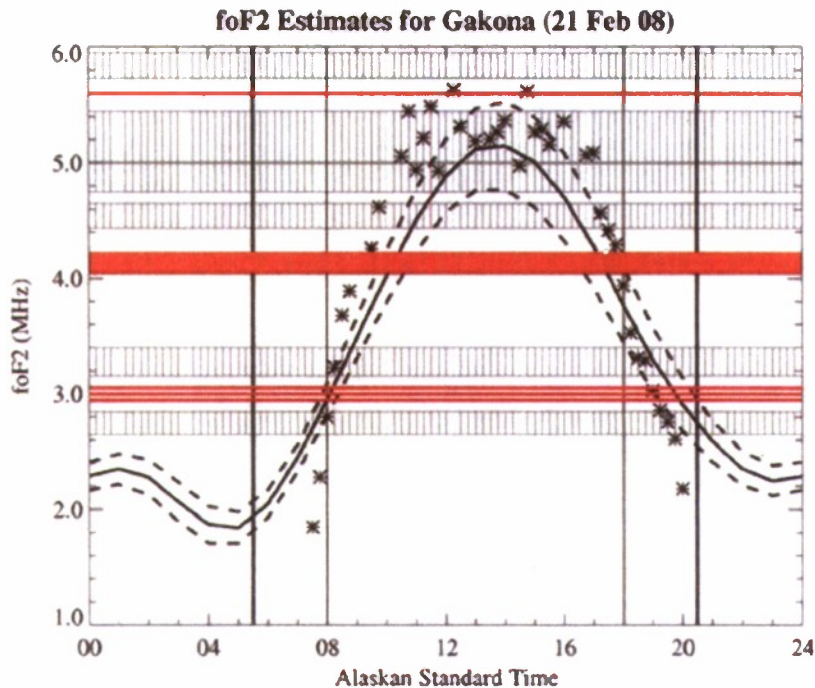


Figure 3. Variation in the F-layer critical frequency, f_oF_2 as a function of time of day. Cross-hatched and solid horizontal bands indicate HAARP transmitter permanent and temporary frequency authorizations respectively. 0000 Universal Time is equivalent to 0900 AST.

The final factor affecting campaign scheduling is operator duty cycle. HAARP has developed guidelines allowing up to 10-11 hours of continuous operation followed by an equivalent rest period.

Taking all of these factors into account resulted in the following scheduling criteria:

1. Artificial irregularity research should be conducted during the early afternoon to evening to take advantage of high f_oF_2 and potentially high HAARP transmitter ERP.
2. Because artificial irregularity research requires quiet geomagnetic conditions (low K_p), the research should be scheduled prior to the recurring disturbed period starting on about 27 February.
3. Comparing Figures 1 and 2 indicates that selecting a campaign period running from 21 February to 3 March would include several days of quiet geomagnetic conditions prior to lengthy dark periods beginning on 24 February.
4. Although some of the days at the end of the campaign might coincide with higher K_p conditions, this was acceptable or even desired for several of the proposals.

The initial campaign experiment execution schedule was developed and posted to the campaign web site on February 5, 2008. This initial schedule was adjusted several times prior to the beginning of the campaign to accommodate travel plans of individual investigators. The final schedule is shown in Figure 4 with time of day in both Alaska Standard Time (AST) and Universal Time (UTC) along the left axis in 15 minute increments for simplicity. At the beginning of the campaign, operations were scheduled to run in ten hour blocks from late morning through late afternoon to take advantage of high f_oF_2 during the daylight hours and anticipated low K_p . The ten hour block was then “slipped” as the campaign progressed, to take advantage of the increasing hours of darkness beginning on 25 February. Satellite passes are

indicated in Figure 4 as alphanumeric entries indicating the satellite and experiment number (eg, FM4 30, indicating satellite FM4, experiment 30). More exact schedules were produced each day of the campaign, to identify the exact times for satellite rise and set times.

Other diagnostic facilities participated in the campaign including the SuperDARN Kodiak facility and the University of Alaska magnetometer string. Several participants brought specialized instruments and set them up at locations away from the HAARP facility. Among these were remote ULF receivers, a Stimulated Electromagnetic Emission (SEE) receiver set up at Gakona, 8 miles from HAARP, and a slant looking optical imager set up at Delta Junction. Campaign investigators made use of multiple satellites including NIMS (OSCAR and Transit), COSMIC, DMSP (F15 and F16), CHAMP, DEMETER and GPS. Experiments were also planned with the FAST and ALOS satellites but could not be carried out.

Table 1 is a listing of all of the experiments as actually conducted during the HAARP 2008 irregularities and optical emissions campaign. The table indicates the principal investigator, the number of the experiment (as shown in the experiment schedule, Figure 4, and the specific appendix to this report where a quick-look report of the experiment can be found. There were a total of 31 experiments conducted by 28 principal investigators collaborating with an additional 33 associate investigators.

AST	UTC	21-Feb	22-Feb	23-Feb	24-Feb	25-Feb	26-Feb	27-Feb	28-Feb	29-Feb	1-Mar	2-Mar
09:00	18:00				D15 30							
09:15	18:15				FM4 30							
09:30	18:30		G0 19	G06 19	G06 19							
09:45	18:45	G06 19	33	33	33							
10:00	19:00	33	33	33	33							
10:15	19:15	33	33	G21 19	G21 19	G21 19	G21 19					
10:30	19:30	G21 19	G21 19	8	8	8	4					
10:45	19:45	35	35	8	8	8	4					
11:00	20:00	35	35	8	4	4	4					
11:15	20:15	35	35	8	4	4	4	1				
11:30	20:30	35	FM6 30	DMTR 23	4	4	4	1				
11:45	20:45	35	35	13	4	4	CHMP 20	ALOS 1				
12:00	21:00	35	CHMP 20	13	8	8	8	DMTR 23				
12:15	21:15	35	35	13	8	8	8	22/34				
12:30	21:30	35	35	13	8	8	8	22/34				
12:45	21:45	35	35	13	8	8	FM2 30	22/34				
13:00	22:00	35	35	13	8	13	22/34	22/34				
13:15	22:15	35	35	13	3	13	22/34	22/34				
13:30	22:30	35	35	13	O25 3	13	22/34	22/34				
13:45	22:45	35	35	O32 30	O25 3	13	22/34	22/34				
14:00	23:00	35	35	O23 30	8	13	22/34	22/34	31	21	21	
14:15	23:15	35	35	14	8	13	22/34	22/34	31	21	21	
14:30	23:30	35	35	14	8	13	22/34	22/34	31	21	21	
14:45	23:45	35	35	14	8	13	14	22/34	31	21	21	
15:00	00:00	31	31	14	8	3	14	22/34	31	14	14	
15:15	00:15	31	31	14	FM5 30	FM5 3	14	22/34	31	14	14	
15:30	00:30	31	31	14	22/34	13	14	22/34	31	14	14	
15:45	00:45	31	31	14	22/34	13	14	22/34	31	14	14	
16:00	01:00	31	31	14	22/34	29	14	22/34	31	14	14	
16:15	01:15	31	31	14	22/34	29	14	22/34	31	3	14	
16:30	01:30	31	31	FM4 30	3	29	14	22/34	31	O25 3	14	
16:45	01:45	3	31	O25 30	O25 3	29	14	22/34	31	14	14	
17:00	02:00	O25 3	31	14	8	8	14	36	31	14	14	
17:15	02:15	31	31	14	8	8	14	36	31	14	14	
17:30	02:30	31	31	14	8	8	14	36	FM6 30	14	14	
17:45	02:45	31	31	14	8	8	14	36	G20 30	14	14	
18:00	03:00	31	31	14	8	8	29	4	12	12	4	21
18:15	03:15	4	27	12	4	29	29	4	12	12	4	21
18:30	03:30	4	27	12	4	29	29	4	12	12	4	21
18:45	03:45	FM6 30	27	12	D15 30	29	29	4	12	12	4	21
19:00	04:00	FM6 30	27	12	G23 30	29	36	27	17	5	5	17
19:15	04:15	G23 30	27	12	36	29	36	27	17	5	5	10
19:30	04:30	5	27	12	36	D16 2	D16 2	27	17	11	10	17
19:45	04:45	5	27	12	D16 2	5	36	27	17	11	10	10
20:00	05:00				36	5	36	27	17	11	10	17
20:15	05:15				36	FM2 30	36	27	17	11	10	10
20:30	05:30				36	G13 30	36	4	4	4	10	11
20:45	05:45				36	5	36	4	4	4	10	11
21:00	06:00							4	4	4	10	11
21:15	06:15							4	FAST 25	4	ELF*	11
21:30	06:30							DMTR 23	4	ELF*	DMTR 23	11
21:45	06:45							4	ELF*	ELF*	ELF*	11
22:00	07:00								DMTR 23	ELF*	ELF*	DMTR 23
22:15	07:15								ELF*	ELF*	24	24
22:30	07:30								ELF*	ELF*	24	24
22:45	07:45								ELF*	ELF*	24	24
23:00	08:00								ELF*	ELF*	24	24
23:15	08:15								ELF*	ELF*	24	24
23:30	08:30								ELF*	ELF*	24	24
23:45	08:45								ELF*	ELF*	24	24
00:00	09:00								ELF*	ELF*	ELF*	
00:15	09:15								ELF*	ELF*	ELF*	
00:30	09:30								ELF*	ELF*	ELF*	
00:45	09:45								ELF*	ELF*	ELF*	

Nautical twilight
 Astronomical twilight
 Dark

Figure 4. Final campaign schedule. Times are shown in 15 minute increments to the left. Numbers refer to Experiment/Proposal number. Alphanumerics refer to satellite passes with experiment number at the end. On March 3 (UTC) experiments continued until 1400 UTC. ELF* indicates Experiment 38, which was pre-empted when ionospheric conditions were suitable for optics experiments.

Table 1
HAARP 2008 Winter Campaign Schedule as Executed

Date UTC	Start UTC	Stop UTC	Experiment Number	Q-L Report Appendix	Principal Investigator
20 February	23:28:00	23:59:59	33	Q	Spaleta
21 February	00:00:00	00:21:17	33	Q	Spaleta
	01:53:00	03:19:07	33	Q	Spaleta
	18:45:00	19:24:30	33	Q	Spaleta
	19:25:00	19:45:00	30	D	Secan
	20:00:00	21:15:00	35	W	Yampolski
	22:00:00	23:59:30	35	W	Yampolski
22 February	00:09:00	03:14:30	31	T	Sheerin
	03:15:00	03:44:30	4	F	Leyser
	03:47:00	04:13:00	30	D	Secan
	04:27:00	05:00:00	5	Y	Hughes
	18:06:38	18:15:42	5	Y	Hughes
	18:30:00	19:18:00	33	Q	Spaleta
	19:21:00	19:40:30	19	N	Milikh
	19:42:00	20:17:00	35	W	Yampolski
	20:22:00	20:46:30	30	D	Secan
	20:56:00	21:15:30	20	K	Mishin
	21:20:00	23:55:00	35	W	Yampolski
23 February	00:08:00	03:01:30	31	T	Sheerin
	03:15:00	05:00:00	12	S	Pedersen
	18:00:00	19:15:00	33	Q	Spaleta
	19:18:00	19:36:30	19	N	Milikh
	19:37:00	20:28:30	8	AB	Isham
	20:29:00	20:48:30	23	L	Papadopoulos
	20:49:00	22:39:30	13	B	Kuo
	22:40:00	23:04:30	30	D	Secan
	23:05:00	23:59:59	14	U	M-C Lee

Date UTC	Start UTC	Stop UTC	Experiment Number	Q-L Report Appendix	Principal Investigator
24 February	00:00:00	01:30:00	14	U	M-C Lee
	01:31:00	01:55:30	3	*	Groves
	01:57:00	03:14:30	14	U	M-C Lee
	03:15:00	05:01:00	12	S	Kosch
	17:50:00	18:15:00	3	*	Groves
	18:28:00	18:47:30	19	N	Milikh
	18:48:00	19:12:30	33	Q	Spaleta
	19:13:00	19:32:30	19	N	Milikh
	20:00:00	20:59:30	4	F	Leyser
	21:00:00	22:14:30	8	AC	Isham
	22:17:00	22:47:00	3	*	Groves
	23:02:00	23:59:30	8	AC	Isham
	25 February	00:02:00	00:25:00	3	*
00:33:00		01:59:30	22	I	Oyama
02:00:00		03:14:30	8	AC	Isham
03:15:00		03:43:30	4	F	Leyser
03:44:00		04:18:30	30	D	Secan
04:20:00		04:46:30	36	J	Gustavsson
04:47:00		5:07:00	2	M	Chang
19:09:00		19:28:30	19	N	Milikh
19:46:00		19:59:30	8	AC	Isham
20:00:00		20:59:30	4	F	Leyser
21:00:00		21:59:30	8	AC	Isham
22:00:00		23:59:00	13	B	Kuo
26 February		00:00:00	00:59:00	13	B
	01:04:00	01:59:30	29	G	Sales
	02:00:00	03:14:30	8	AC	Isham
	03:19:00	04:33:30	29	G	Sales
	04:34:00	04:53:30	2	M	Chang
	04:54:00	05:08:30	5	Y	Hughes
	19:05:00	19:24:30	19	N	Milikh
	19:25:00	20:38:30	4	F	Leyser
	20:39:00	20:58:30	20	K	Mishin
	20:59:00	21:17:00	38	***	Inan
	21:20:00	21:49:30	8	AC	Isham
	22:00:00	23:29:30	34	H	Watkins
	23:30:00	23:59:30	14	U	M-C Lee

Date UTC	Start UTC	Stop UTC	Experiment Number	Q-L Report Appendix	Principal Investigator
27 February	00:00:00	02:59:30	14	U	M-C Lee
	03:00:00	03:49:00	29	G	Sales
	03:58:26	04:19:30	36	J	Gustavsson
	04:20:00	04:39:30	39	*	Wuerker
	04:40:00	05:57:30	36	J	Gustavsson
	05:58:00	06:18:00	38	***	Inan
	20:55:00	21:14:00	23	L	Papadopoulos
	21:16:00	22:42:30	34	H	Watkins
	22:43:00	22:49:30	3	*	Groves
	23:06:00	23:59:59	34	H	Watkins
28 February	00:00:00	01:59:30	34	H	Watkins
	02:10:00	02:59:30	36	J	Gustavsson
	03:00:00	06:26:30	4	F	Leyser
	06:27:00	06:46:30	23	L	Papadopoulos
	06:48:00	06:59:30	4	F	Leyser
	22:28:53	22:29:30	36	J	Gustavsson
	23:00:00	23:59:59	31	T	Sheerin
29 February	00:00:00	01:29:30	31	T	Sheerin
	01:37:00	01:42:00	3	*	Groves
	02:08:00	02:59:30	31	T	Sheerin
	03:00:00	03:58:00	36	J	Gustavsson
	04:00:00	05:29:30	17	Z	Marshall
	05:30:00	06:17:00	4	F	Leyser
	06:20:00	06:29:30	25	*	Parent
	06:30:00	06:57:30	4	F	Leyser
	06:59:00	07:19:00	38	***	Inan
	07:20:00	08:49:30	6	C	Hysell
	08:50:00	10:00:00	37	**	Inan
23:00:00	23:59:30	21	X	Moore	
1 March	00:00:00	02:59:30	14	U	M-C Lee
	03:00:00	03:59:30	4	F	Leyser
	04:03:00	06:29:30	11	R	Kosch
	06:30:00	07:47:30	37	**	Inan
	07:50:00	08:40:30	26	P	Pedersen
	08:41:00	09:38:30	37	**	Inan
	09:39:00	10:00:00	26	P	Pedersen
	23:00:00	23:59:30	21	X	Moore

Date UTC	Start UTC	Stop UTC	Experiment Number	Q-L Report Appendix	Principal Investigator
2 March	00:02:00	02:59:30	14	U	M-C Lee
	03:00:00	03:59:30	4	F	Leyser
	04:00:00	05:42:00	10	E	Kendall
	05:51:00	06:20:30	37	**	Inan
	06:21:00	06:40:30	23	L	Papadopoulos
	06:41:00	07:14:30	37	**	Inan
	07:15:00	08:59:30	24	V	Parent
	09:00:00	10:00:00	37	**	Inan
	20:10:00	20:24:13	37	**	Inan
3 March	03:00:00	03:59:30	21	X	Moore
	04:00:00	05:29:30	10	E	Kendall
	05:30:00	06:51:30	11	R	Kosch
	06:52:00	07:11:30	23	L	Papadopoulos
	07:15:00	08:59:30	24	V	Parent
	09:00:00	10:30:30	37	**	Inan
	10:31:00	10:57:00	26	P	Pedersen
	11:02:00	14:00:00	37	**	Inan

* Quick Look Report was not received.

** ELF/VLF experiment not part of the campaign, was run during conditions not suitable for irregularities/optics experiment.

*** ELF/VLF satellite experiment not part of the campaign, run as higher priority experiment.

3. Preliminary Campaign Results

All principal investigators were required to submit quick-look reports in a standard format describing the research objective, the procedure or observation technique, and preliminary results. Submission of the reports was requested within 6 weeks of the end of the campaign. With one exception, all of the campaign participants submitted the requested reports. Several of the participants indicated that they were still awaiting data from the facility or from collaborating investigators. In other cases, there was insufficient time to analyze the data.

However, a number of investigators were able to show early reports of new and exciting results. Some examples include unusual Stimulated Electromagnetic Emission (SEE) spectra seen during a new HF operating mode used for the first time in any ionospheric research experiment (Experiment 4), use of the new HAARP imaging riometer to study ionospheric absorption (Experiment 35), the methodical study of ionospheric saturation effects as a function of radiated power (Experiment 33), and the apparent self-scattering of HF signals into ionospheric ducts (Experiment 29) among others. It is reasonable to expect that this campaign will produce several published papers on new scientific findings.

All of the submitted quick look reports are contained in the Appendix section of this report, beginning with Appendix B.

4. Campaign Organizers Report

Previous HAARP research campaigns have been organized by government personnel or by a combination of government and support contractor personnel. NorthWest Research Associates was tasked to organize this campaign as a new paradigm for future general science (as distinct from DoD applications-related) campaigns at HAARP.

Organization efforts began immediately following the decision in late December 2007 to conduct the campaign. A general announcement was sent out on December 31, 2007 to a list of scientists who had previously participated in irregularities or optical research campaigns at the HAARP facility. A special campaign web site was set up as a repository for information about the campaign and a formal campaign announcement was posted on this web site on January 4, 2008, requesting the submission of proposals by January 18 to be prepared following a standard format. A total of 33 proposals were received by the deadline. Three NWRA scientists reviewed the proposals and a summary document was produced with a prioritized listing of participants showing diagnostic instruments requested, satellites to be used, environmental constraints (e.g., day/night, geomagnetic conditions, etc.) and additional factors that could affect schedule placement.

As discussed in Section 2. of this report, the campaign dates were selected based on apportioning campaign time between irregularities and optics, allocating the first four days exclusively to irregularities research, shifting toward emphasis on optical emissions as the campaign progressed. The initial schedule was developed beginning with placeholders for all of the requested satellite passes. Proposals justifying requirements for large, continuous blocks of time were accommodated next followed by those experiments constrained by the need for high f_0F_2 . The most difficult aspect of scheduling was placement of optical emission experiments since, in general, these experiments require complete darkness (end of astronomical twilight) with f_0F_2 no lower than the lowest HAARP frequency allocation. Since this campaign was conducted during the minimum of sunspot cycle 23, the amount of time where these conditions were satisfied each evening was very short, making it possible to allocate the best time slot to only one principal investigator each campaign day. Campaigns in future years will not be as time-constrained since solar flux levels will be higher as we move into solar cycle 24.

The campaign began as planned on February 21 (one experiment was conducted on February 20 as part of the pre-campaign preparations). With minor variations, all experiments were performed although some principal investigators did not receive all of the experiment time they had initially requested. Requests for dedicated operation of participating diagnostic facilities, most notably, SuperDARN, could not be satisfied in every case due to the short amount of lead time. Overall, however, the campaign was extremely successful with several new and unexpected scientific results reported. Another measure of the campaign's success was the nearly flawless operation of the HAARP facility, including the HAARP HF transmitter (the Ionospheric Research Instrument or IRI) and the on-site diagnostic suite. The extensive use of a web site to disseminate campaign information was also a valuable addition.

5. Concluding Remarks

The HAARP 2008 winter irregularities and optical emission campaign was conducted at the HAARP Gakona Facility over the period February 20 through March 3, 2008. The experiments executed during the campaign, exploited the facility's state-of-the-art design. The diversity of

participants and the willingness of the HAARP staff to work with those participants have resulted in development of new and often ground breaking methods for exploiting the versatile performance parameters of the IRI and its diagnostics.

Although only preliminary results are available at this point, it is apparent that new scientific findings will be reported as a result of this campaign. This is due not only to the enhanced and more powerful capabilities of the facility but also to the serendipitous effect of a collaborative campaign, cooperative facility staff and collegial spirit among all of the participants. Future campaign planning and execution should be acutely aware of the value of these intangibles and strive to preserve them with careful consideration of any new and restrictive requirements.

The organization effort required for a campaign of this scope and participation level should not be overlooked. Campaign planning activities including proposal solicitation, review, schedule development, communication with participants and reporting is a multi-person, dedicated effort requiring concomitant assistance from site staff and program managers during all phases. All of those factors came together for this campaign producing an inevitably successful conclusion.

Appendix A

Geophysical Conditions During the Campaign Interval.

This appendix provides graphical and tabular information characterizing the geophysical conditions during the twelve days of the HAARP campaign interval. Data were obtained from instruments located at and near the HAARP facility, from satellite instruments, and from the Association of Geomagnetism and Aeronomy (IUGG).

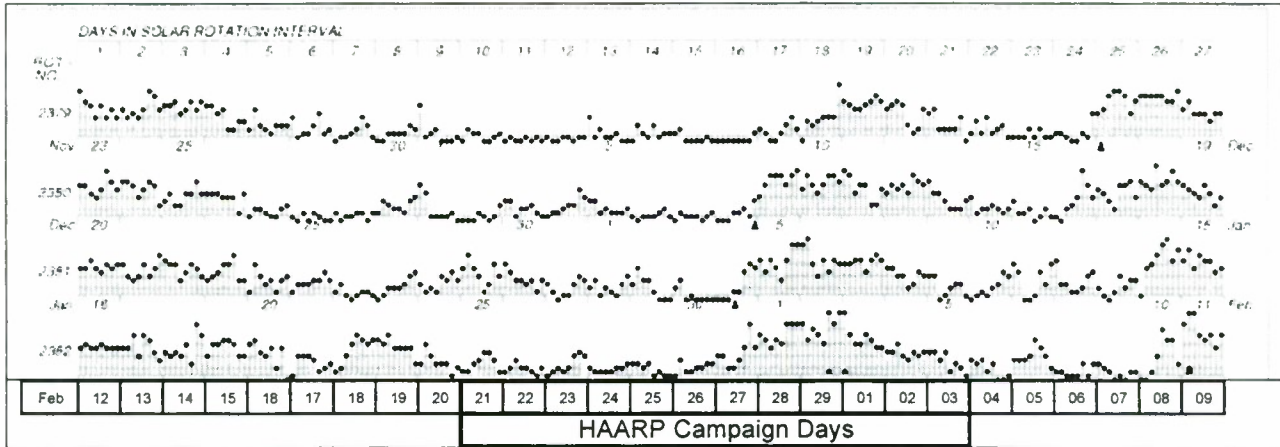
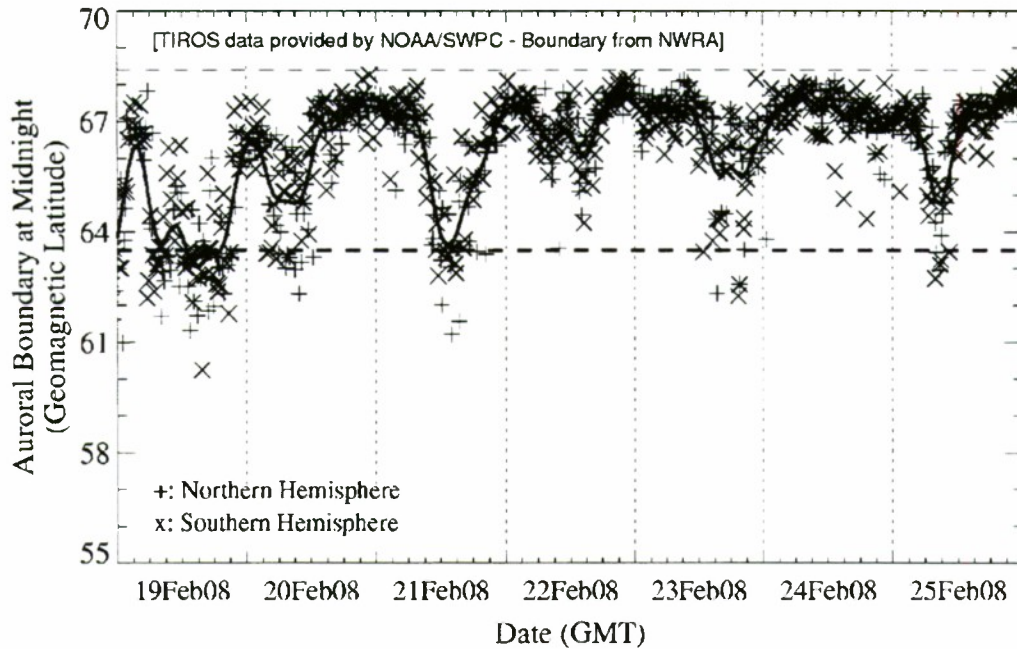


Figure A1. Plot of the K_p "musical diagram" indicating the HAARP campaign interval.

Table A1. Definitive K_p , A_p , and C_p indices from the Association of Geomagnetism and Aeronomy International Service of Geomagnetic Indices (GeoForschungsZentrum Potsdam).

Date	Kp three-hourly								Sum Kp	Ap	Cp	Char
	1	2	3	4	5	6	7	8				
19 Feb	3+	3o	4-	3-	3-	3-	3-	1+	22o	14	0.8	
20 Feb	1+	3o	2o	1+	1+	1+	0+	1o	12-	6	0.3	
21 Feb	1-	1-	1+	2-	2+	2+	2-	1-	11+	6	0.2	Q0
22 Feb	1-	1o	2-	1o	1o	1-	0+	1o	7+	4	0.1	Q3
23 Feb	0+	1-	1o	1-	1o	2o	2+	2o	10o	5	0.2	Q8
24 Feb	1o	1-	1-	1-	1-	1o	1o	1+	7o	4	0.1	Q1
25 Feb	1+	1+	1o	1+	0+	1-	0+	0+	7-	4	0.1	Q2
26 Feb	0+	2-	1-	1-	1o	1o	1+	1+	8o	4	0.1	Q4
27 Feb	2o	2o	1o	1o	2-	3-	4+	3-	17+	10	0.6	
28 Feb	4-	3+	3-	3+	3o	4+	4+	4+	29o	23	1.1	D2
29 Feb	4+	3+	4o	4-	3o	5+	4+	5o	33o	31	1.3	D1
01 Mar	5+	4-	3o	3o	4-	3+	3-	3-	27+	22	1.1	D5
02 Mar	2+	2+	3o	2o	2-	2+	2o	2+	18o	9	0.5	
03 Mar	2+	2+	2-	2+	1-	1+	1o	0+	12o	6	0.3	Q9

NOAA TIROS Auroral Boundary Estimate



NOAA TIROS Auroral Boundary Estimate

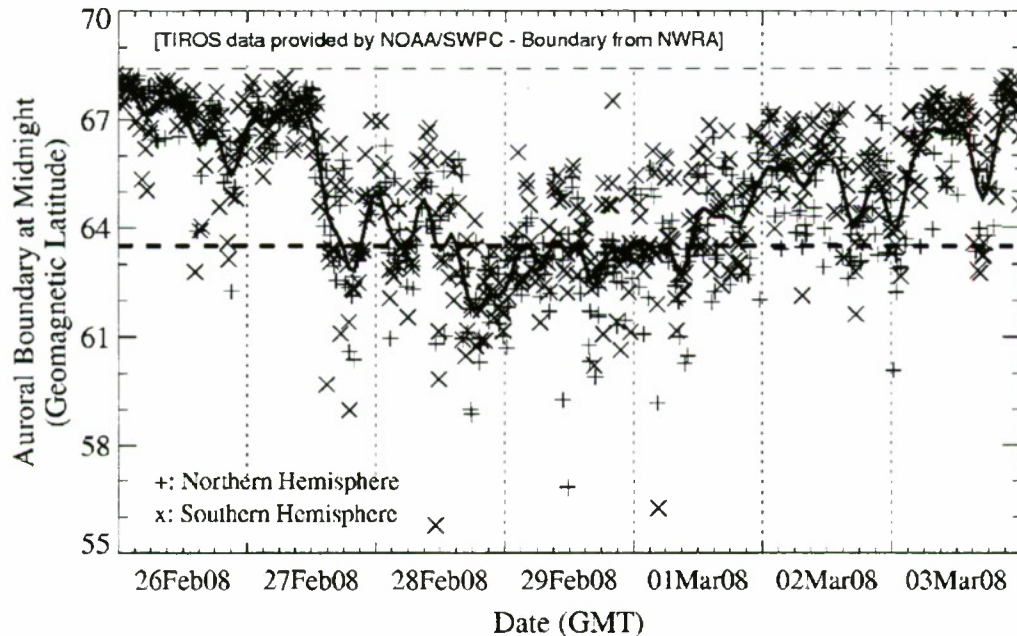


Figure A2. Estimated location of the equatorial boundary of the diffuse aurora as derived from precipitating electron data observed by TIROS and MetOp satellites. Light dashed line indicates the highest boundary latitude (corresponding to lowest activity level) possible; the heavy dashed line indicates the HAARP latitude; and the heavy curve is a three-hour smoothed boundary location. Data from both northern and southern hemisphere are included in these plots.

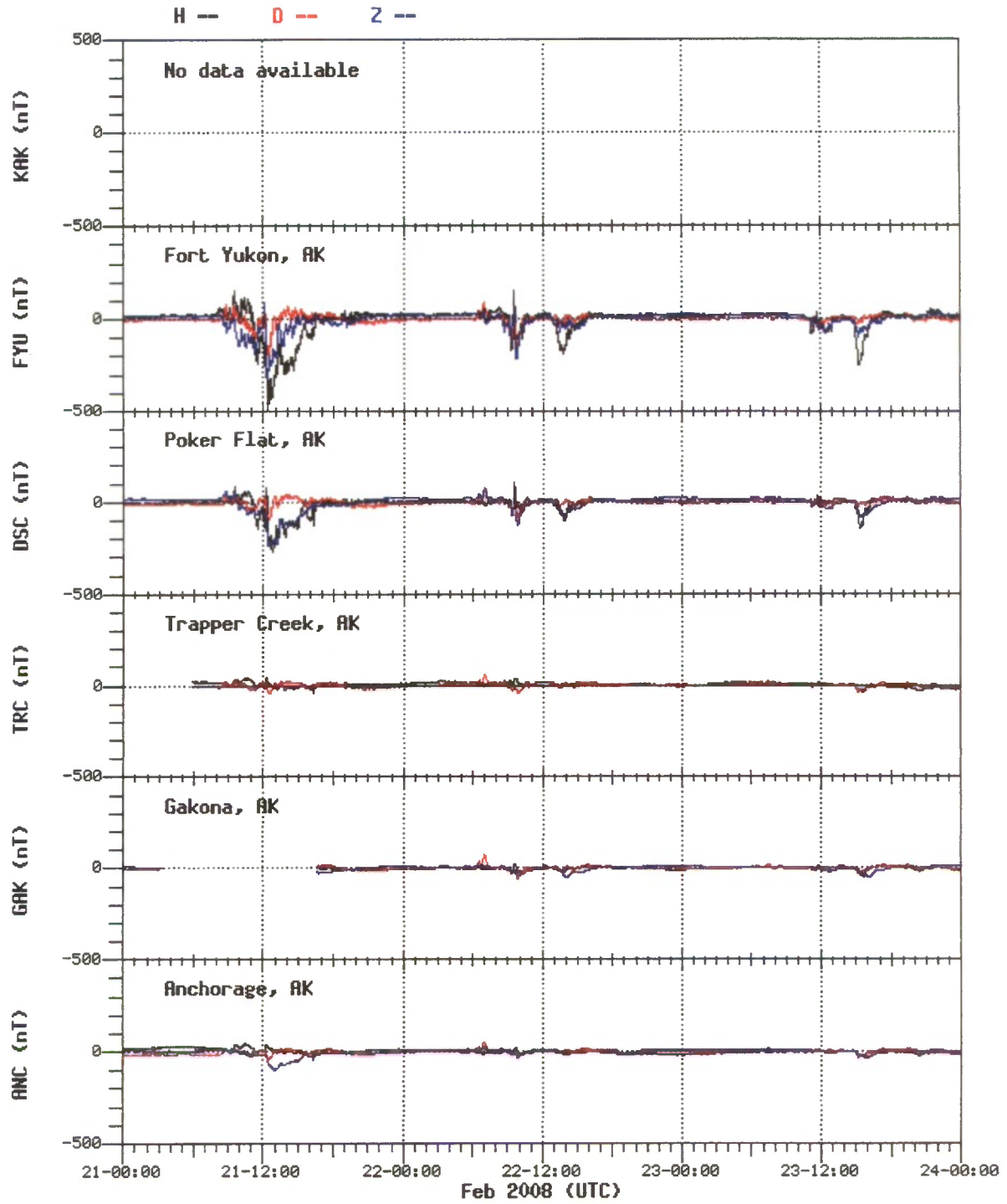


Figure A3. Data from the University of Alaska Geophysical Institute Magnetometer Array for 21 through 24 February 2008.

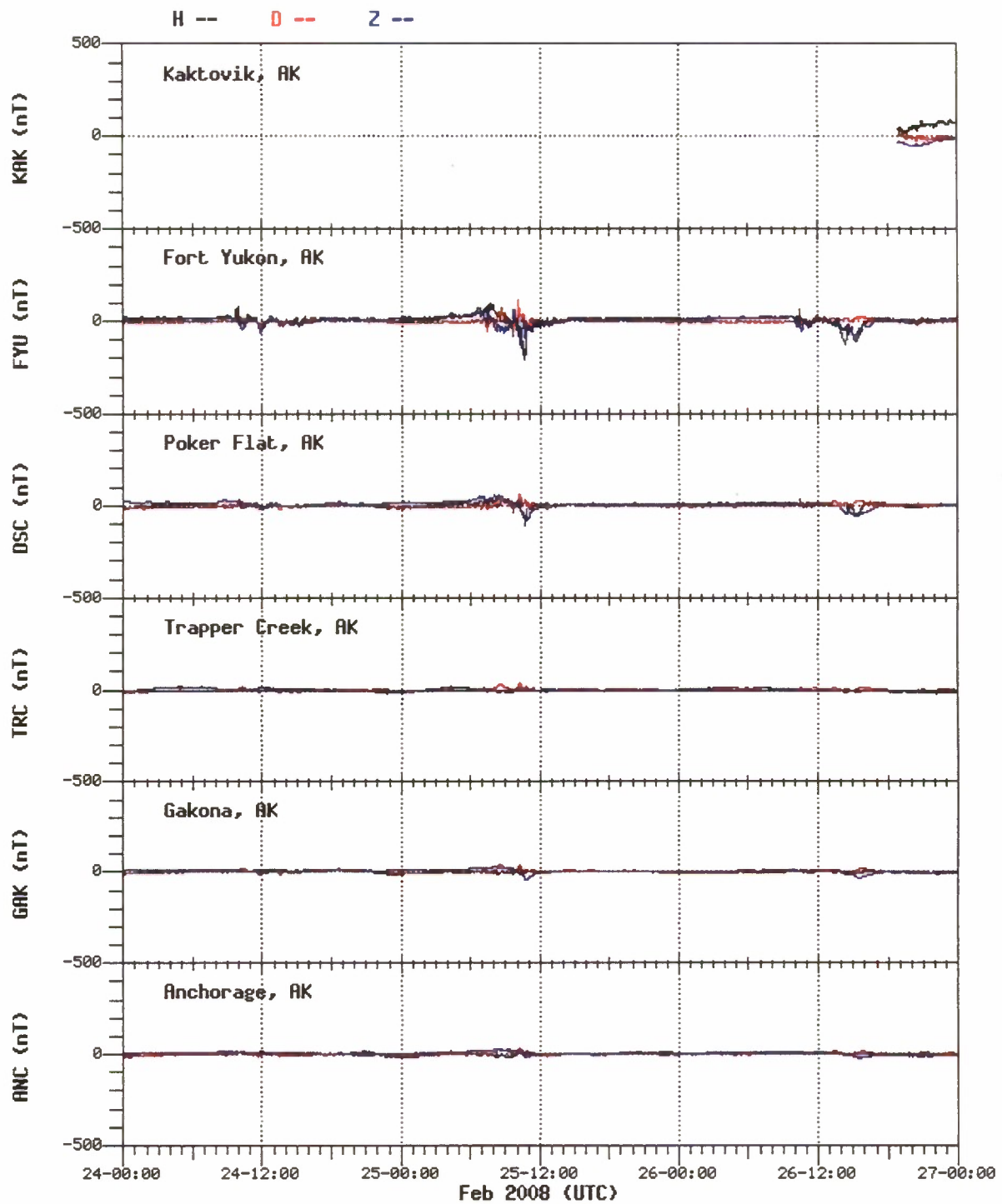


Figure A4. Data from the University of Alaska Geophysical Institute Magnetometer Array for 25 through 26 February 2008.

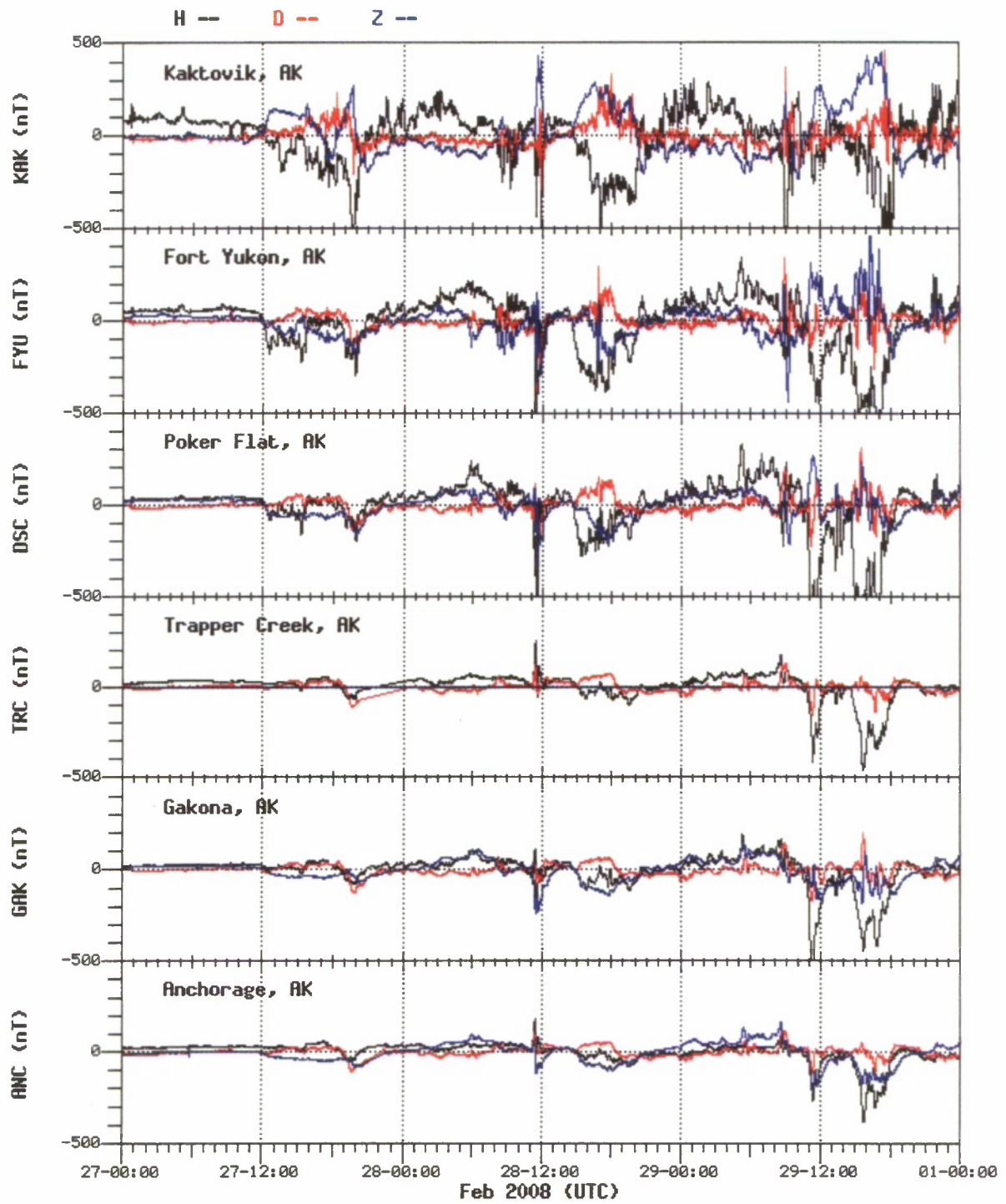


Figure A5. Data from the University of Alaska Geophysical Institute Magnetometer Array for 27 through 29 February 2008.

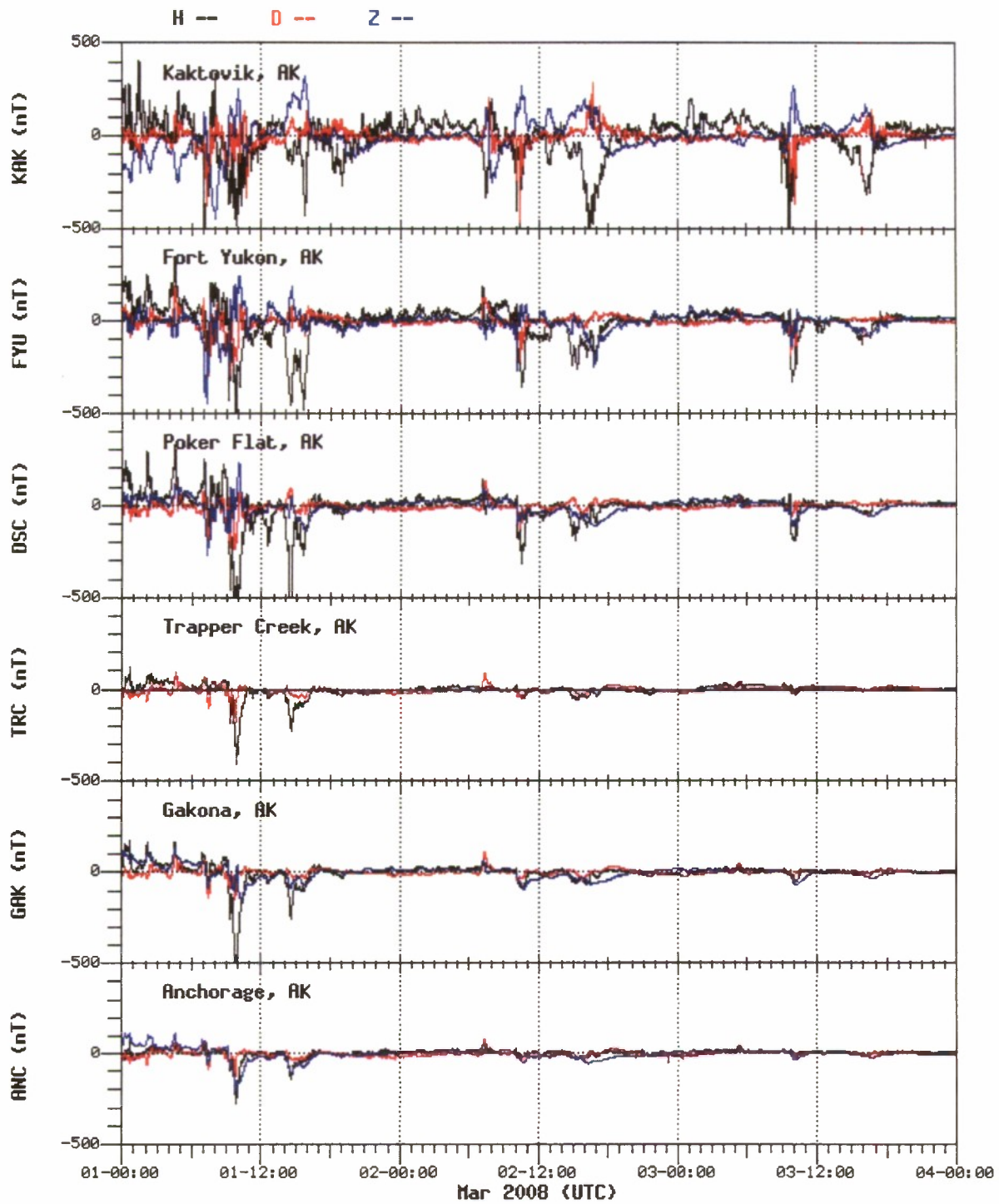


Figure A6. Data from the University of Alaska Geophysical Institute Magnetometer Array for 01 through 03 March 2008.

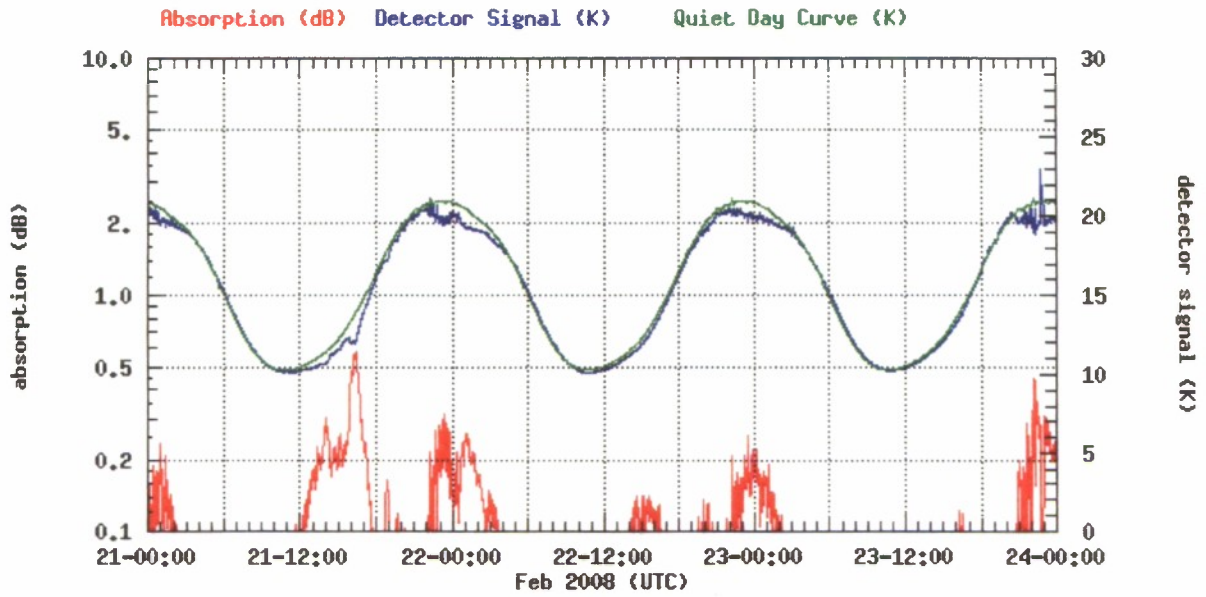


Figure A7. Data from the HAARP riometer for 21 through 23 February 2008.

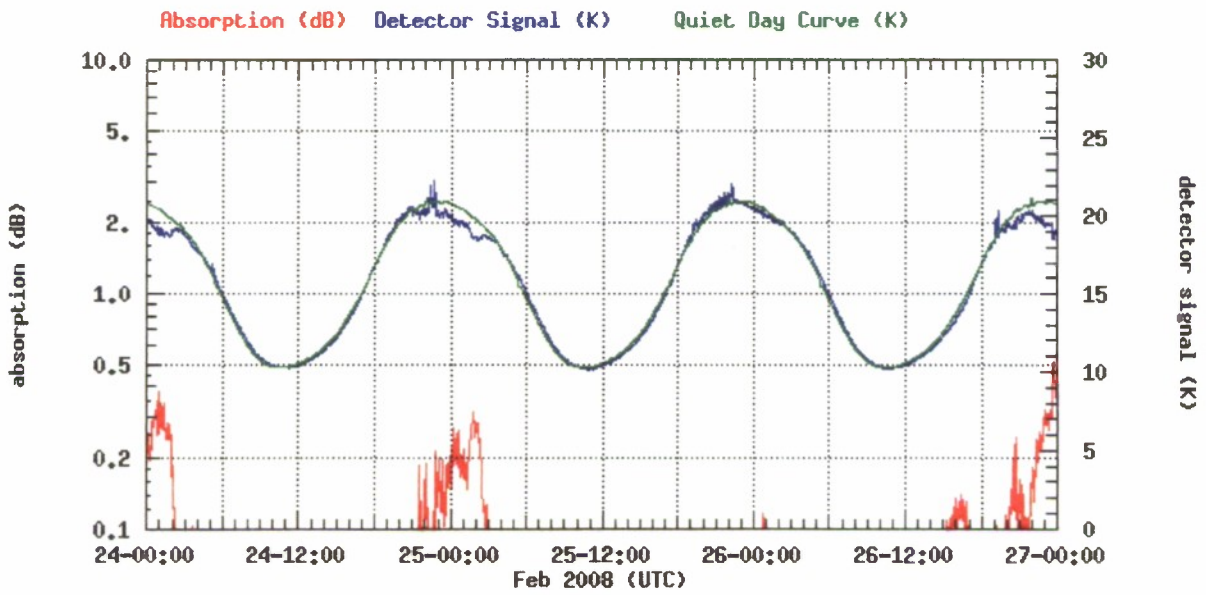


Figure A8. Data from the HAARP riometer for 24 through 26 February 2008.

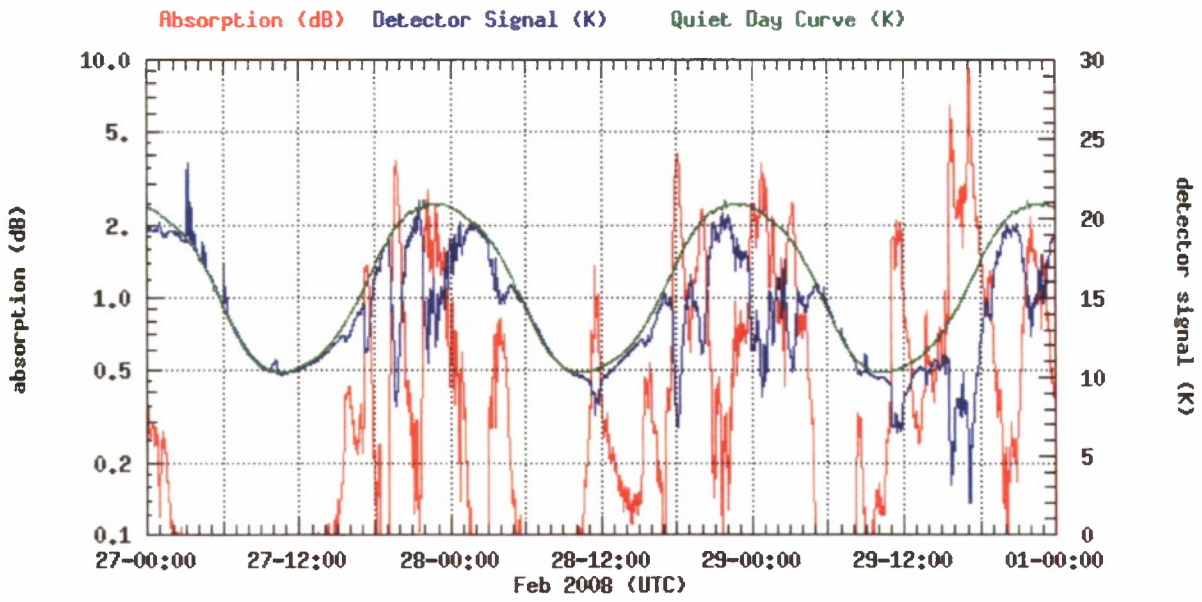


Figure A9. Data from the HAARP riometer for 27 through 29 February 2008.

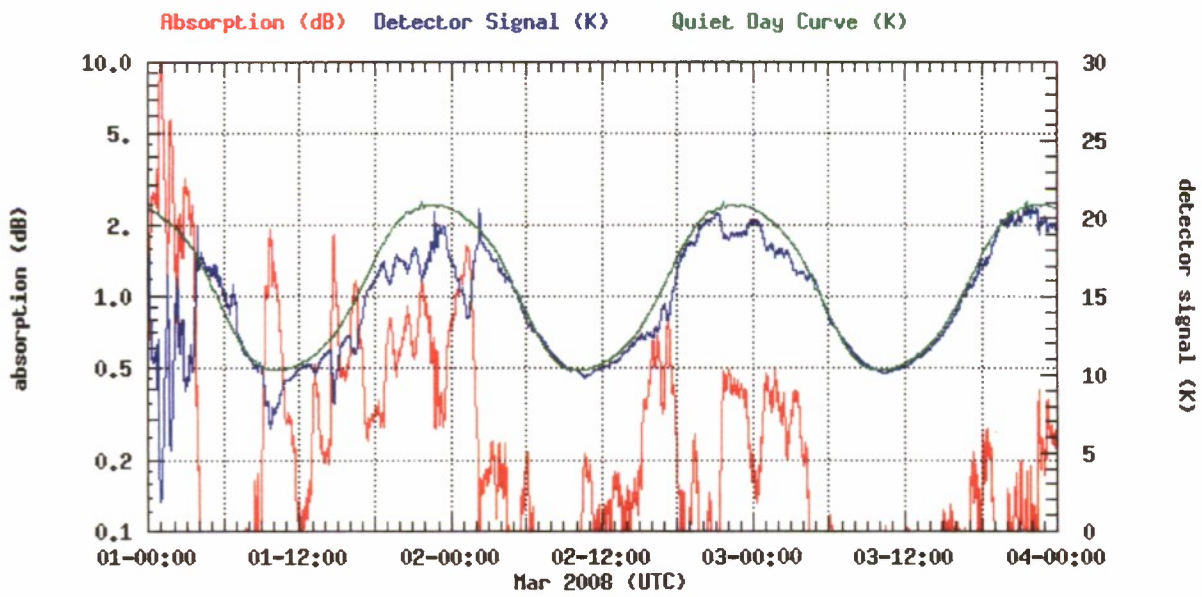


Figure A10. Data from the HAARP riometer for 01 through 03 March 2008.

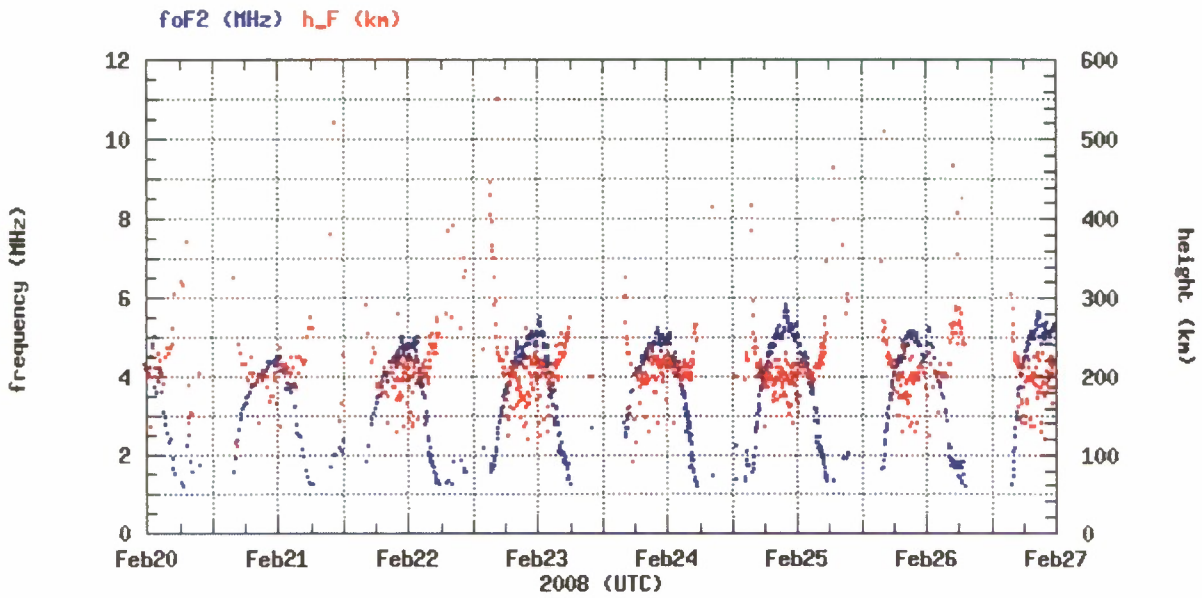


Figure A11. Data from the HAARP Digisonde for 20 through 26 February 2008. The observed f_oF2 is plotted in blue, the observed h_mF2 in red.

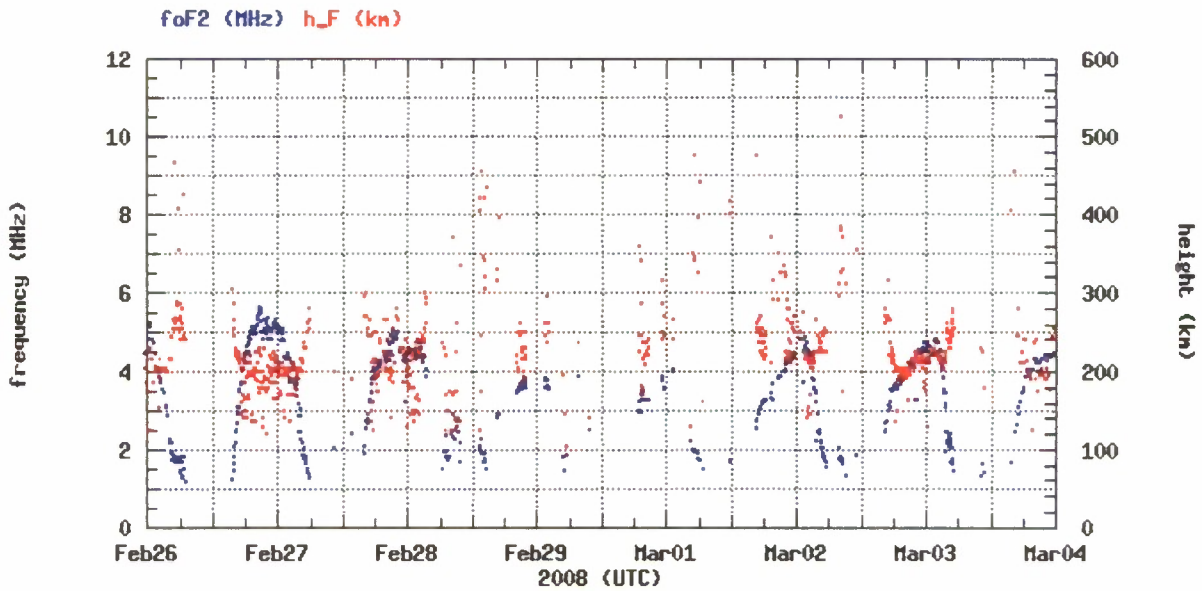


Figure A12. Data from the HAARP Digisonde for 26 February through 03 March 2008. The observed f_oF2 is plotted in blue, the observed h_mF2 in red.

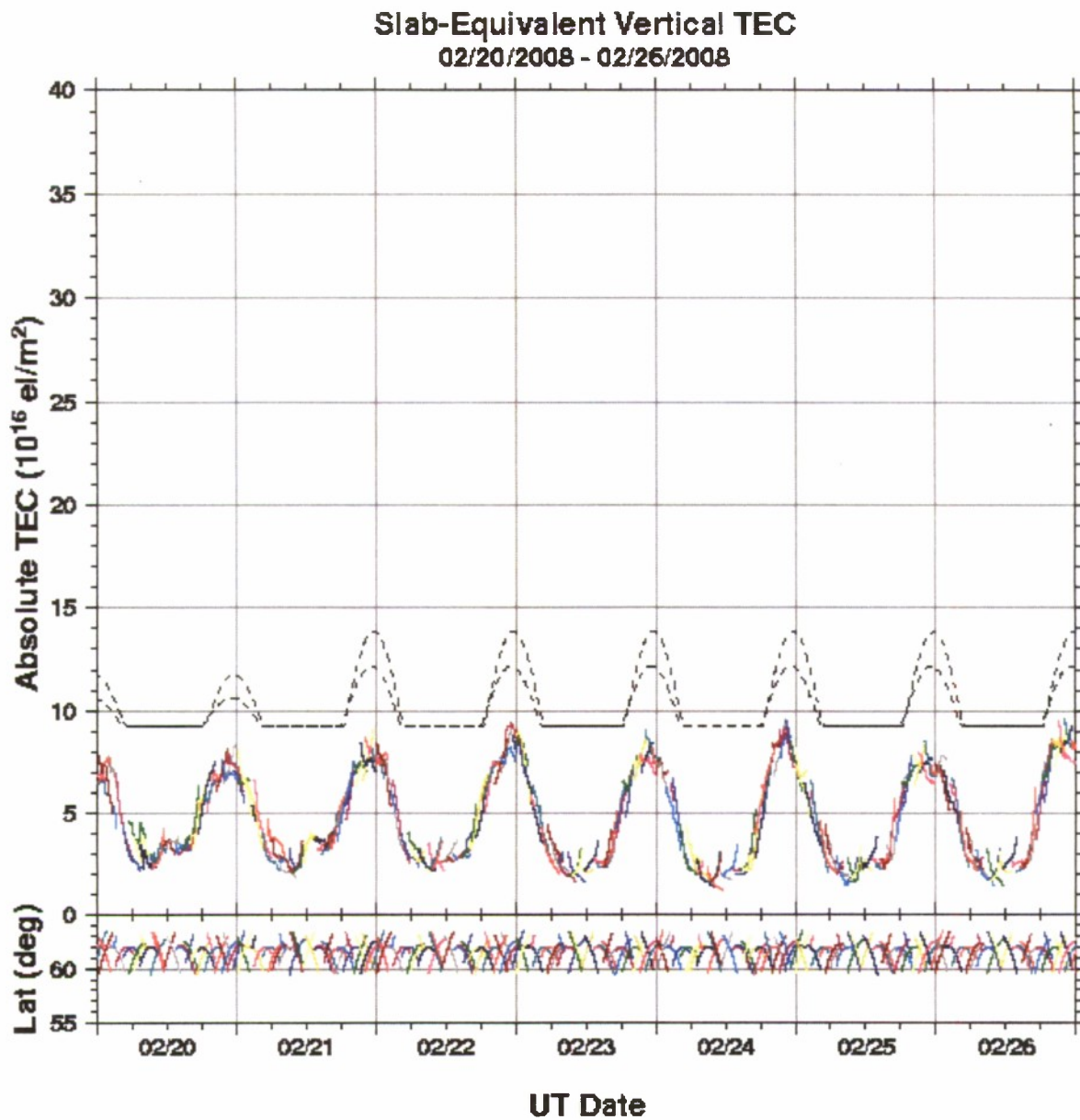


Figure A13. Total Electron Content derived from the HAARP GPS receiver for the period 20 February through 26 February 2008. Different colors indicate data from different GPS satellites. The black dashed curve is the vertical TEC obtained from the GPS single-frequency user TEC model.

Slab-Equivalent Vertical TEC
02/26/2008 - 03/03/2008

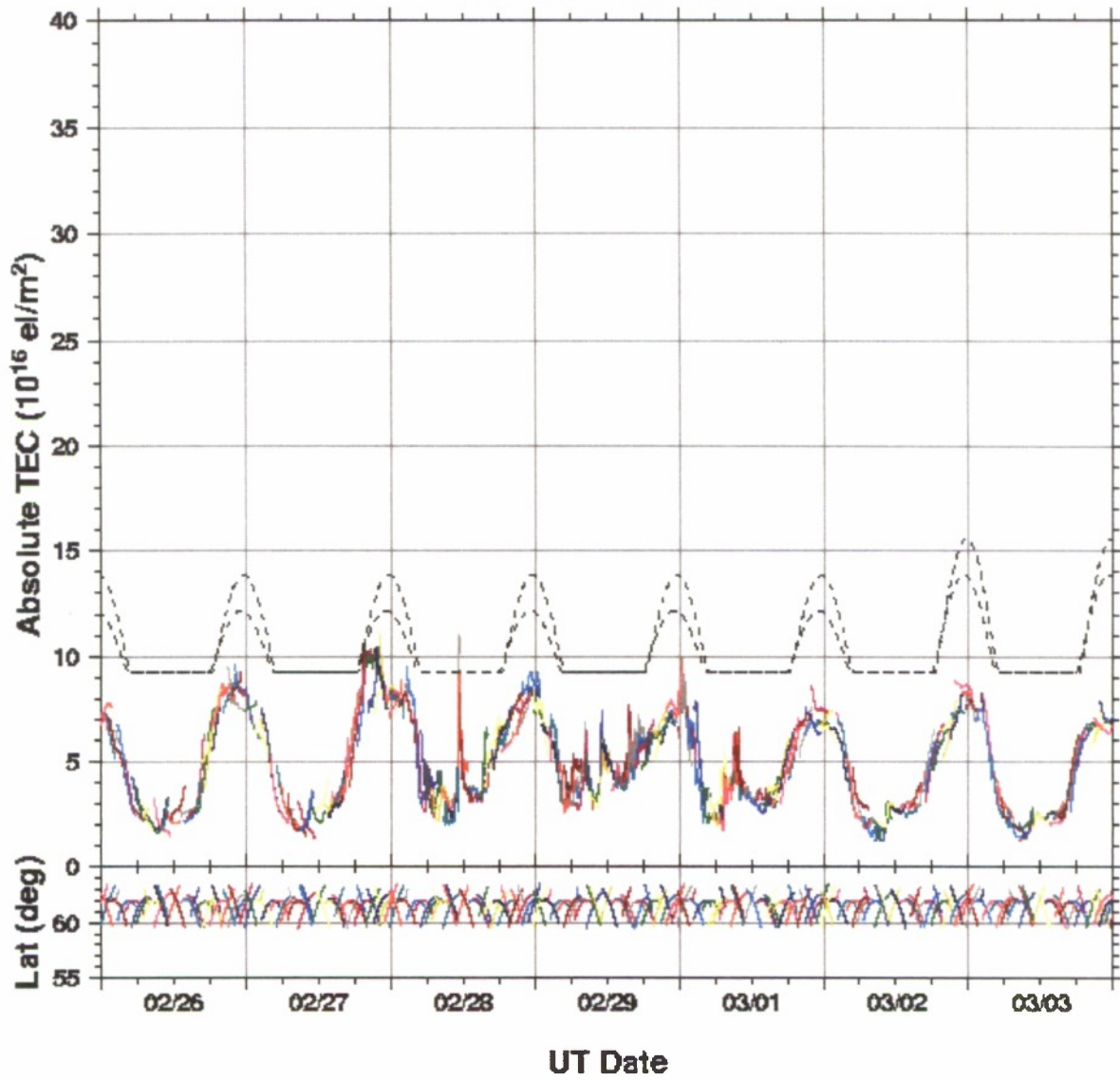


Figure A14. Total Electron Content derived from the HAARP GPS receiver for the period 20 February through 26 February 2008. Different colors indicate data from different GPS satellites. The black dashed curve is the vertical TEC obtained from the GPS single-frequency user TEC model.

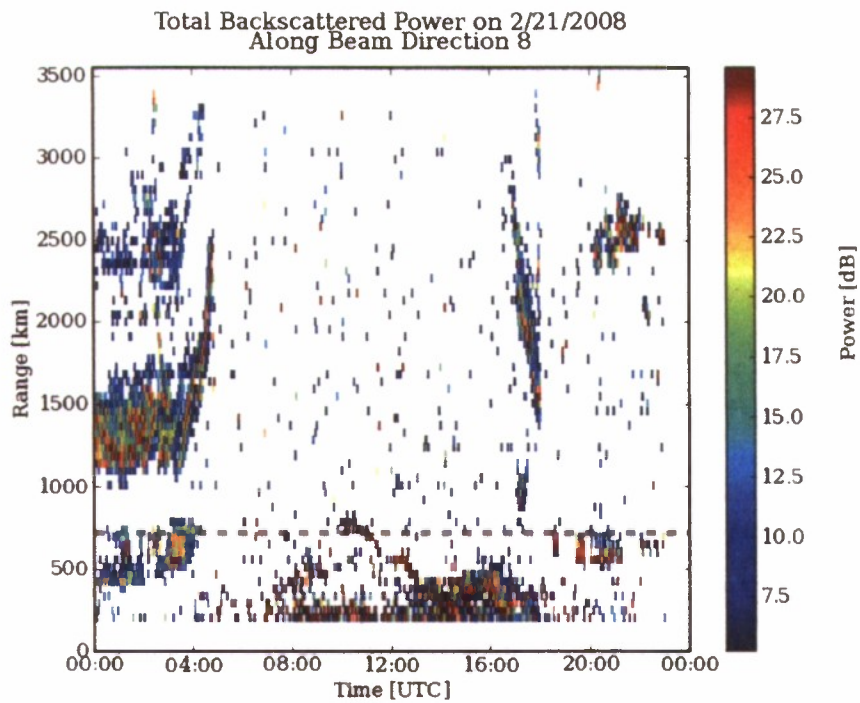


Figure A15. Total backscattered power from the Kodiak SuperDARN radar along Beam 8 on 21 February 2008.

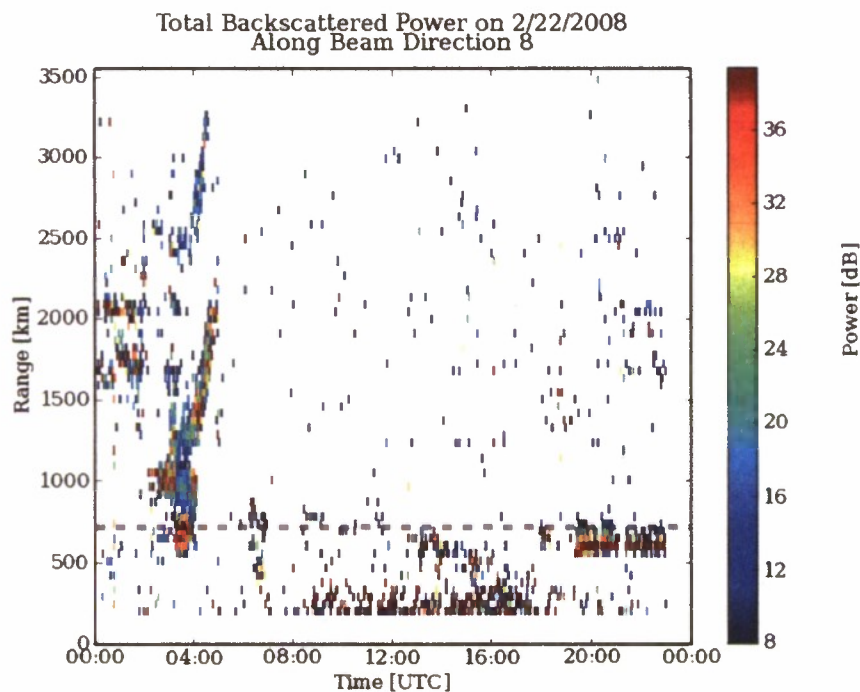


Figure A17. Total backscattered power from the Kodiak SuperDARN radar along Beam 8 on 22 February 2008.

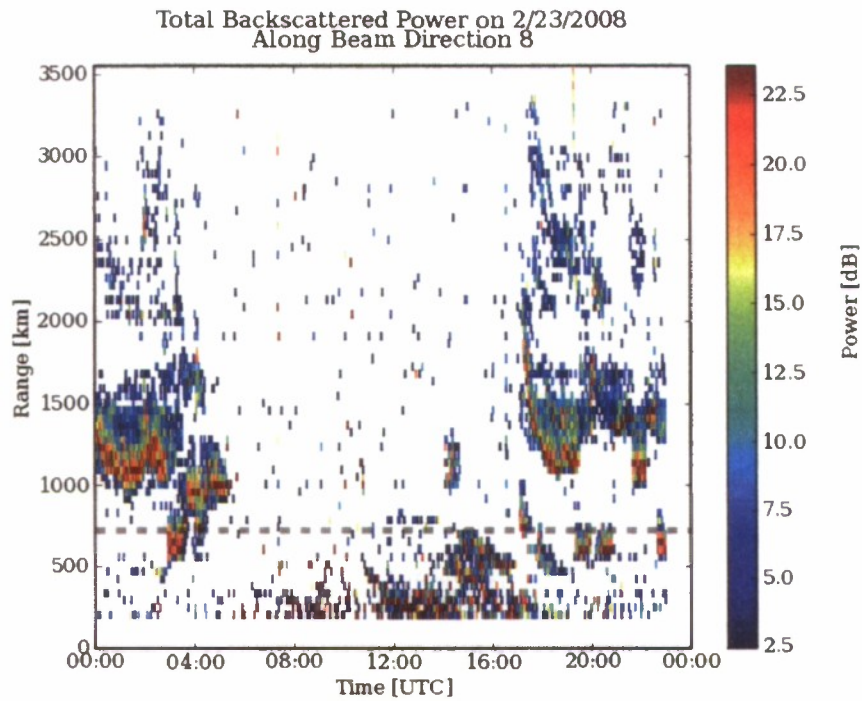


Figure A18. Total backscattered power from the Kodiak SuperDARN radar along Beam 8 on 23 February 2008.

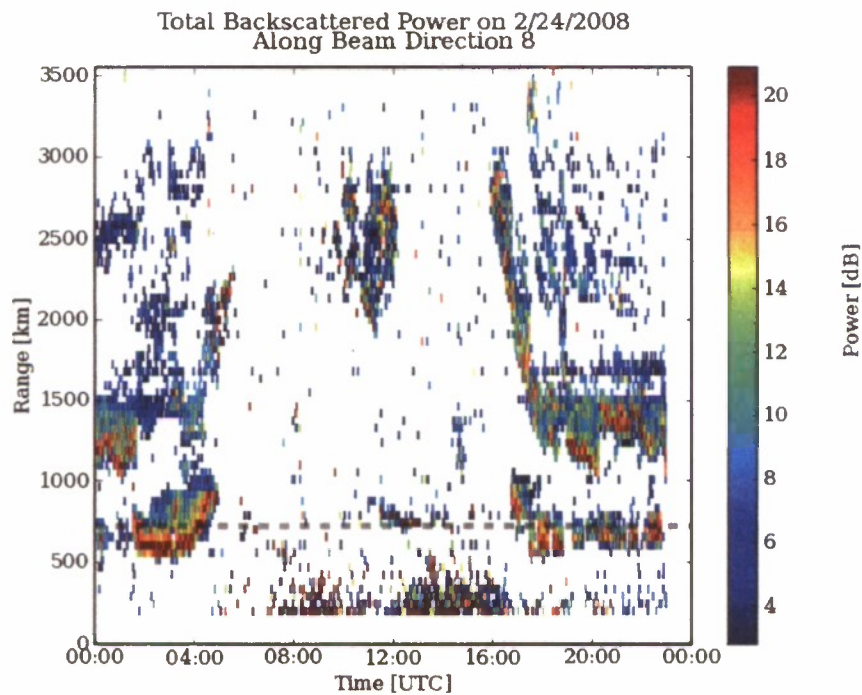


Figure A19. Total backscattered power from the Kodiak SuperDARN radar along Beam 8 on 24 February 2008.

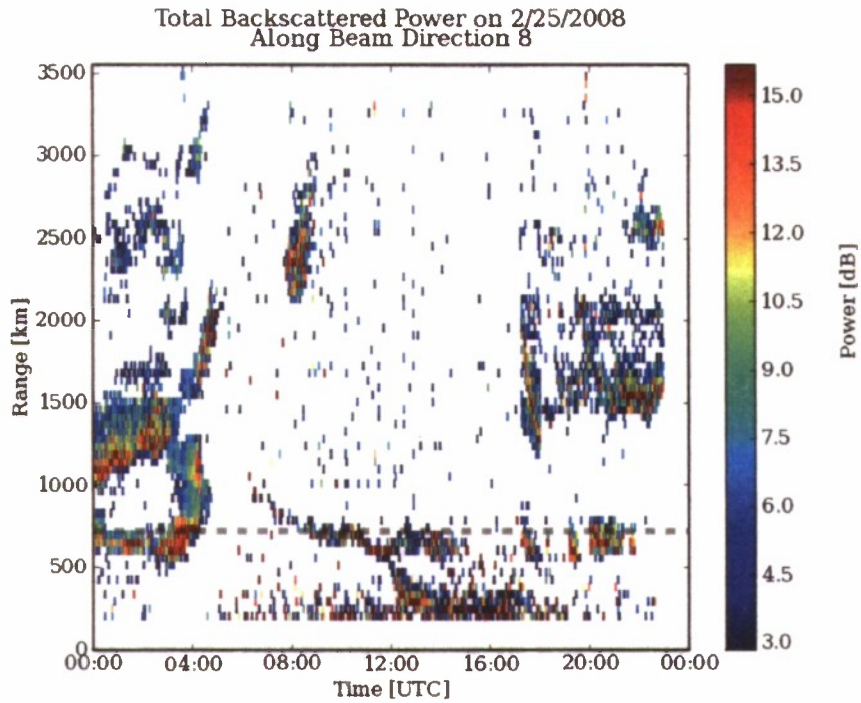


Figure A20. Total backscattered power from the Kodiak SuperDARN radar along Beam 8 on 25 February 2008.

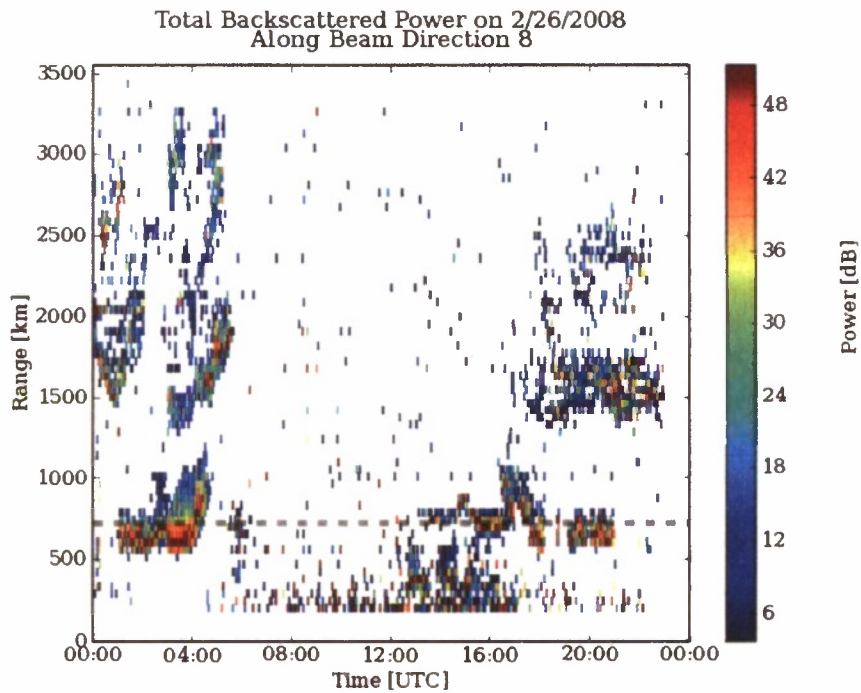


Figure A21. Total backscattered power from the Kodiak SuperDARN radar along Beam 8 on 26 February 2008.

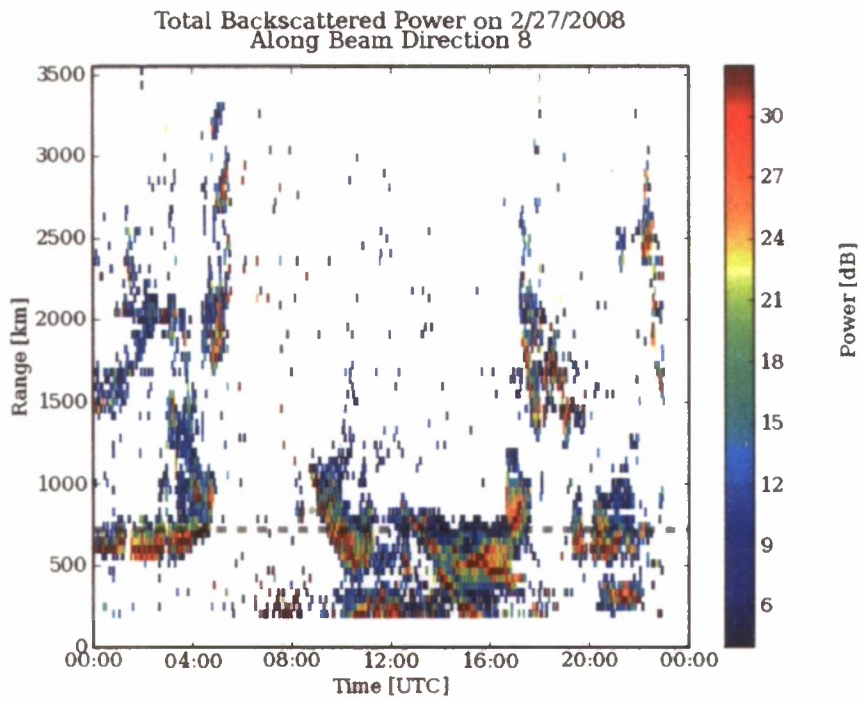


Figure A22. Total backscattered power from the Kodiak SuperDARN radar along Beam 8 on 27 February 2008.

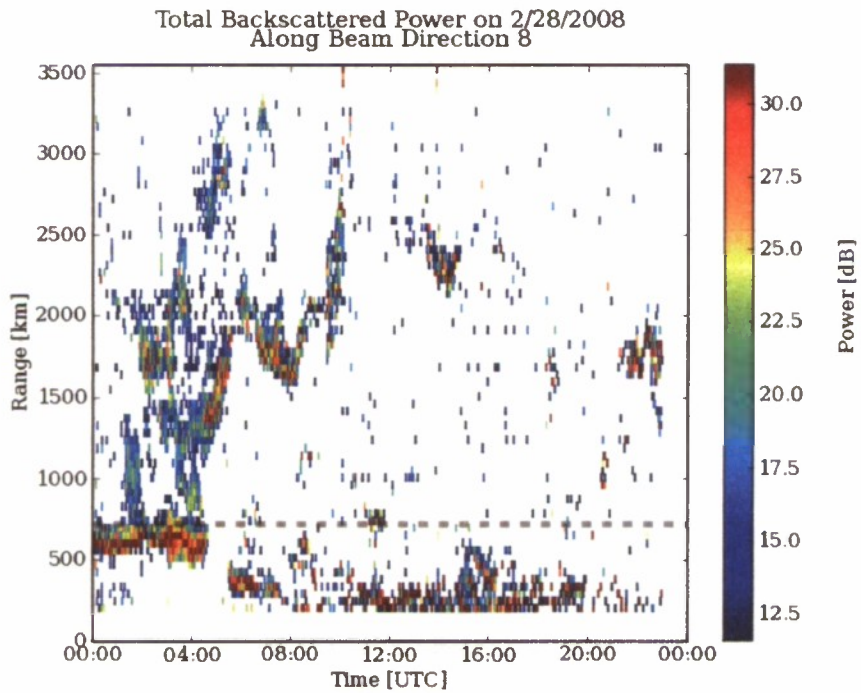


Figure A23. Total backscattered power from the Kodiak SuperDARN radar along Beam 8 on 28 February 2008.

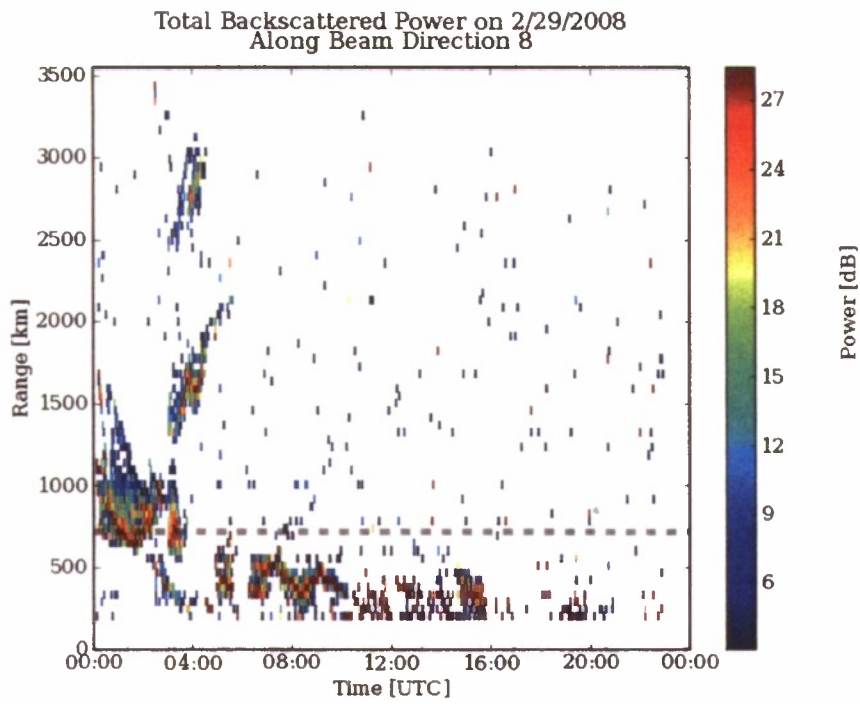


Figure A24. Total backscattered power from the Kodiak SuperDARN radar along Beam 8 on 29 February 2008.

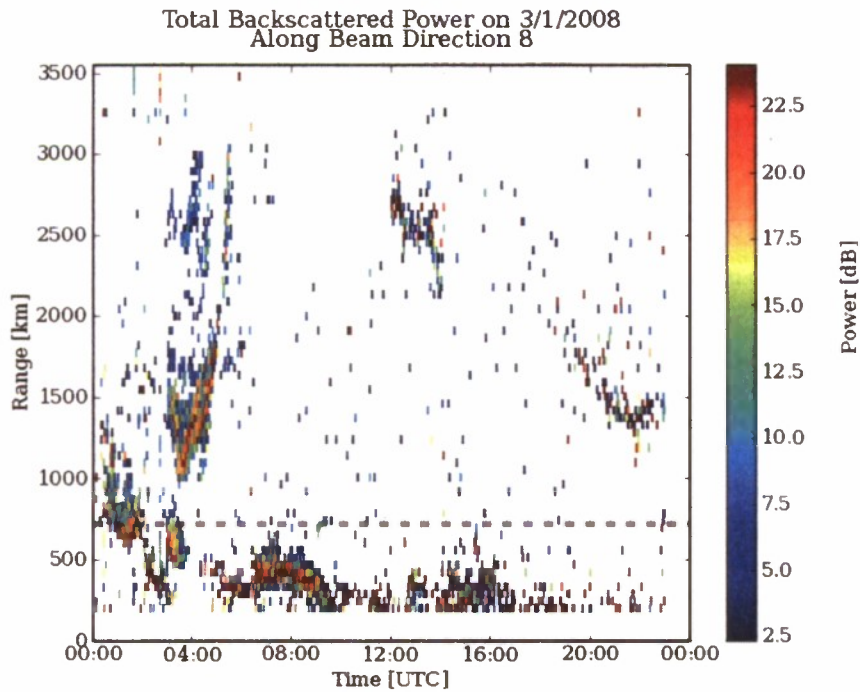


Figure A25. Total backscattered power from the Kodiak SuperDARN radar along Beam 8 on 01 March 2008.

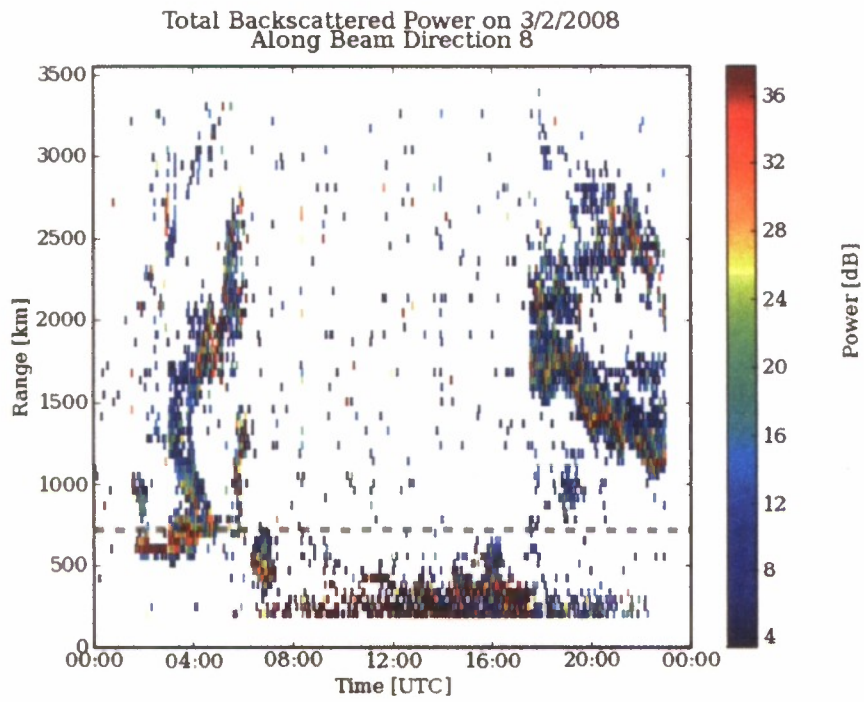


Figure A26. Total backscattered power from the Kodiak SuperDARN radar along Beam 8 on 02 March 2008.

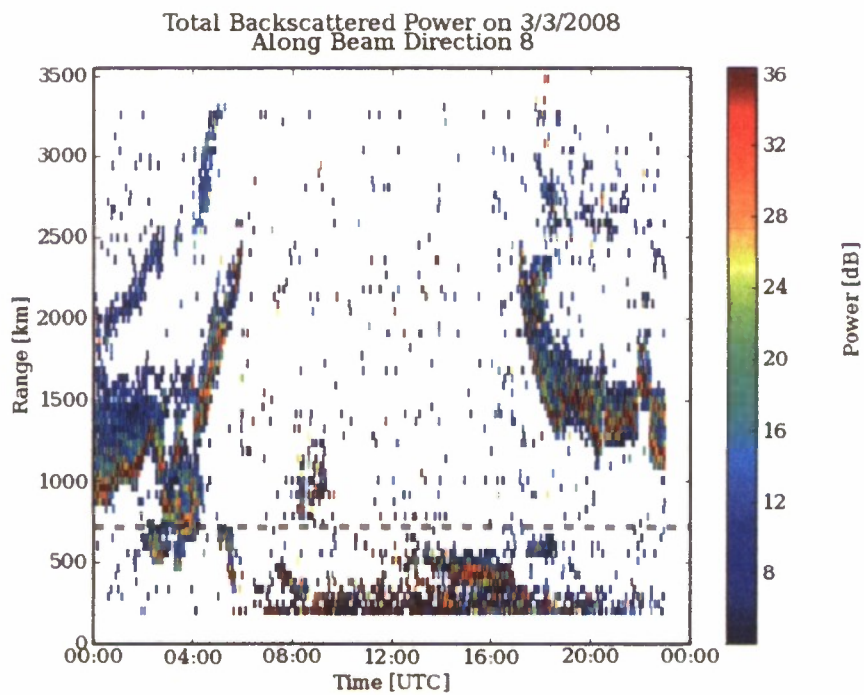


Figure A27. Total backscattered power from the Kodiak SuperDARN radar along Beam 8 on 03 March 2008.

Appendix B

Generation of Large-scale Density Irregularities and Geomagnetic Micropulsations

Investigators

Spencer Kuo and Wei-te Cheng, *Polytechnic University, Brooklyn, New York*

Min-Chang Lee, *MIT, Cambridge, MA*

Keith Groves, *Air Force Research Laboratory, Hanscom AFB, MA*

Brent Watkins, *Geophysical Institute, University of Alaska Fairbanks, Fairbanks, AK*

Objective

A large-amplitude HF heater propagating to near the reflection height can excite filamentation instability [Kuo and Schmidt, 1983; Kuo and Lee, 1983]. The HF heater and the excited high frequency sidebands interacting through the nonlinearity of the plasma produce a differential Ohmic heating force \mathbf{F} acting only on electrons. This force gives rise an $\mathbf{F} \times \mathbf{B}_0$ drift motion in the electron fluid and induces an electron drift current flowing in the direction perpendicular to both the background magnetic field \mathbf{B}_0 and the alignment direction (i.e., wave vector \mathbf{k}) of the generated density irregularity. This experiment is to verify that magnetic field fluctuation $\delta\mathbf{B}$, parallel to the background magnetic field \mathbf{B}_0 , will be induced by the HF heater via the filamentation instability, which also generates large-scale density irregularities.

Observation Technique

The experiment was carried out from 25 February 22:00 UTC to 26 February 01:00 UTC. From 22:00 to 23:00 UTC, full power X-mode heater wave at the frequency of 4.5 MHz was applied, and the heater frequency was switched to 2.7 MHz from 23:00 to 01:00 UTC. The induced magnetic field variation was monitored by the Fluxgate Magnetometer. The density irregularities were monitored by the Ionosonde.

Preliminary Results

The magnetic field variations in three directions (H, D, and Z) recorded by the fluxgate magnetometer from UTC 20:00 to 04:00 are shown in the plots of Figure B1. As shown, B_H and B_D were not affected by the HF heater; however, B_Z had a step jump, by about 1.65 nT, during the heater on period. This is consistent with the theory that the magnetic field perturbation induced by the filamentation instability is in the vertical direction (i.e., parallel to the background magnetic field).

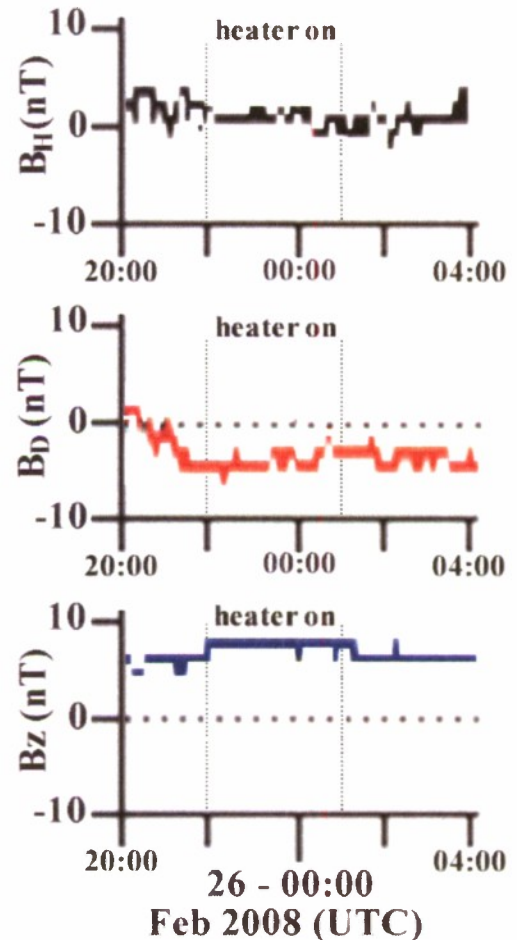


Figure B1. Magnetic field variations recorded by the fluxgate magnetometer.

The generation of large-scale density irregularities by the filamentation instability near the HF reflection height can be evidenced by the variation of the reflection height of the sounding waves in the frequency region around the HF heater frequency. Significant anomalous absorption (i.e., reduction the backscattering) of the sounding waves by the generated density irregularities can cause the return trace of the sounding waves in the ionogram to disappear. Digisonde data was then analyzed to extract the evidence. From UTC 22:00 to 23:00, heater wave frequency was 4.5 MHz. As shown in Figure B2, the return of the sounding waves recorded in the ionogram from 4.4 to 4.6 MHz was reduced considerably. After UTC 23:00, the heater frequency was switched to 2.7 MHz, the return of the sounding waves reappeared in the ionogram. Similarly, as shown in Figure B3, the return trace from 2.5 to 3 MHz in the ionogram disappeared during the period from 23:00 to 01:00 UTC when the heater was run at 2.7 MHz. Again, one could see that the return trace reappeared after the heater was turned off. These results provide indirect, but convincing evidence on the generation of large-scale density irregularities, which together with the simultaneous generation of magnetic field presented in Figure B3 also evidence the excitation of filamentation instability.

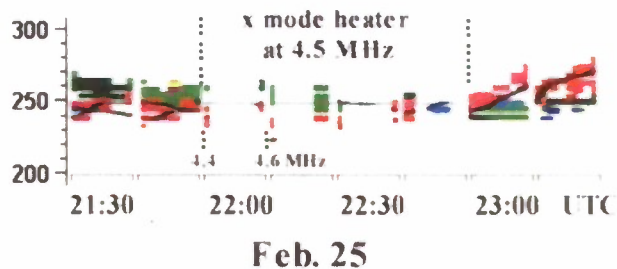


Figure B2. Composite ionogram showing the variation of the reflection height of the sounding waves from 4.4 to 4.6 MHz in every 15 minutes. The sounding waves appeared to be anomalously absorbed when the x mode HF heater at 4.5 MHz was turned on.

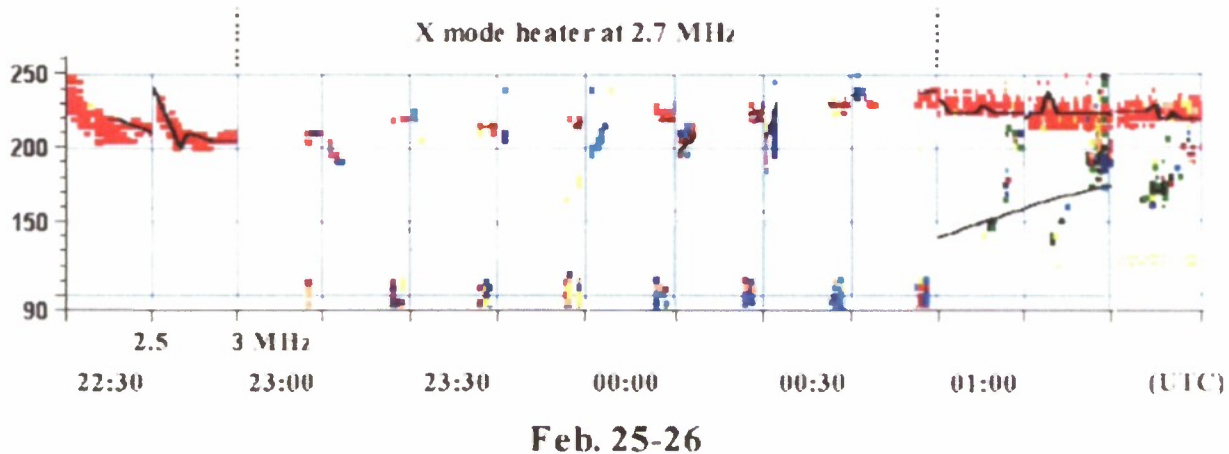


Figure B3. Composite ionogram showing the variation of the reflection height of the sounding waves from 2.5 to 3 MHz in every 15 minutes. The sounding waves appeared to be anomalously absorbed when the x mode HF heater at 2.7 MHz was turned on.

References

- S. P. Kuo and G. Schmidt, "Filamentation Instability in Magneto Plasmas", *Phys. Fluids*, 26, 2529-2536, 1983.
- S. P. Kuo and M. C. Lee, "Earth Magnetic Field Fluctuations Produced by Filamentation Instabilities of Electromagnetic Heater Waves", *Geophys. Res. Lett.*, 10(10), 979-981, 1983.

Appendix C

Observing artificial *E* region field-aligned irregularities over HAARP

Investigators

David Hysell and Eliana Nossa, *Department of Earth and Atmospheric Sciences, Cornell University, Ithaca, NY.*

Objective

The goal of our experiments was to generate *E* region artificial field aligned irregularities over HAARP, observe and diagnose them with the new imaging coherent scatter radar in Homer, and investigate the thermal oscillating two stream and resonance instabilities thought to be responsible. The 30 MHz radar permits us to study the morphology and dynamics of the irregularities in three spatial dimensions unambiguously, measure their aspect sensitivity interferometrically, measure their rise and fall times precisely, and estimate their cross-section at 30 MHz.

Preliminary experiments were run successfully in the fall of 2007. The present objective was to refine the experiments and address more quantitative aspects of artificial FAI generation. Whereas the 2007 experiments involved ordinary daytime *E* layers, experiments performed during the 2008 winter campaign were more likely to involve nighttime sporadic *E* layers. This presents the possibility of imaging irregular structures in the layers and studying their behavior.

Observation Technique

A number of experimental modes were defined for the campaign. Of those, two were actually run during the evening ELF time slots when sporadic *E* layers were present and absorption was minimal. The modes are defined below.

1. Alternate heating between frequencies 50 kHz above and below 3 MHz. Use full power, O-mode, 1-min on, 1-min off, heating at zenith. The objective was to assess the impact of heating above and below the second electron gyro-harmonic.
2. Alternate between magnetic zenith and zenith, 1-min on, 1-min off, O-mode, full power, 2.75 MHz heating frequency. The objective was to assess the impacts of magnetic zenith heating and possible Z-mode leakage.

The 30 MHz radar was also run in support of a number of other heating experiments in the winter campaign. However, echoes were not detected during heating experiments which were not designed explicitly for artificial *E* region FAI generation.

Preliminary Results

Sporadic *E* layers occurred on the nights of 29 February – 3 March. The densest and longest-lived echoes occurred on the first of these nights and produced the radar echoes shown in Figure C1. Heating mode 1 was employed before 0820 UT. The figure shows that weak backscatter was observed during 1-min. heating intervals. Significantly, backscatter intensity was about 5 dB

stronger at 3.045 MHz than at 2.945 MHz. These results are consistent with theories governing the double resonance and with observations obtained in the F region using HF radars.

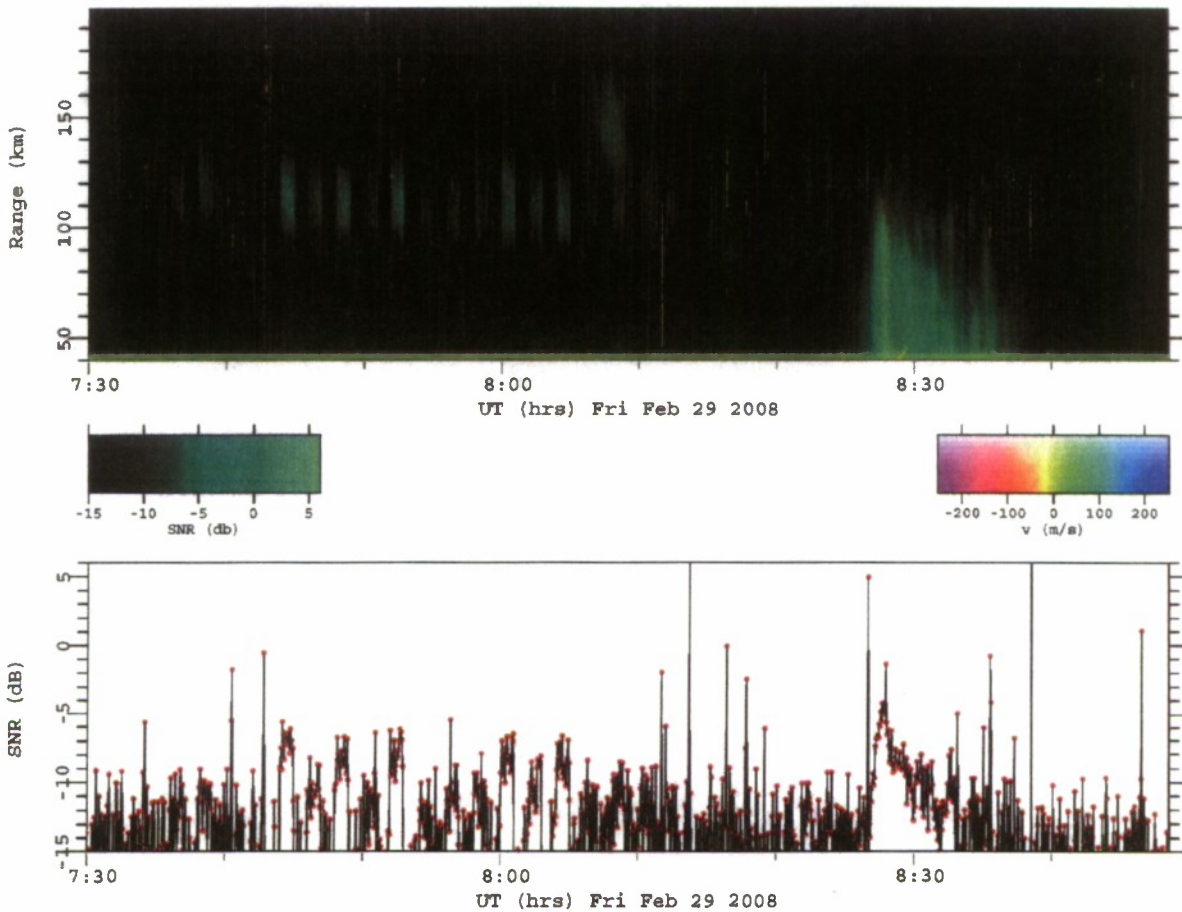


Figure C1. 30 MHz radar range time intensity versus universal time and apparent range for Feb. 29, 2008. True range from Homer is apparent range + 370 km. (upper panel) Backscatter signal-to-noise ratio, Doppler shift, and spectral width represented by pixel brightness, hue, and saturation, respectively. Artificial irregularities occupy ranges between 90–130 km, and natural auroral echoes occupy other ranges. (lower panel) Average signal-to-noise ratio in ranges between 90–130 km.

After 0820 UT, heating mode 2 was utilized. Despite the reduction in the pump mode frequency, artificial FAIs were no longer observed. Generating FAIs in sporadic E layers is actually rather difficult due to the narrowness of any possible upper hybrid frequency interaction layer and grows more difficult the greater the difference between the heating frequency and the E layer critical frequency. Note that echoes received during the 2007 experiments had signal-to-noise ratios nearly 20 dB stronger than what is depicted in Figure C1.

Finally, whereas the echoes observed in 2007 in daytime E layers had uniformly small Doppler shifts and spectral widths, the echoes shown in Figure C1 have large Doppler shifts of about 150 m/s with spectral widths between 150–200 m/s. The large Doppler shifts likely reflect the presence of strong auroral convection, prerequisite for naturally-occurring auroral echoes. The large spectral widths are predicted by the theory of ionospheric interactions at the double resonance. Note that wide spectra prohibit further signal-to-noise ratio improvement through additional coherent integration.

Appendix D

Beacon and In Situ Observations of IRI-Generated Plasma-Density Structures

Investigators

J. A. Secan, *NorthWest Research Associates, Inc.*

J. F. Smith and C. M. Smith, *Northwest Research Engineering, Inc.*

G. R. Wilson, *Air Force Research Laboratory/RVBX, Hanscom AFB, MA*

K. R. Martin, *Boston College, Boston, MA*

Objective.

The overall objective of the experiments was to observe plasma-density structures generated by the HAARP IRI using both transionospheric probing via coherent transmitters on both LEO and GPS satellites and *in situ* observations of the ionosphere from the Defense Meteorological Satellite Program (DMSP) Special Sensor for Ions, Electrons, and Scintillation (SSIES) instrument. NWRA has made prior observations of scintillation-scale structures generated by the IRI during both daytime and nighttime operations in prior campaigns, and one goal of this campaign was to compare the structure generated using the fully completed IRI system with results obtained with the smaller array. To our knowledge, observations of heater-generated structure from DMSP altitudes (nominally 840 km) have not been made prior to this campaign.

Observation Technique.

Ionospheric structures were generated using the IRI in two modes: a focused beam pointed at the magnetic zenith (standard mode), and a beam broadened in the north-south array alignment (NS mode). In both modes, the IRI transmitted a CW O-mode signal at a frequency selected to be just below the observed F_2 -region critical frequency (f_oF_2). Instrumentation used included the NWRA ITS10S receivers located at Gakona, Cordova, and Delta Junction; the new NWRA mobile receiver (ITS30m); the NWRA GPS receiver located at Gakona; and the DMSP SSIES Scintillation Meter (SM) and the Drift Meter (DM) instruments on the DMSP F15 satellite. The mobile receiver was repositioned for each satellite pass to obtain a geometry in which the 220-km (nominal h_mF_2) ionospheric penetration point (IPP) track of the satellite beacon passed as nearly as possible through the center of the region the IRI was operating on.

Table D1. NWRA HAARP campaign experiment times

Case	Satellites	Program	Freq MHz	UT			AST		
				Date	Start	End	Date	Start	End
Milikh	G21	STD	3.4	21-Feb	19:25:00	19:45:00	Thu, 21-Feb	10:25:00	10:45:00
1	FM6/G23	STD	2.84	22-Feb	03:47:00	04:13:00	Thu, 21-Feb	18:47:00	19:13:00
2	FM6	STD	4.5	22-Feb	20:22:00	20:46:30	Fri, 22-Feb	11:22:00	11:46:30
3	O32	STD	5.2	23-Feb	22:40:00	23:04:30	Sat, 23-Feb	13:40:00	14:04:30
4	O25	NS	4.2	24-Feb	01:31:00	01:55:30	Sat, 23-Feb	16:31:00	16:55:30
5	F15	NS	3.4	24-Feb	17:50:00	18:15:00	Sun, 24-Feb	08:50:00	09:15:00
Groves	O23	NS	5.2	24-Feb	22:17:00	22:47:00	Sun, 24-Feb	13:17:00	13:47:00
6	FM5	NS	4.8	25-Feb	00:02:00	00:25:00	Sun, 24-Feb	15:02:00	15:25:00
7	F15	STD	2.7	25-Feb	03:44:00	04:10:00	Sun, 24-Feb	18:44:00	19:10:00
7	G23	30sOnOff	2.7	25-Feb	04:10:30	04:18:00	Sun, 24-Feb	19:10:30	19:18:00

Table D1 provides a summary of the experiment times NWRA was provided. In this table, the Case column specifies the case number we assigned the experiment (the Milikh case is time assigned originally to Gennady Milikh, the Groves case is the experiment we ran collaboratively with Dr. Keith Groves of AFRL), the Satellites column indicates which satellites were involved (“G” for GPS with the GPS PRN, “FM” for FORMOSAT, “O” for NIMS, and “F” for DMSP), the Program column indicates the configuration of the IRI beam, the Freq column is the IRI frequency, and the UT and AST columns provide the date and start/end times of the IRI use. The three programs shown were STD for standard mode, NS for NS mode, and 30sOnOff is the standard mode with a 30-seconds on, 30-seconds off operation.

Figure D1 shows the mobile ITS30m system as it was deployed on a rental SUV. The antenna is placed on the top of the vehicle, which serves as a limited ground plane. The receiver and laptop computer controlling the receiver are located inside the vehicle. This system was deployed and operated by F. J. Smith and C. M. Smith. AFRL also fielded a mobile system (the door of their vehicle can be seen behind the NWRA vehicle), which they deployed with the NWRA system in order to compare results.



Figure D1. The NWRA ITS30m receiver system deployed near Gakona.

Preliminary Results.

Preliminary review of the GPS data from the three passes indicated in Table D1 has found little evidence of IRI-generated structure. This is not wholly unexpected given that these passes were during the early-morning and late-afternoon times when there was little ionospheric plasma available to structure, and that the GPS signals are at L-band, which requires fairly strong ionospheric irregularities to generate observable scintillation.

Preliminary review of the LEO data has shown that while there are a few good cases that deserve further study, problems with the beacon signals for many of the newer satellites (FORMOSAT-3 and DMSP) have severely reduced the amount of useful data from those satellites. Data collected from the older Navy Ionospheric Measurement System (NIMS) satellites (OSCAR satellites) will be the focus of future in-depth analysis.

We have, however, found what appears to be a clear example of a plasma structure in the DMSP SSIES data that was likely generated by the IRI heater. Figure D2 shows data from the DMSP F15 satellite SSIES SM (left panels) and DM (right panels) instruments, taken from a period when the field line at the DMSP altitude mapped down to the region being heated by the IRI (at 220 km altitude). Both the density and vertical-drift features shown within the region that maps to the IRI region (within the 3dB points of the beam) were isolated from naturally occurring ionospheric structures. Our working hypothesis is that this is the signature of plasma that has been moved out of the heated region along the field lines. The small-scale structuring evident in the top-left panel could either be structure mapped from the lower heated region, or it could be structuring that has occurred in the plasma at the satellite altitude due to drift-driven instabilities. This is still to be determined.

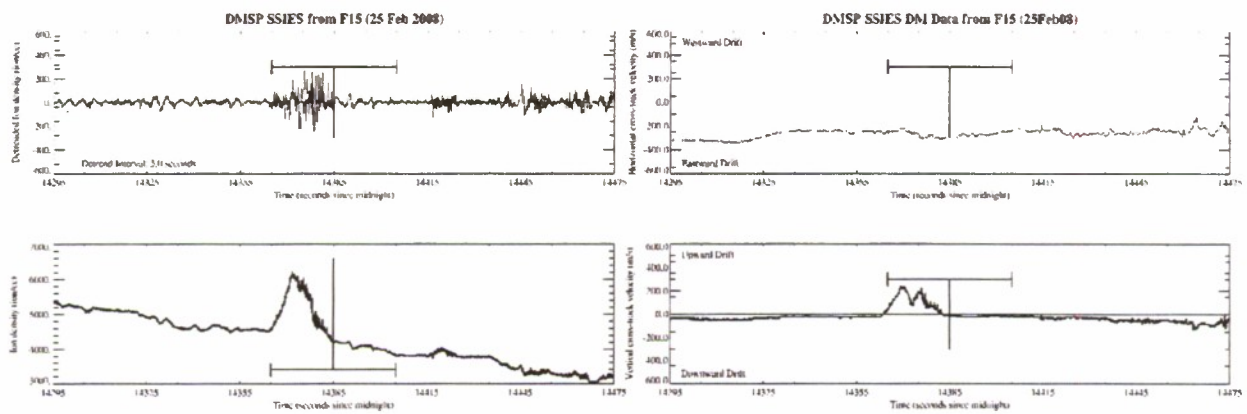


Figure D2. (Left panels) Total ion density data from the DMSP SM sensor (bottom) and detrended density (top). (Right panels) Horizontal (top) and vertical (bottom) ion drift velocity from the DMSP DM sensor. Horizontal bars indicate times the field lines at DMSP altitude were within the IRI heated region (within the beam pattern 3dB points).

Appendix E

Characterization of decameter-scale ionospheric irregularities through imaging of HAARP-induced airglow

Investigators

Elizabeth Kendall, Craig Heinselman and Kostas Kalogerakis *SRI International*

Objective.

HF heater-induced artificial airglow observations can be used to diagnose electron energies and distributions in the heated region, illuminate natural and/or artificially induced ionospheric irregularities, determine $\mathbf{E} \times \mathbf{B}$ plasma drifts [Bernhardt et al., *J. Geophys. Res.*, 94, 7003, 1989], and measure quenching rates by neutral species. Unlike the typically smooth electron density variations at equatorial and middle latitudes, the lower ionosphere at high latitudes is in general extremely turbulent, with many natural electron density perturbations or irregularities present [e.g., Kelley, 1989, p. 345].

Observation Technique.

Our primary goal was to conduct observations of decameter scale airglow structure using the new HAARP telescopic imager, shown in Figure E1.

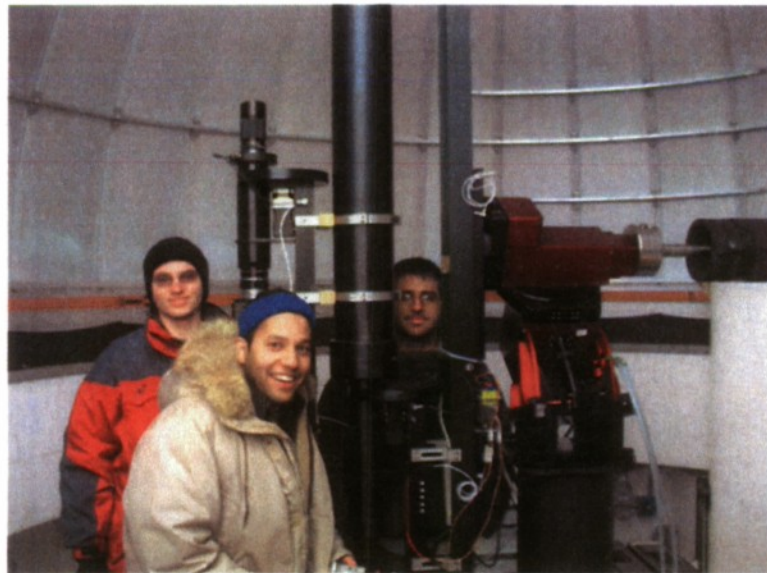


Figure E1. The telescopic imaging system and WPI student interns during the HAARP Winter 2008 campaign.

In May 2005, a new optical shelter with a 14 ft telescope dome was installed at HAARP. This new facility provides a platform for instruments to be mounted outdoors with an unimpeded view of the sky. The new telescopic system has a resolution of ~20 m in the F layer and ~10 m in the E layer, which allows decameter- and kilometer-scale features to be observed. Any HAARP transmission which produces airglow emissions is useful for accomplishing these observations.

Preliminary Results.

Bright structured airglow was observed on several nights during the winter HAARP campaign. Detailed analysis of the images collected has not yet been performed, however an example image is shown in Figure E2. This data will be used to support other experimenters as well as set new limits on the smallest airglow features observed at HAARP.

Participants: Elizabeth Kendall (SRI), Jorge Alejandro (WPI), Muzhtaba Islam (WPI), and Thomas Niemczycki (WPI)

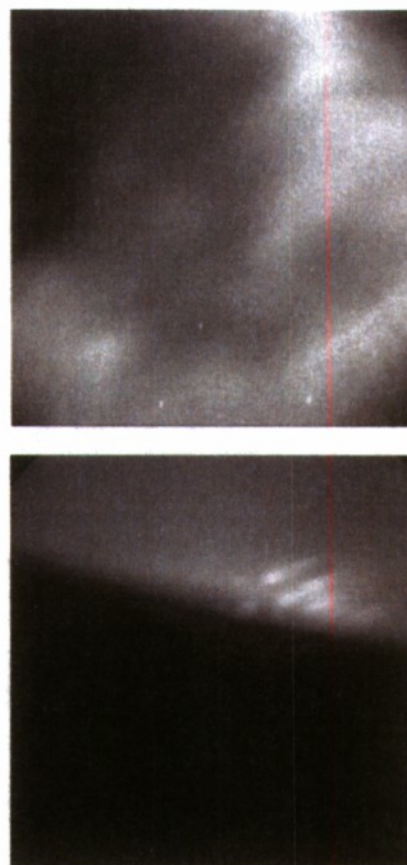


Figure E2. Data from the 2008 campaign. The top panel shows an image from the telescope with fine structured airglow at 557.7 nm (15 seconds exposure). The bottom panel shows an image from the wide field of view imager (also 15 seconds, 557.7 nm). Note that the dome was blocking part of the wide imager's field of view.

References

Bernhardt, P. A., L. M. Duncan, C. A. Tepley, Heater-induced cavities as optical tracers of plasma drifts, *J. Geophys. Res.*, 94, 7003, 1989.

Kelley, M.C., The Earth's Ionosphere, ISBN 0-12-404013-6, Academic Press, San Diego, CA, 1989.

Appendix F

HAARP twisted-beam experiments

Investigators

T. B. Leyser, *Swedish Institute of Space Physics, Uppsala, Sweden.*

L. Norin, *Department of Physics and Astronomy, Uppsala University, Uppsala, Sweden.*

T. Pedersen, *Air Force Research Laboratory, Hanscom Air Force Base, Massachusetts*

B. Gustavsson, *University of Tromsø, Tromsø, Norway*

M. McCarrick, *BAE SYSTEMS, Advanced Technologies Electronics & Integrated Solutions, Washington, DC*

Objective

HAARP was used to perform what we believe were the first experiments on plasma turbulence pumped by a radio beam with electromagnetic orbital angular momentum (OAM). HAARP with its phased antenna array appears presently to be the only HF research facility in the world which can transmit the required twisted beam to exert OAM on the ionosphere. Figure F1 shows a numerically computed power pattern in a cross section of the HAARP beam. The characteristic ring-shape of the beam with the intensity minimum in the centre is clearly seen.

Observation Technique

An analogue-to-digital converter (ADC) capable of up to 20 Msamples/s was brought from Sweden to receive stimulated electromagnetic emissions (SEE) on the ground. The ADC was connected to a wideband HF antenna provided by HAARP. Figure F2 shows the ADC and laptop computer used to control the system at the receiving site at the Riverview Bed-and-Breakfast near HAARP. In addition to detecting the SEE, optical emissions from the pumped plasma turbulence were observed during hours of darkness.

Preliminary Results

The HAARP transmitters were typically cycled 30 seconds ON / 30 seconds OFF during the daytime experiments. In the night time experiments longer cycles were used. The OAM

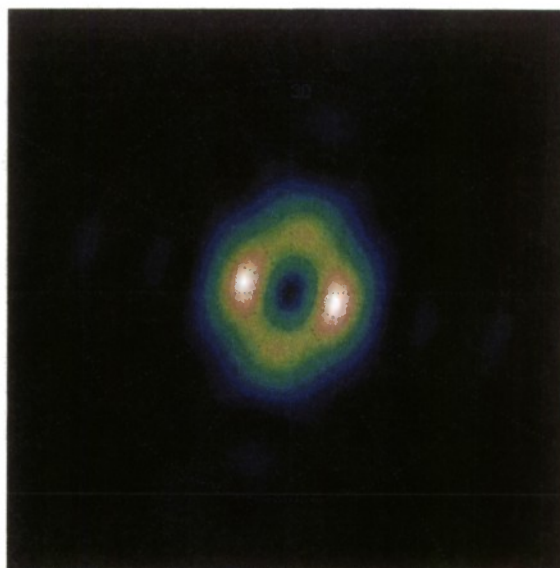


Figure F1. Power pattern of vertical HAARP beam as the field phases turn through 2π while turning once around the array, for a frequency of 4.8 MHz.



Figure F2. The Hewlett-Packard E1437A 20 Msamples/s, analogue-to-digital converter, and laptop computer used sample the electromagnetic emissions.

of the HAARP beam was alternated between zero (usual plane wave) and nonzero (twisted beam) in successive pump pulses, all for ordinary mode polarization.

It soon became clear that there was a significant dependence of the SEE on the OAM of the beam. Figure F3 displays two superposed frequency spectra of the SEE, for a pump frequency of 4.5 MHz and maximum pump power. The ionospherically reflected pump wave is seen as the strongest peak in the centre of the spectra. The blue spectrum is for a usual plane wave ($l=0$) and the red spectrum is for a twisted beam ($l=-3$), where l is the integer number of 2π that the pump field changes in a plane across the vertical beam axis at a given height and time. It is seen that the blue spectrum exhibits a very strong peak downshifted from the pump frequency by a few kilohertz which reaches approximately 20 dB above the SEE at the same frequency for OAM-pumping. In the upper sideband the SEE is slightly stronger in the red spectrum than in the blue spectrum.

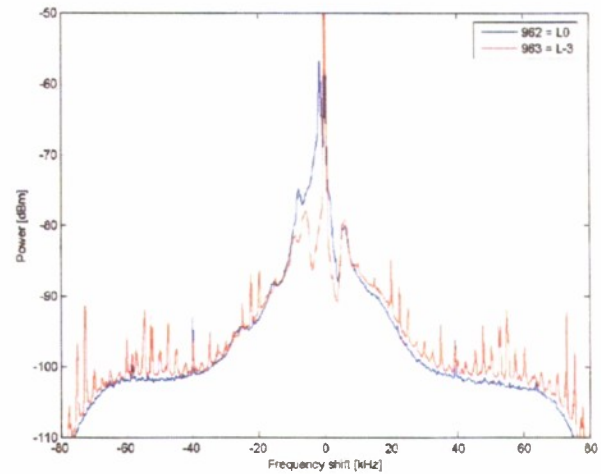


Figure F3. Two overlaid SEE spectra. The blue spectrum is for a usual pump beam with zero OAM and the red spectrum is for a beam with nonzero OAM. The frequency span shown is 160 kHz wide.

The prominent downshifted peak in the blue spectrum is identified as the so called narrow continuum maximum (NCM) which is attributed to Langmuir turbulence. The NCM feature has never been observed to be this well developed in our previous experiments at the EISCAT (Norway) and Sura (Russia) facilities. We attribute this to the very high effective radiated power transmitted by HAARP.

At the present very preliminary stage of the data analysis we speculate that the much stronger SEE at frequencies just below that of the pump might be due to the much stronger pump power in the centre of the beam for $l=0$ than for $l\neq 0$. The transmitted power in the centre of the beam for $l\neq 0$ is zero because of the phase ambiguity in the pump field (see Figure F1). However, if this is the case, then why is the SEE relatively well developed for OAM pumping at frequencies further downshifted and upshifted from the pump?

Appendix G

Using the HAARP heating facility to investigate the self-scattering of high power radio waves.

Investigators

G.S. Sales, B.W. Reinisch, V.V. Paznukhov. *University of Massachusetts Lowell Center for Atmospheric Research*

Yu.M. Yampolski, V.G. Galushko. *Institute for Radio Astronomy, Kharkov, Ukraine*

Objective

To investigate the scattering of high power HF radio waves from the HAARP heater by ionospheric irregularities which are produced by the same HF emission (the “self-scattering effect”)

This research is a joint effort between the University of Massachusetts Lowell, Center for Atmospheric Research (UMLCAR) and the Institute of Radio Astronomy, Ukraine. Previously the Ukrainian group has reported the long-distance detection of transmissions from both the EISCAT (Norway) and SURA (Russia) HF heating facilities including observed motions of the irregularities generated by the heaters using the measured Doppler shifts of the received signals. Our experimental proposal for the 2008 Winter HAARP Campaign was to conduct similar experiments using HAARP transmissions and to improve the detection and analysis of these effects by using an array of geographically dispersed receivers.

Observation Technique

The HAARP HF radio waves self-scattered from the irregularities generated by the heater transmissions were monitored at seven sites remote from the HAARP facility. The location of these receivers is shown in Figure G1.

At five of the sites shown (College, King Salmon, Pt. Arguello, Quaanaaq, and Millstone Hill) digisonde sounding systems (<http://umlcar.uml.edu/digisonde.html>) were used as receivers. UMLCAR has developed a special “listen-only” mode using the existing digisondes to receive the scattered signals. The Ukrainian group operated receivers at Svalbard and Kharkov. Another part of this experiment was to study scattering at several frequencies to investigate the dimensions of the heater induced irregularities. The HAARP operating modes used in these

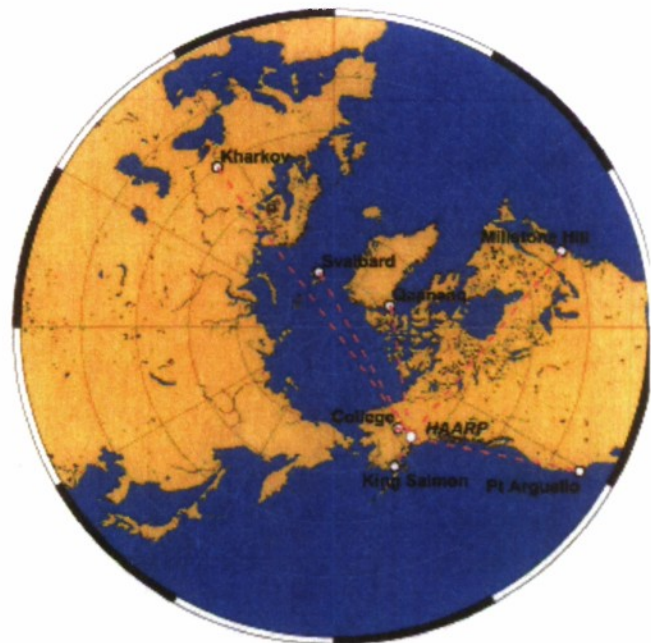


Figure G1. Locations of the receiver sites operated during the Winter 2008 HAARP Campaign. Approximate propagation paths are shown as well. The map is made using OMC tool.

experiments are summarized in Table G1. At all remote locations, except Svalbard, the systems were tuned to receive two HAARP operating frequencies simultaneously.

Table G1 HAARP operation mode summary

Heating intervals	Operating frequencies (and transmit power)	Polarization	Operation sequence	Beam orientation
26.02.08 0100-0200 UT	4,100,063 Hz (3.5 MW/120 kW) 8,095,063 Hz (120 kW)	O-mode O-mode	7.5 min Hi* / Low* CW	Zenith N/A
26.02.08 0315-0445 UT	2,755,063 Hz (3.5 MW/120 kW) 5,475,063 Hz (120 kW)	O-mode O-mode	7.5 min Hi* / Low* CW	Zenith N/A
27.02.08 0300-0349 UT	2,675,058 Hz (3.5 MW) 2,835,058 Hz (120 kW)	O-mode O-mode	7.5 min Hi / OFF CW	Zenith N/A

* 'Hi' denotes high power (3.5 MW) transmission, while 'Low' denotes transmission at 120 kW.

Preliminary Results

Preliminary results are very encouraging. HAARP transmissions were reliably detected at all the observation sites during the three time intervals for the experiments given in Table G1. The most interesting result revealed so far is the observed variations of the received signal strength during the experiment conducted on 26 February 2008 at 0330-0430 UT at the operating frequency of 2,755,063 Hz. These measurements, shown in Figure G2, display the data collected at the

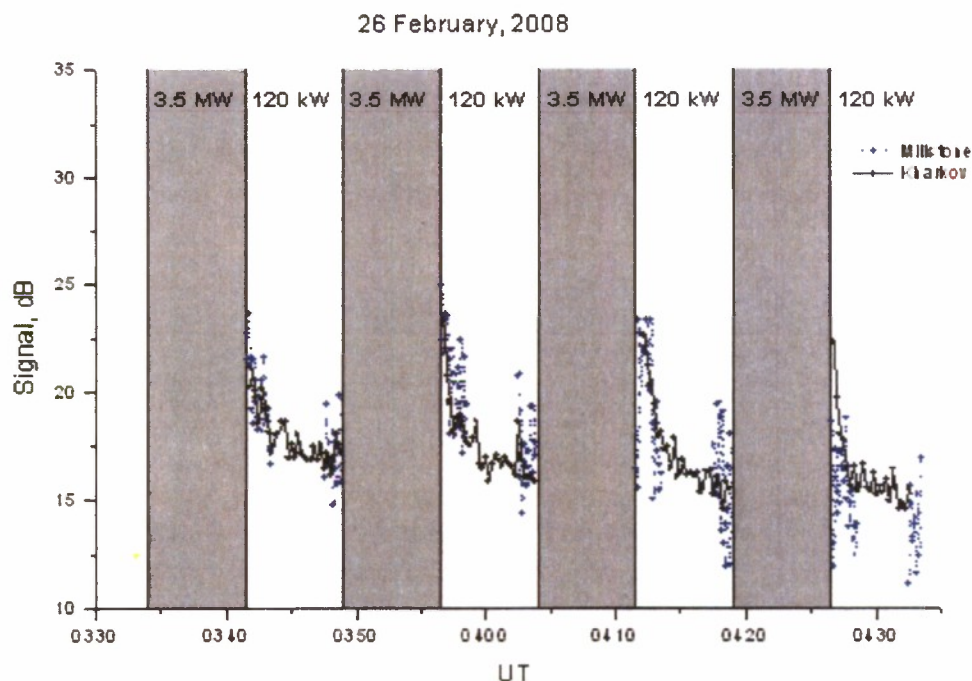


Figure G2. Variations in the signal strength during the OFF (low power) period observed at Millstone Hill (blue) and Kharkov (black) at the operating frequency of 2,755,063 Hz. Signal amplitudes recorded during the full-power heating are considerably larger and are not shown to simplify the graph.

Millstone Hill and Kharkov observatories. After the HAARP transmission is switched from “high power” (3.5 MW) to “low power” (120 kW) the recorded signal intensity at the two remote sites gradually decreases. This is likely caused by the fact that the observed signals were self-scattered from the ionospheric irregularities that slowly decay with a certain time constant of a few minutes, after the HF heating is turned off.

Future Effort

- The complete dataset from the other stations are currently being processed to assess the geographical character of the received signal strength variations. These data in conjunction with a scattering model will make it possible to describe the spatial characteristics of the heater induced irregularities. The angular distribution of the received scattered signals will be used to determine the dynamics of the stimulated ionospheric irregularities over the HAARP and to better understand the scattering mechanism. The complete datasets will also make it possible to investigate different possible mechanisms for generation of the artificially produced plasma irregularities.

Appendix H

HF power dependence on the cascade spectrum of HF-enhanced plasma lines

Investigators

B.J.Watkins, *Geophysical Institute, University of Alaska, Fairbanks, AK*
S.Oyama, *Solar -Terrestrial Environment Lab, Nagoya Univ, Japan*

Objective

This experiment was designed to evaluate the variability (if any) of the cascade spectrum of HF-enhanced plasma lines when the HF power is varied. Since the HAARP system is now complete and operating at full power a new opportunity exists to test this idea over a wide range of HF power levels. Initial previous experiments at EISCAT have suggested no power dependence, although later experiments at higher power indicate a possible power dependence. However past experiments elsewhere conducted at different times are inconclusive because of differing ionospheric temperatures and conditions. Theoretical considerations by Kuo and Lee (2005) point to an HF-power effect on the number and amplitude of the cascade spectrum of Langmuir waves generated by the parametric decay instability and oscillating two stream instability and our experiments seek to evaluate the compatibility of experiment and theory.

Observation Technique

The MUIR UHF diagnostic radar was operated with a 1 ms uncoded pulse and an inter-pulse period of 10 ms. Power spectra of MUIR signal returns were obtained every 10 ms; the altitude of the samples covered the interaction region of the HF pulse with the ionosphere which in this case was about 220 km altitude. The HF transmitter was cycled on for 2 seconds and off for 58 seconds. Data were acquired at differing HF power levels, cycling through full-power, $\frac{3}{4}$, $\frac{1}{2}$, $\frac{1}{4}$ -power to determine possible HF power dependencies.

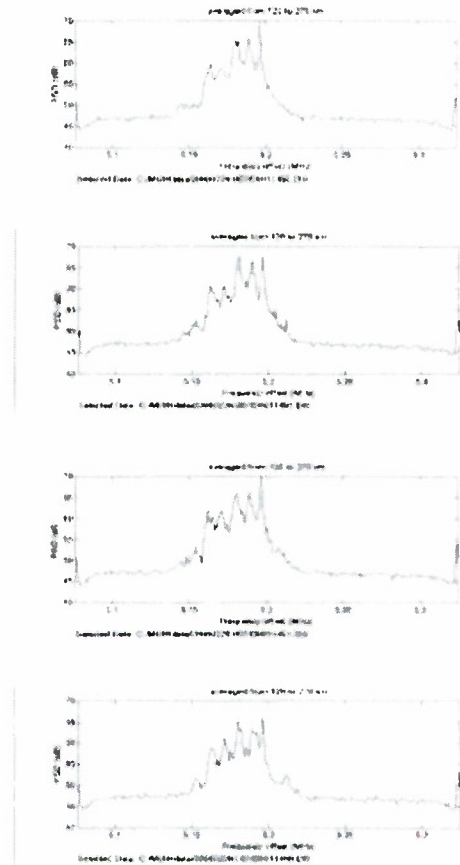


Figure H1. Cascade spectra of HF-enhanced plasma lines for full-power (bottom plot), $\frac{3}{4}$ power, $\frac{1}{2}$ power, and $\frac{1}{4}$ power (top plot) of the HAARP HF transmitter array operated at 5.2 MHz.

Preliminary Results

Some sample data are shown in Figure H1 for the four HF power levels. The spectra all show the usual 'decay' line near 5.2 MHz, and for all power levels there are four strong cascade lines corresponding to the electrostatic waves generated by the instabilities mentioned above. There is a fifth weaker cascade line that is also evident at all power levels. These data seem to contradict the theoretically-derived suggestion that the number of cascade lines depends on HF power.

Appendix I

Aspect sensitivity of HF-induced plasma line measured with MUIR

Investigators

Shin-ichiro Oyama, *Solar-Terrestrial Environment Laboratory, Nagoya University, Japan.*
Brenton J. Watkins, *Geophysical Institute, University of Alaska, Fairbanks, AK*

Objective

The objective of this study is to understand the aspect sensitivity of HF-induced plasma lines (HFPL). During the 2005 optical campaign at HAARP, persistent enhancements of the HF induced plasma line were measured with MUIR [Oyama *et al.*, 2006]. Furthermore, during the 2005 PARS summer school, MUIR detected plasma lines that could be generated in association with up-propagating Langmuir waves generated via oscillating two-stream instabilities produced by upper hybrid waves. While these two results were brought through analyses using data obtained for geomagnetic field-aligned experiments with MUIR, there may be aspect sensitivities to the field line as suggested by a recent publication using data from the Tromsø UHF radar of the EISCAT facility [Dhillon and Robinson, 2005].

Observation Technique

The HF heating facility was operated with 960 kW power (6x8 array) O-mode field-aligned beam at 4.5 MHz from 00:33:00 to 01:59:30 UT on 25 February 2008. The heater duty cycle was 5 seconds on and 25 seconds off. Nine directions around the magnetic field line were measured with the MUIR phased array system (see Figure I1). The direction was changed every IPP.

Preliminary Results

Figure I2 shows the power spectrum density (PSD) of upshifted HFPL averaged for the first 100 ms after HF turn-on at four of the nine MUIR-beam positions approximately along the magnetic meridian. The spectrum signatures are strongly dependent on the MUIR beam direction as we expected. The magnitude becomes

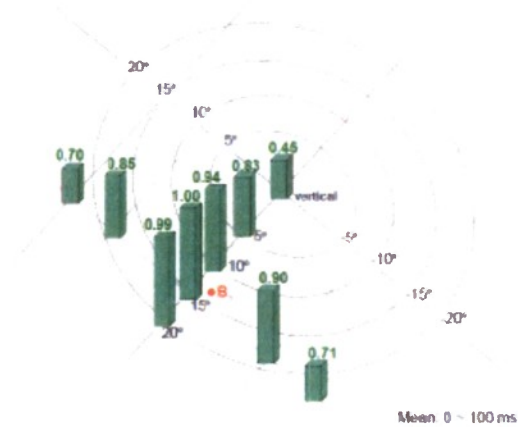


Figure I1. Horizontal pattern of relative magnitude of the unshifted HFPL averaged for the first 100 ms after HF turn-on.

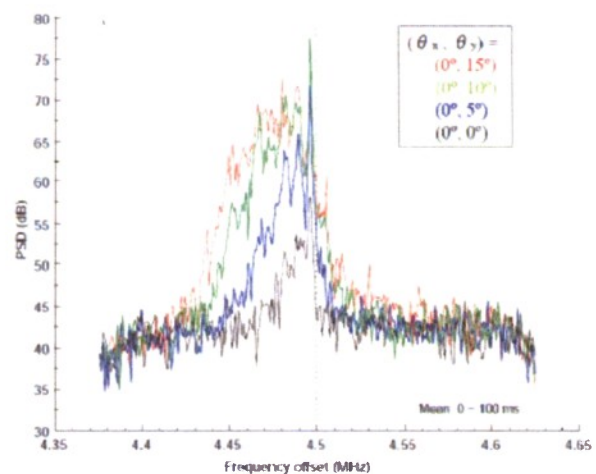


Figure I2. Mean PSD (dB) of the upshifted HFPL measured with the MUIR phased-array system. The magnetic zenith is close to (0°, 15°) beam position (red).

weaker with going far from the magnetic zenith (close to red one). Figure I1 shows the horizontal pattern of the relative magnitude of the mean PSD. The peak magnitude appeared at the magnetic zenith then weakening with going away from magnetic zenith.

Acknowledgment

The HAARP program is a Department of Defense project managed jointly by the U.S. Air Force and the U.S. Navy. This research was supported by grant N00014-03-1-0165 and other grants from the Office of Naval Research (ONR). The authors wish to thank HAARP personnel for their assistance in operating the experiments. The support of Lewis Duncan and William Gordon for assistance in initiating this research is greatly appreciated. The UHF diagnostic radar is a cooperative effort with the National Science Foundation and the HAARP program. The assistance of SRII personnel with the development of the radar under difficult environmental conditions has been most helpful.

Appendix J

HAARP 2008 Winter Campaign Effects of additional X-mode pumping on radio induced optical emissions

Investigators

B. Gustavsson, *University of Tromsø, Tromsø, Norway*

M. Kosch, *Lancaster University, Lancaster, UK*

T. B. Leyser and L. Norin, *Swedish Institute of Space Physics, Uppsala, Sweden*

M. McCarrick, *BAE SYSTEMS, Advanced Technologies Electronics & Integrated Solutions, Washington, DC*

T. Pedersen, *Air Force Research Laboratory, Hanscom Air Force Base, Massachusetts*

B. Bristow, J. Spaleta, B. Watkins, *Geophysical Institute, University of Alaska Fairbanks, Fairbanks, AK*

Objective

The objective with this experiment is to investigate the relation between small scale density depletions induced by the HF-pumping and the processes that accelerate electrons which cause enhanced optical emissions. It has been shown that high latitude radio induced optical emissions are suppressed when the pump-frequency matches the double resonance condition [Kosch et al. 2005, Gustavsson et al. 2006], when the pump frequency, f_0 , equals the upper hybrid (UH) frequency, f_{UH} , and a multiple of the electron gyrofrequency, f_e , at the same altitude. Then upper hybrid turbulence is suppressed, which leads to reductions in enhancement of electron temperature and optical emissions, as well as reduced back-scatter from artificial field aligned irregularities and absence of certain features in Stimulated Electromagnetic Emission (SEE) spectra [e.g. Carozzi 2002]. By simultaneously transmitting an X-mode beam with a frequency that is about $f_e/2$ higher than the O-mode frequency the growth rate of the UH-related SEE features can be significantly reduced [Frolov 1999]. This provides another means to investigate the processes that create radio induced optical emissions. With combined observations of SEE spectra, enhanced optical emissions and coherent radar back-scatter it will be possible to determine if the existence of density striations are a necessary condition for efficient acceleration of ionospheric electrons.

Observation Technique

Two experiments were attempted during the campaign, the first with 3 minute transmission periods with alternating X + O-mode and O-mode only transmission separated by 2 minutes without transmission, the second with 90 s X+ O-mode followed by 90 s O-mode only with a 2 minute off period. For both experiments the beams were directed towards local magnetic zenith, for the first experiment the array was split into approximately $3/4$ transmitting X-mode and $1/4$ transmitting O-mode making the O-mode beam wider. For the second experiment the array was split 50-50 giving the beams approximately the same shape, with X-mode frequency at 3.4 MHz and the O-mode frequency at 2.7 MHz.

Preliminary Results

During the first experiment, the ionospheric critical frequency was too low, resulting in no observable response. For the second experiment f_0F_2 was high enough for 20 minutes which

provided us with some preliminary results. It appears, as can be seen in Figure J1, that the enhancement at 6300 Å is suppressed by the additional X-mode transmission. However, these observations will need either corroborating support from simultaneous photometer, SEE, Super-DARN, and ISR observations or additional experiments to make a clear enough picture to allow us to draw clear conclusions. Additional experiments should include different pumping schemes, with additional variations of the ones already attempted.

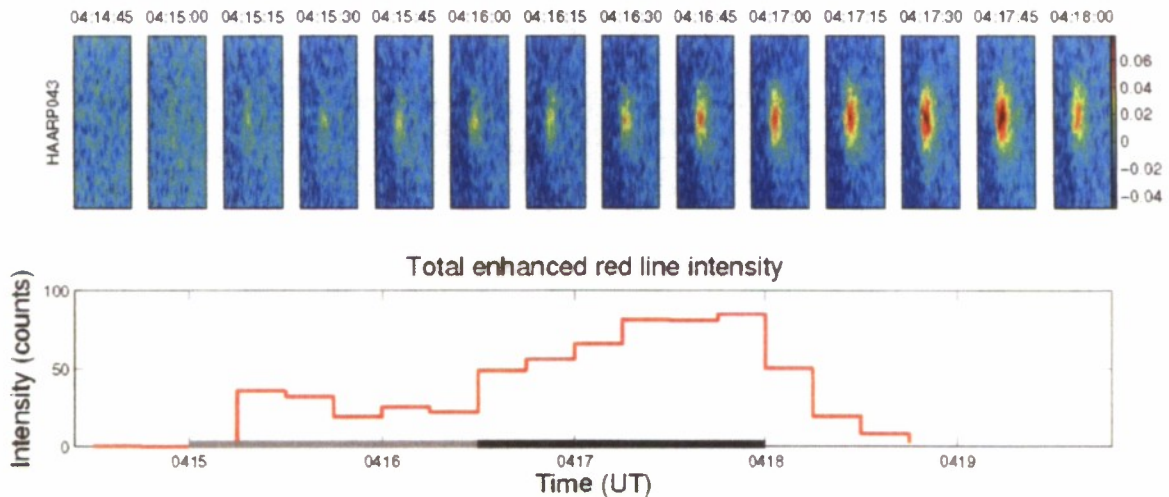


Figure J1. During the HF-transmission pulse from 0415 to 0418 UT on February 26th, it appears as if the enhancement in 6300 Å was limited to a very narrow region and that the intensity was suppressed during the initial 90 s when there were additional X-mode transmission. For the time period from 0416:30 UT the region with enhanced emissions at 6300 grows and the total intensity increases by a factor of 3.

Bibliography

Carozzi T. D., B. Thide, S. M. Grach, T. B. Leyser, M. Holz, G. P. Komrakov, V. L. Frolov, and E. N. Sergeev. Stimulated electromagnetic emissions during pump frequency sweep through fourth electron cyclotron harmonic. *J. Geophys. Res.*, 107(A9):1253, 2002.

Frolov V. L., L. M. Kagan, E. N. Sergeev, G. P. Komrakov, P. A. Bernhardt, J. A. Goldstein, L. S. Wagner, C. A. Selcher, and P. Stubbe. Ionospheric observations of F region artificial plasma turbulence, modified by powerful X-mode radio waves. *J. Geophys. Res.*, 104:12695--12704, June 1999.

Gustavsson B., T. B. Leyser, M. Kosch, M. T. Rietveld, A. Steen, B. U. E. Brandstrom, and T. Aso. Electron gyro-harmonic effects in ionization and electron acceleration during high-frequency pumping in the ionosphere. *Phys. Rev. Lett.*, 97(19):195002, 2006.

Kosch M. J., T. Pedersen, J. Hughes, R. Marshall, E. Gerken, A. Senior, D. Sentman, M. McCarrick, and F. T. Djuth. Artificial optical emissions at HAARP for pump frequencies near the third and second electron gyro-harmonic. *Ann. Geophys.*, 23(5):1585--1592, 27th~ 2005.

Appendix K

In-situ detection of the ionospheric irregularities due to HF heating

Investigators

Evgenii Mishin, *Boston College*

Chia-Lie Chang, *BAE SYSTEMS, Advanced Technologies Electronics & Integrated Solutions, Washington, DC*

Gennady Milikh, *University of Maryland, College Park, MD*

Hermann Luehr, *Geoforschungszentrum Potsdam, Germany*

Objective

Strong HF heating of the F₂ region of the ionosphere generates a broad spectrum of irregularities from kilometer down to meter scale. The CHAMP satellite moving along a low polar orbit with a height of about 330 km creates a unique opportunity to detect long scale irregularities in-situ.

Observation Technique

The CHAMP satellite has a number of on board detectors including a fluxgate magnetometer, and digital ion drift meter. The magnetometer with the maximum resolution 10 pT has the sample rate of 50 Hz which corresponds to the spatial resolution 150 m and will measure ULF emissions. The ion drift meter measures the ion density in the range 10⁰ – 10⁶ cm⁻³, and ion temperature in the range 200 – 55,000K with a sample rate up to 16 Hz which corresponds to the spatial resolution 500 m.

The satellite measurements are complemented by the ground based observations: Ionograms to select the proper heating frequencies. SuperDARN (Kodiak) diagnostics and optical measurements were requested to provide us with the knowledge of irregularities caused by the HF heating.

Preliminary Results

Two observations were conducted, 02/22 and 02/26. Each of these days the HF-heating lasted for 20 minutes around 21 UT. The radio beam of 4.95 MHz, O-mode, maximum ERP, square pulse modulation with 0.7 Hz modulation frequency was used. The beam was directed toward the magnetic zenith. In the both observations we had favorable ionospheric conditions including a smooth F-layer with f_oF₂ between 5 and 6 MHz, and no electrojet. Thus HAARP produced strong irregularities near the peak of the F₂ layer as shown by the Kodiak backscatter plots.

There were 20 minute time slots designated for each of these two observations based on the preliminary orbits. The latter were supplied by us two weeks prior to the campaign. Unfortunately for low flying satellite, such as Champ, all long time orbit predictions are inaccurate, as a result we missed the Champ's over fly by about 15 minutes. For future campaigns we have to plan the experiments with Champ so that we will be able to make the final choice of the operational time a day before the experiment.

Appendix L

Generation of Ionospheric Ducts by HF-heating

Investigators

Dennis Papadopoulos, Gennady Milikh, *University of Maryland, College Park, MD*

Chia-Lie Chang, *BAE SYSTEMS, Advanced Technologies Electronics & Integrated Solutions, Washington, DC*

Objective

Ducts in the Earth's ionosphere along magnetic field lines - defined by their density gradients perpendicular to the magnetic field, enhancing refractive indices and acting as wave guides to whistler-range waves - have implications to the transmission of ELF radio waves across the globe. Strong HF ionospheric heating has been shown to create a depletion of electrons at the heated region, and could lead to a pressure perturbation that propagates along the entire magnetic field line. The objective of this experiment is to detect the artificial ducts by instruments on the board of Demeter satellite over flying HAARP.

Observation Technique

The experiments were conducted by using the maximum HAARP ERP at the chosen frequency. O-mode F-region heating was used, the heating frequency was selected to match the f_oF_2 peak. Square modulation was used with the modulation frequency 1.4 Hz. The HF beam was directed along the magnetic field line. Besides, we allocated one specific experimental slots (see below) where we used a different procedure.

The satellite measurements are complemented by the ground based observations: Ionograms to select the proper heating frequencies. The Kodiak radar observations and optical measurements will provide us with the knowledge of irregularities caused by the HF heating.

Preliminary Results

Four observations were conducted:

1. 23 February 20:29 – 20:48:30 UT
2. 27 February 20:55 – 21:14 UT
3. 28 February 06:27 – 06:46:30 UT
4. 2 March 06:21 – 06:40:30 UT.

On 23 February and 27 February the heating frequency was $f = 4.2$ MHz, while during 28 February and 2 March, the heating frequency was $f=2.83$ MHz.

In all of the cases except 27 February, square modulation was used with a modulation frequency of 1.4 Hz. On 27 February, the array was split into two halves with one radiating O-mode at a frequency of $f = 4.2$ MHz and the other half radiating X-mode at $f = 3.2$ MHz.

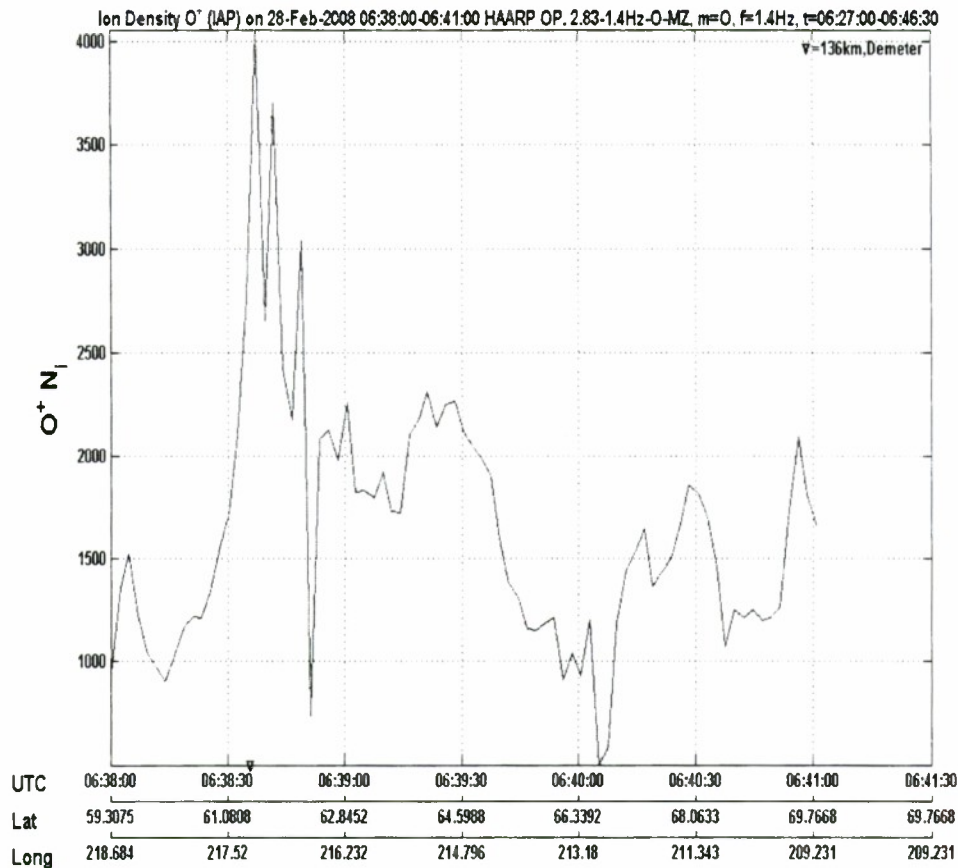


Figure L1. Density of ionized atomic Oxygen (O⁺) as a function of time, and as a function of the respective latitude / longitude of the satellite

During the first two days we got favourable ionospheric conditions with a smooth F-layer and weak E-layer. The Kodiak SuperDARN backscatter plots show strong reflected signals during these two days. For the two last days the ionosphere was perturbed, and during this time the backscatter was weak.

This is a work in progress; however, some preliminary findings are illustrated in Figure L1.

This figure shows the density of O⁺ ions in cm⁻³ versus time, and of the respective latitude / longitude of the satellite. The closest distance between the footprint of the Demeter orbit and HAARP was 136 km, it was reached at 06:38:40. The figure shows three fold increase of the ion density due to the HF-heating. The density increases over 1 min which corresponds to 480 km distance.

Therefore the experiment was able to detect artificial ducts when over flying HAARP which confirms our theoretical predictions [Perrine et al., *Radio Sci.* 41, doi:10.1029/2005RS003371, 2006]. Correlation analysis which includes detailed optical and HF radar data will be applied to underline the physics of the observed effect.

Appendix M

Generation of Ion outflow by HF-heating

Investigators

Chia-Lie Chang, *BAE SYSTEMS, Advanced Technologies Electronics & Integrated Solutions, Washington, DC*

Gennady Milikh, *University of Maryland, College Park, MD*

Evgenii Mishin, *Boston College, Boston, MA*

Objectives

Strong HF heating of F₂ region of the ionosphere has been shown to enhance the electron and ion temperature, and produces the ion outflow that propagates along the entire magnetic field line. This process changes the local ion composition by pushing light hydrogen ions upward. The objective of this experiment is to detect the ion outflow by instruments on the board of DMSP-16 satellite over flying HAARP at the height of about 850 km.

Observation Technique

The experiments were conducted by using the maximum ERP at the chosen frequency. O-mode F-region heating was used, the heating frequency was selected to match the f₀F₂ peak. The experimental procedure is specified below.

Two instruments onboard F16 were used, the ion density meter and the ion temperature detector. The satellite measurements are complemented by the ground based observations: Ionograms to select the proper heating frequencies. Kodiak diagnostics is requested along with the optical measurements to provide us with the knowledge of irregularities caused by the HF heating.

Preliminary Results

Two observations were conducted, 02/25 and 02/26. Each of these days the HF-heating lasted for 20 minutes around 5 UT. The radio beam of O-mode, of the maximum ERP was used. It was directed toward the magnetic zenith. The sampling rate of the F16 ion density meter was 24 Hz, while the sampling rate by the ion temperature detector is only 1 per 8 s. During both observations there was a smooth F-layer with the f₀F₂ at approximately 3 MHz, and there was no electrojet.

1. During the DMSP-16 over-fly (02/25/08) the heater array was split into two halves; one half radiated 2.85 MHz almost matching f₀F₂ frequency, and other half at a frequency shifted by -1.4 Hz. This could allow in addition to studying the ion outflow to measure potential F-region generation of 1.4 Hz ULF waves.
2. During the DMSP-16 over-fly (02/26/08) the heater array was split into two halves; one half radiated 2.85 MHz O-mode almost matching f₀F₂ frequency, and other half at frequency 3.2 MHz and X-mode modulated at 2 kHz. This will allow in addition to studying the ion outflow measure possible injection of 2 kHz VLF waves in the duct.

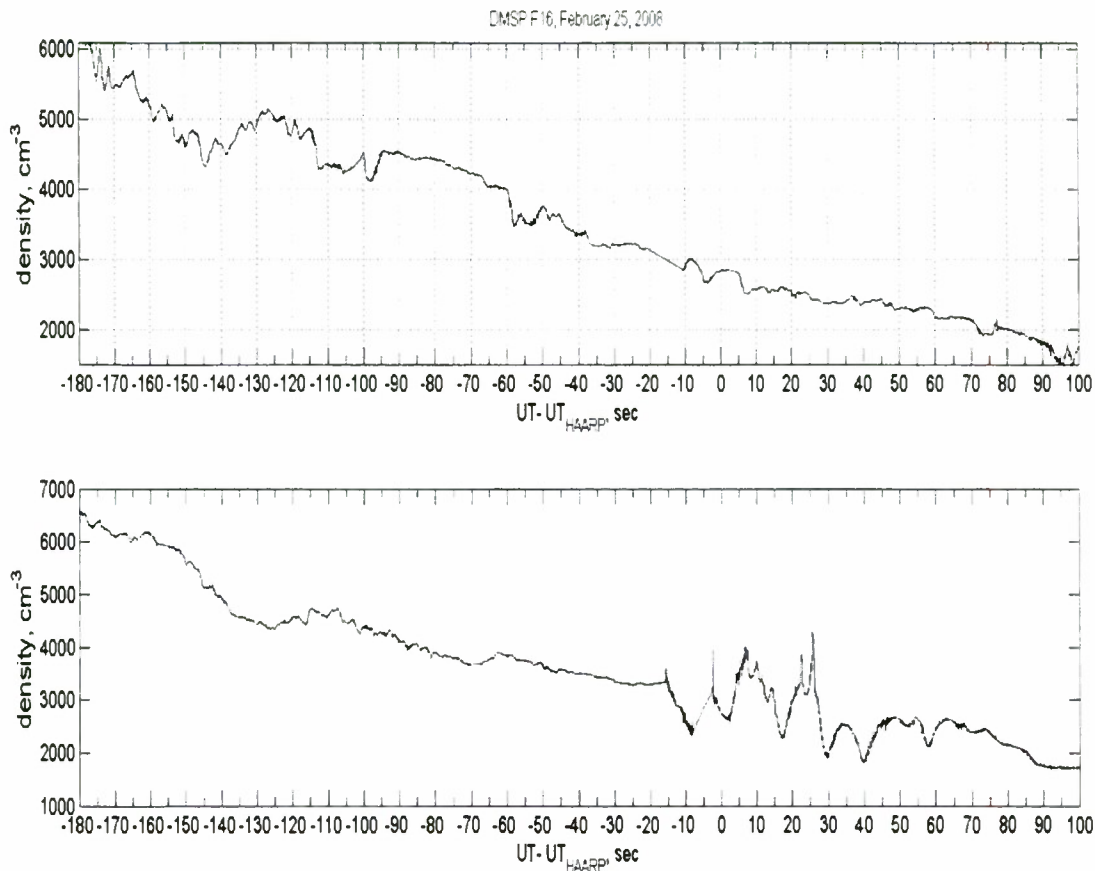


Figure. M1. The measurements made by the F16 ion density meter 02/25 (the top panel), and 02/26 (the lower panel). Zero time corresponds to F16 fly over HAARP.

Preliminary results of our experiments are illustrated by Figure M1. The lower panel shows data from 26 February 2008 under quiet ionospheric conditions. The closest distance from F16 to the HAARP field line was about 300 km. The ion outflows lasted for about 60 seconds which corresponds to 500 km in space. Its amplitude $\delta n/n$ is of order of unity. This is similar to the Demeter observations of ion outflows.

Data from the experiment conducted on 25 February 2008 are shown in the upper panel of Figure M1, also at quiet ionospheric conditions. However, in this case the closest distance from F16 to the HAARP field line was about 500 km. A small bump lasted for 15 s which could be indicative of the ion outflows was detected as shown at the top panel.

Due to poor sensitivity and low time resolution of the ion temperature detector we could not find any related temperature changes. Some backscattering is shown by the quick look SuperDARN RTI plots during the above heating intervals.

Thus we can summarize that for the first time the ion outflows due to the HF heating by HAARP was detected by the ion density meter onboard F16. Some correlation analysis which includes detailed optical and HF radar data will be applied to underline the physics of the observed effect.

Appendix N

Detection of super small scale irregularities generated by the HF-heating of triple gyrofrequency

Investigators

Gennady Milikh, *Departments of Physics and Astronomy, University of Maryland, College Park, MD*

Alex Gurevich, Kiril Zybin, P.N. Lebedev Institute, Russian Academy of Sciences

Jim Secan, *NorthWest Research Associates, Inc.*

Objective

Recent theoretical models predict that super small scale electron irregularities of the size of tens centimeters can be excited by radio waves having a frequency equal to the multiple gyrofrequency ($n > 2$). Such irregularities could scatter UHF signals such as GPS, and thus play an important role in some applications. The objective of this experiment is to detect small-scale irregularities of the electron density caused by the HF-heating at a frequency close to three times the gyrofrequency ($3f_B$).

Observation Technique

The critical diagnostic instrument is the GPS receiver located at HAARP which detects the changes in phase of GPS signals passing through the HF-heated spot. We used square pulses having pulse width of 10 seconds, O-mode, and maximum ERP. The beam was directed towards the chosen GPS satellite such as PRN06 or PRN21. During last 5 minutes of the designated observational time we switched to 0.2 seconds square pulse modulation in order to check the rising time of the causal instability. We observed differential carrier phase and differential group delay of GPS signals. The data were provided by Jim Secan.

SEE observations conducted by Thomas Leiser could provide a test for matching the resonance conditions since the shape of the SEE spectrum changes when the resonance condition is met. We used ionograms to select the proper heating frequencies. Kodiak radar diagnostics along with the optical measurements will be used to obtain the spectrum of irregularities caused by the HF heating.

Preliminary Results

Six observations were conducted, 02/22, 02/23, 02/24 (twice at 18:28 and 19:13), 02/25 and 02/26. Each of these days the HF-heating lasted for 20 minutes around 19 UT. We used $f = 3f_B$ which depends upon the altitude and ranges between 4.24 MHz at 250 km and 4.05 MHz at 350 km. The exact choice of the heating frequency changed from day to day depending upon the local ionospheric conditions. The experiments were conducted under quiet or normal geomagnetic conditions.

In three out of 5 observations (in one case the data were corrupt) we found that after the start of the heating the phase of the probe signals changes abruptly in about 10 seconds, and then oscillates with the period of HF-heating, 20 seconds. The oscillations lasted for 4-5 minutes and then disappear, presumably when the resonance condition is not fulfilled, although the HF-heating continues. This is illustrated in Figure N1 showing data obtained on 23 February 2008. The encircled area in the left panel shows the oscillations with 20 second period. The right panel is a close-up of the circled area.

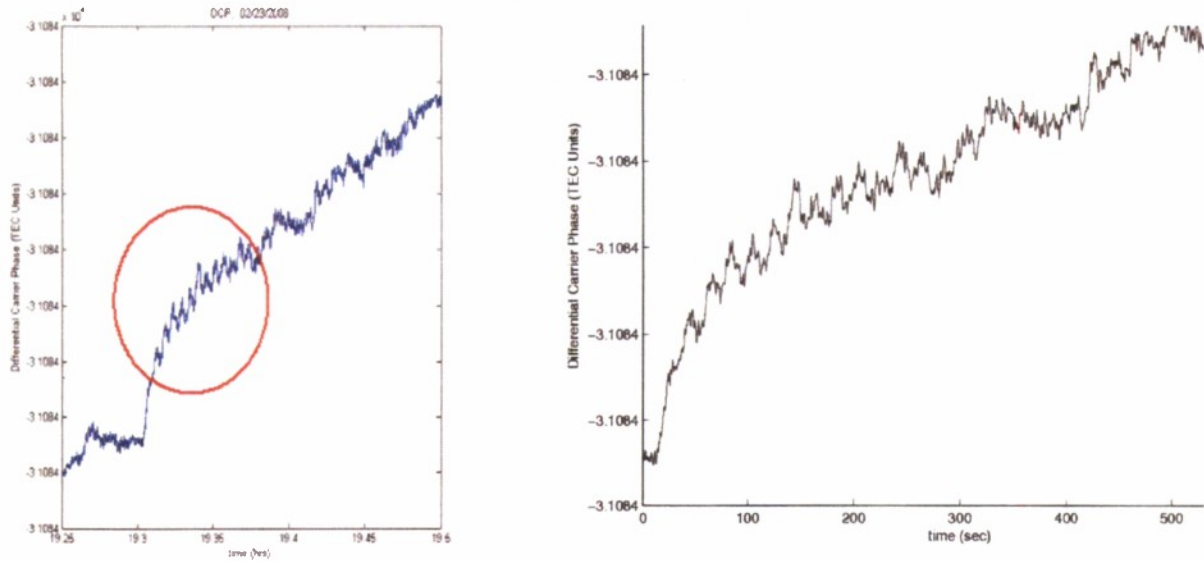


Figure N1. The differential carrier phase in arbitrary units measured 02/23/08. The ionospheric heating started at 19.3 UT and lasted for 0.3 h. The left panel shows phase oscillations with the period 20 s, corresponding to the heating pulses. The encircled area in the left panel shows the oscillations. The circled region is zoomed in the right panel where zero time corresponds to 19.3 h.

The detail SEE observations will be used to find if the heating frequency has matched the resonance conditions $f = 3f_B$ during these experiments. Besides, the optical and radar observations will be used for the same purpose since both are sensitive to the multiple gyro-resonance.

In conclusion, we report for the first time detection of the artificial scattering of the GPS signals. It indicates the presence of small-scale irregularities of the electron density caused by the HF-heating at the frequency close to $f = 3f_B$. Future analysis will be focused on the spectrum and intensity of the detected small-scale irregularities.

Appendix O

3-D Determination of Artificial Optical Emission Structure

Investigators

T. Pedersen, T. Mills, and S. Jimenez, *Air Force Research Laboratory RVBXI, Hanscom AFB, MA*

B. Gustavsson, *University of Tromso, Tromso, Norway*

Objective

The objective of this experiment was to determine the altitude dependence of artificial optical emissions at multiple wavelengths using the HAARPOON remote imager network and an imaging spectrometer variant of a HAARPOON system. This experiment represents the first scientific test of the HAARPOON network. Determination of the altitude of emissions at 557.7 and 630.0 nm can be used to investigate the altitude dependence, and therefore frequency dependence, of the excitation mechanism, as well as properties of the electron energy spectrum and neutral atmosphere. The imaging spectrometer is capable of observing emissions over a wide range of wavelengths, allowing the altitude dependence of a number of emissions to be determined simultaneously. This includes the possible presence of OH emissions as well as other less commonly observed lines.

Observation Technique

Optical data was collected using the HAARP imager at the HAARP site, the HAARPOON 2 system located in Delta Junction, ~250 km north of HAARP. The HAARPOON 1 system and the HAARPOON imaging spectrometer were deployed on a temporary basis during the campaign at Delta Junction, the HAARP site, and a roadside site near Eureka Lodge. Deployments were based on weather considerations and equipment readiness. As pointing of the temporarily deployed systems, especially the spectrometer, was difficult to establish prior to observations, the HAARP transmitter was run in a mode alternating between magnetic zenith and vertical to maximize the chances of the systems intercepting the emission region. This also provided for a direct comparison between emissions in the two regions, at least for the instruments with wider fields of view.

Preliminary Results

Excellent optical data were acquired by the HAARP imager and HAARPOON 1 and 2 systems on the night of 23 Feb 2008. Since both HAARPOON systems were at the same site on this night, the field-widening mirror was removed from the HAARPOON 1 system, allowing simultaneous wide- and narrow-field imaging at both 557.7 nm and 630.0 nm. Dramatic emissions were observed in both the magnetic zenith and the vertical as shown in Figures O1 and O2. In both the magnetic zenith and the vertical the dominant features of the emissions were a relatively homogenous central spot near the beam center and rings of irregular structure surrounding the central spot well outside the main beam. Significant evolution of the central spot and ring structure during the 3 min on periods was also apparent in the 15 sec resolution data from the HAARPOON systems, although accurate discrimination between altitude changes and horizontal motion will require a full analysis to be performed. Significant emissions from N₂⁺ at 427.8 nm were observed with the HAARP imager during this experiment, suggesting that significant artificial ionization may have been achieved.

Unfortunately, the spectrometer setup was incomplete during the first run early in the campaign, and weather and ionospheric conditions were unfavorable during the second run of this experiment later in the campaign. It is possible that spectrometer data of HAARP emissions were obtained during some other experiments, but this search has not yet been completed.



Figure O1. 630.0 (left) and 557.7 (right) nm wide-field images of HAARP-induced optical emissions from the $\sim 90^\circ$ FOV HAARPOON system at Delta Junction during the experiment on 23 Feb 2008. Note that north is toward the bottom of these quick-look images.

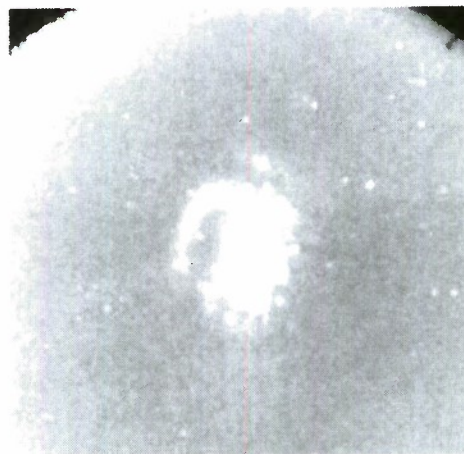


Figure O2. Central spot and partial ring in the vertical as seen at 557.7 nm looking up from the HAARP site on 23 Feb 08 at approximately the same time as the images in Figure O1.

Appendix P

Excitation of Optical Emissions and Irregularities in the Ionospheric E-Region

Investigators

T. Pedersen and T. Mills, *Air Force Research Laboratory RVBXI, Hanscom AFB, MA*

Objective

The objective of this experiment is to determine the mechanism responsible for generation of bright optical speckles and km-scale irregularities in the E-region by heating in sporadic and auroral E layers at different frequencies.

E-layer optical effects from HF heating experiments have been observed on only a few occasions in the past, but the original observations from HAARP [Pedersen and Gerken, 2005] have now been joined by a second case providing additional information [Pedersen et al., 2008, manuscript in preparation]. At HAARP, the E region effects take the form of small (~1-2 km) presumably field-aligned irregularities visible as bright spots superimposed on the natural background aurora creating the E layer. The latest results are suggestive of a frequency dependent resonance most likely operating on the topside of the E layer.

Observation Technique

The original technique proposed was to sweep through frequencies near the 5.95 MHz frequency thus far uniquely responsible for producing the E-region structures. However, in practice, runs were possible on only 2 nights, and E-layer densities were not sufficient to allow this frequency range to be explored. On one of the nights, HAARP was cloudy but the experiment proceeded by directing the transmitter toward the north where the E region would be closer to the center of the field of view of the HAARPOON 2 system in Delta Junction, even though the expected km-scale structures are near the lower limit of the system resolution. Transmissions were generally made in a 15 sec on 15 sec off mode allowing artificial structure to be identified by its periodic appearance and disappearance. Imaging at the HAARP site was carried out with the AFRL EM-CCD camera and, after its return from the temporary remote sites, the HAARPOON 1 system.

Preliminary Results

Due to the less-than-ideal ionospheric and weather conditions for the experiment and the very limited amount of time available in the schedule, no observations were made at the target frequency. One possible artificial E-region structure, however, was observed on the last night of the campaign in one image frame during a transmitter on period, but without additional corroborating cases this is inconclusive. A few structures approximately 1 pixel in width were observed later on with the HAARPOON 2 system viewing from Delta Junction, but are most likely cosmic ray streaks. A more detailed analysis will determine whether these could be actual atmospheric emissions, and whether their positions and alignment are consistent with creation in the E-region targeted by the HAARP transmitter beam, although even then the number of cases is likely to be too small to be conclusive.



Figure P1. Possible E-region structure seen during one of the E-region experiments on 3 March 2008.

References

- Pedersen, T., E. Mishin, and R. Esposito (2009), New observations of HF-induced optical emissions from the ionospheric E region, *J. Geophys. Res.*, *114*, A06316, doi:10.1029/2008JA013596.
- Pedersen, T. R., and E. A. Gerken, Creation of visible artificial optical emissions in the aurora by high-power radio waves, *Nature*, *433*, pp. 498-500, 2005.

Appendix Q

Study of High Power Nearly Vertically Incident Skywave Reflections

Investigators

J. Spaleta and R. T. Parris, *Geophysical Institute, University of Alaska Fairbanks, Fairbanks, AK*

Objective

The objective of this experiment was to investigate the ionospheric response to high power transmitter pulses of short duration. The duration and power of a series of transmit pulses were varied systematically in order to parameterize the ionospheric response as a function of both pulse power and pulse length. The response was characterized by comparing recordings of the skywave reflections to recordings of the transmitted groundwave. The recorded groundwave acts as a surrogate for total transmit power, as long as the transmission direction is held constant for all experiments. These experiments utilized the maximum available transmission power of the HAARP facility in order to extend observations beyond what was possible in previous experiments conducted at HIPAS last year. The primary objectives were to confirm the skywave response previously seen and to determine if the characteristic response extends to higher transmit power.

Observation Technique

The parameter scan experiments were performed at an operating frequency near 2.85 MHz, in both X and O mode polarizations with a pulse repetition rate of 20 Hz. Figure Q1 depicts a sequence of calibration pulse data with transmit pulse length and power held constant. The skywave reflection undergoes a large, but relatively slow variation due to ambient ionospheric conditions. In order to make comparisons between the detected groundwave and skywave power during a transmit parameter scan, a normalization must be applied that serves to remove this ambient variation. The normalization chosen was to divide the pulse sequence into short scan groups of 10 pulses (~ 0.5 seconds). Figure Q2 depicts the scan group separation process for a transmit power parameter scan using 200 microsecond long pulses. Neighboring pulses of the same color are members of the same scan group. The detected groundwave and skywave power for each pulse in a scan group is then normalized to the average power recorded in that scan group. Once normalized in this way, normalized powers across all scan groups can be compared as is done in Figure Q3 for O-mode and again in Figure Q4 for X-mode.

Preliminary Results

O-mode power scan observations at HAARP agree with the previous observations at HIPAS for total transmit power below ~900 kW. Below this threshold the skywave reflections appear to be weakly non-linearly dependent on total transmitted power, which can be seen in Figure Q3. Starting at lowest transmit powers, there is higher efficiency of skywave reflection with increasing transmission power. However, there is a noticeable roll-off in reflected skywave power at the highest available transmit powers. Once a certain threshold transmission power is reached, the skywave reflection efficiency begins to sharply decrease.

The significant change in the skywave response near ~900 kW of transmitted power may be an indication of a change in the dominant physics in the interaction region. A more comprehensive study of short pulse skywave response in this power threshold region may provide additional insights.

There also appears to be differences between the high power skywave response for X and O mode. The X mode skywave response is essentially linearly dependent on groundwave power at lower transmission power. More intriguing however, is the observed bifurcation of the X-mode response at higher transmit power in Figure Q4. Work is ongoing to examine this feature more closely

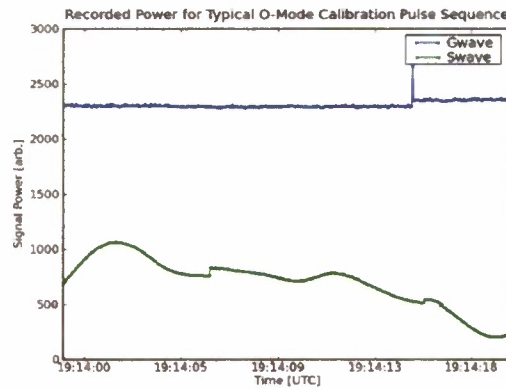


Figure Q1. O-Mode calibration sequence showing slowly varying ambient skywave response.

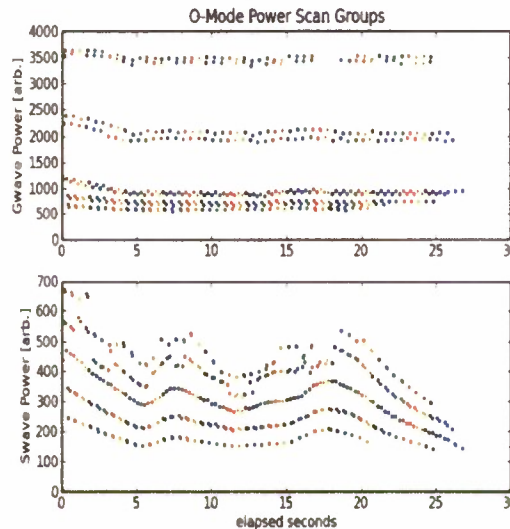


Figure Q2. Depiction of skywave and groundwave recordings separated into scan groups by color. Scan groups are used to normalize the ambient variation that is not the result of changes in transmission power.

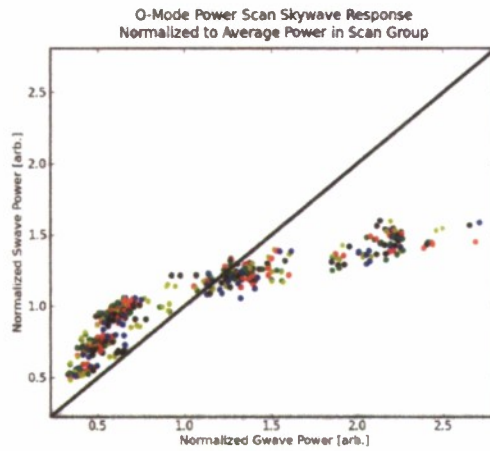


Figure Q3. Comparison of O-mode normalized groundwave and skywave power across multiple scan groups. At lower groundwave power values, the skywave response is weakly non-linear, with increasing reflection efficiency as groundwave power is increased. At higher groundwave power values, a significant roll-off of skywave power is observed at the highest available groundwave power.

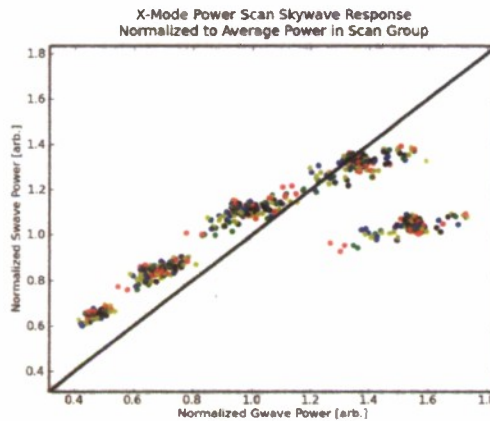


Figure Q4. Comparison of X-mode normalized groundwave and skywave power across multiple scan groups. The X-mode skywave response is strikingly different from the O-mode response across the full range of groundwave power values. In particular, the bifurcation of the response at high power needs to be further analyzed.

Appendix R

Artificial particle precipitation by VLF cyclotron resonance

Investigators

M.J. Kosch, *Lancaster University, UK*

J. Bortnik, *University of California Los Angeles, Los Angeles, CA*

M. Cohen, U. Inan, R. Marshall and R. Newsome, *Stanford University, Stanford, CA*

T. Pedersen and R. Esposito, *Air Force Research Laboratory RVBXI, Hanscom AFB, MA*

R. Friedel, *Los Alamos National Laboratory, Los Alamos, NM*

B. Gustavsson, *University of Tromsø, Tromsø, Norway*

Objective

To produce artificial VLF waves optimized to artificially induce particle precipitation by cyclotron resonance, which will be detected optically.

Observation Technique

The experiment consisted of HAARP pumping at full power with a vertical north-south fan beam on 2.75 or 4.1 MHz, or both simultaneously, in X-mode. The carrier wave is modulated with 6 special VLF envelopes targeting 5 and 10 keV particles and equatorial electron densities of 100, 200 and 400 el/cm³. This combination covers the most likely parameters for success. The frequency-time modulation of the VLF envelope is designed to optimise cyclotron resonance between the incoming target particles and outgoing VLF wave. The prime diagnostic was the AFRL EMCCD imager on wavelength 427.8 nm only at 1 sec cadence. In addition, the Stanford PIPER photometers were operated on multiple wavelengths.

Preliminary results

Very powerful VLF signals with the desired frequency-time modulation were generated. Figure R1 shows an example set of 6 sequential modulations for 5 keV 100 el/cm³, 5 keV 200 el/cm³, 5 keV 400 el/cm³, 10 keV 100 el/cm³, 10 keV 200 el/cm³, and 10 keV 400 el/cm³. No significant difference between using 2.75 or 4.1 MHz, or both together, as the carrier pump frequency could be found. Hence, it is concluded that using the lowest carrier frequency probably is the best.

The run on 1 March 2008 04:03-06:30 UT occurred during overcast sky. The run on 3 March 2008 05:30-06:52 UT occurred under clear optical conditions. However, the optical data are currently not yet available for analysis.

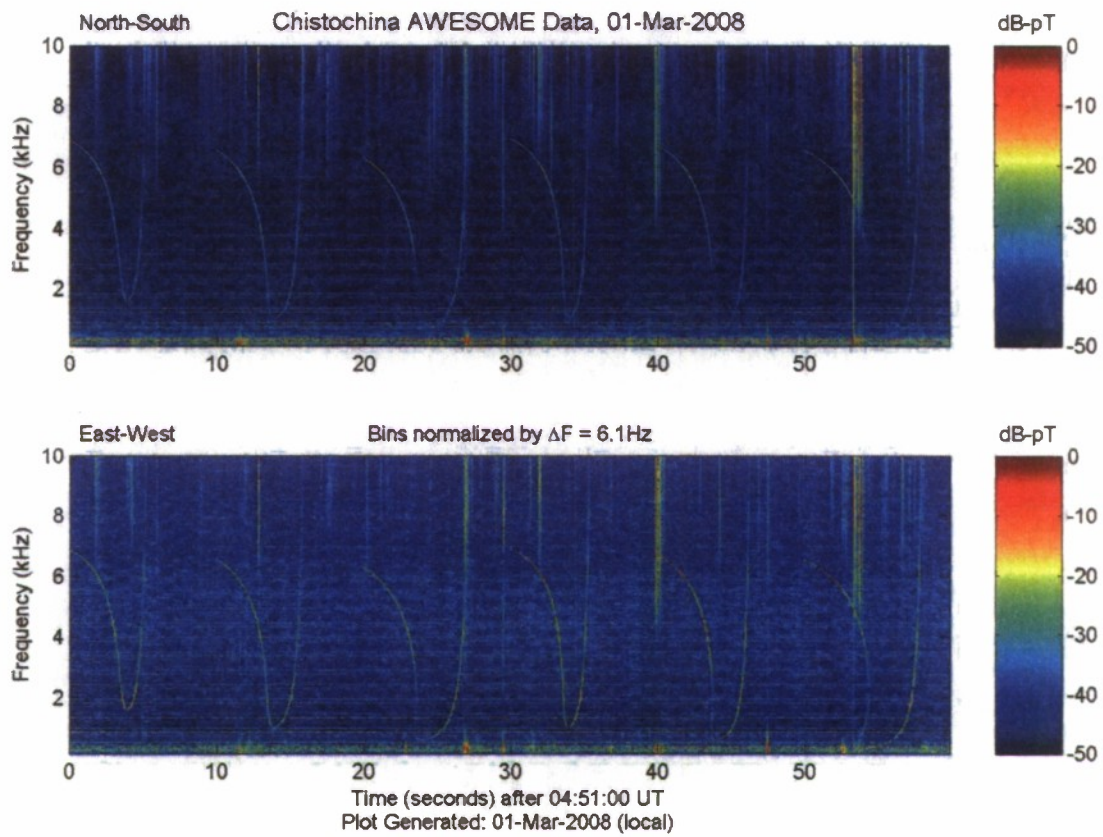


Figure R1. VLF signals observed at Chistochina, AK for six successive HF transmitter modulation waveforms.

Appendix S

The temporal evolution of the magnetic zenith self-focusing effect and accelerated electron energy spectrum using VLF waves as a proxy to detect lower-hybrid waves.

Investigators

M.J. Kosch, Lancaster University, UK

M. Cohen, U. Inan, Marshall and R. Newsome, *Stanford University, Stanford, CA*

G. Ganguli, *Naval Research Laboratory, Washington, DC*

B. Gustavsson, *University of Tromso, Tromso, Norway*

R., S. Oyama, *Solar-Terrestrial Environment Laboratory, Nagoya University, Japan*

T. Pedersen, *Air Force Research Laboratory RVBXI, Hanscom AFB, MA*

J. Spaleta and B. Watkins, *Geophysical Institute, University of Alaska Fairbanks, Fairbanks, AK*

Objective

- 1) To determine the temporal evolution of the magnetic zenith self-focusing effect using high cadence optical images.
- 2) To determine the temporal evolution of the accelerated electron energy spectrum using multi-wavelength optical data.
- 3) Search for indirect VLF evidence for the existence of pump-induced lower-hybrid waves.

Observation Technique

The experiment consisted of HAARP pumping at full power on 2.85 MHz in O-mode pointing into the magnetic zenith with a 2-min ON and 2-min OFF cycle. For objective (1) the prime diagnostic was the HAARP all-sky imager on 557.7 nm only at 10-sec cadence. Auxiliary Lancaster imagers (ST9 and Pike) were operated on 630 at 15-sec cadence. For objective (2) the prime diagnostics are the Stanford photometer and PIPER systems. For objective (3) the prime diagnostic is the Stanford VLF receiver located at Chistochina. In addition, the MUIR and Kodiak radars were operating.

Preliminary results

This experiment was run on 24 February 2008 for 03:15-05:01 UT under optimal clear sky conditions.

Objective 1: Calibrated difference images are not yet available to evaluate the temporal evolution of the self-focusing effect. Figure S1 shows the last 557.7 nm image from the HAARP imager (top row), 630 nm image from the ST9 imager (middle) and 630 nm image from the Pike imager (bottom) before pump-off for two consecutive HAARP cycles, ending 04:21 (left) and 04:25 (right) UT. A bright focused spot is clearly seen surrounded by a more diffuse halo of weaker optical emissions as well as a crescent-shaped region. The 557.7 nm images show significantly more detail than the 630 nm images. Whilst the crescent shape appears very similar to the auroral rings seen at EISCAT, a fundamental difference is that the bright central spot remains. At EISCAT, the central spot extinguished as the crescent developed.

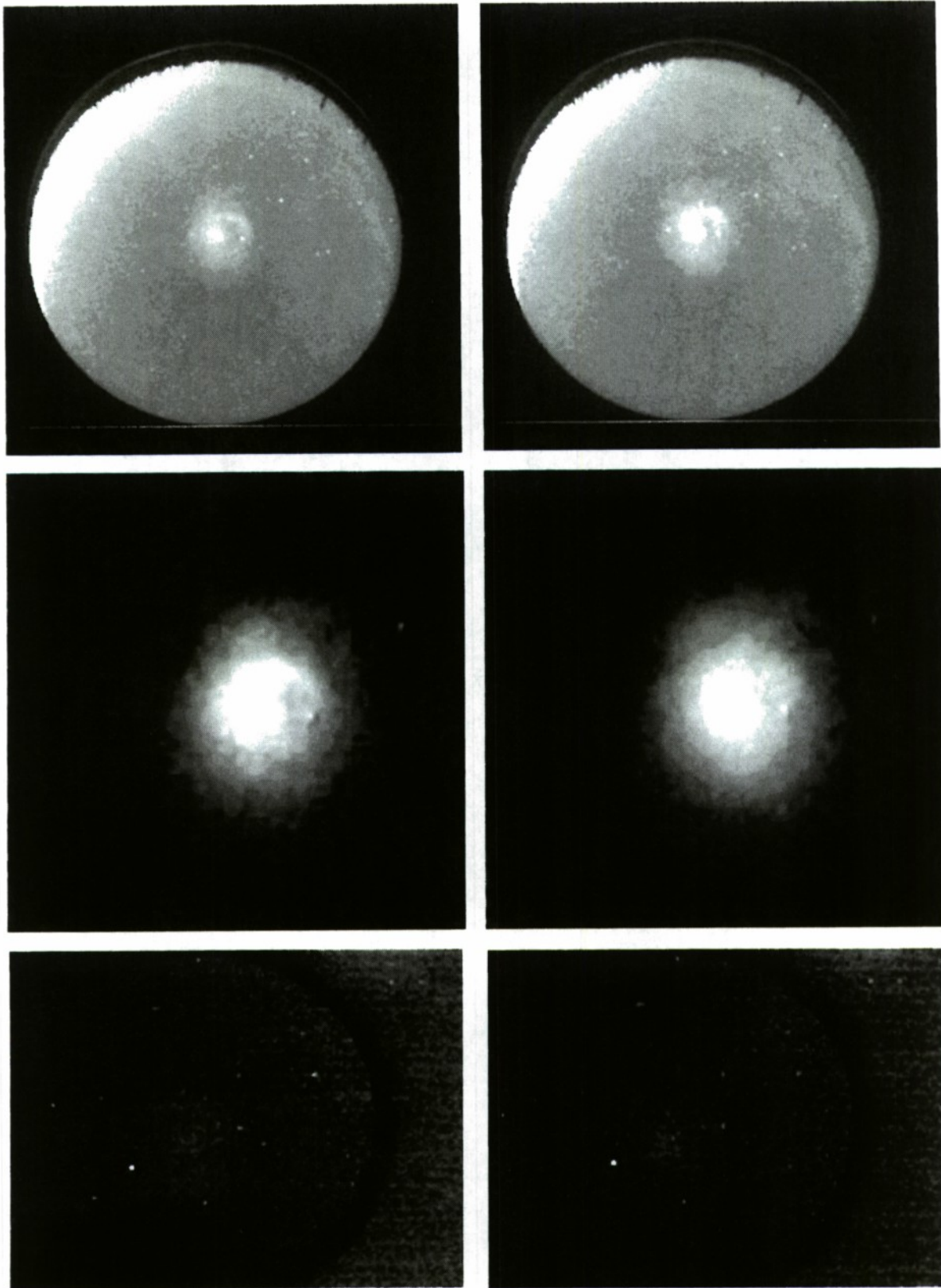


Figure S1. Images from the HAARP imager at 557.7 nm (top row), from the ST9 imager at 630 nm (middle) and from the Pike imager at 630 nm (bottom). Images for the HAARP transmit cycles ending at 04:21 on the left and at 04:25 on the right.

The MUIR radar produced a new observation using the ion-line backscatter, as shown in Figure S2 below. The enhanced backscatter of ion-acoustic waves, associated with Langmuir

turbulence, is clearly seen, indicating the HAARP wave reflection altitude. Note that the reflection altitude descends by five or more kilometers. This is a clear sign of plasma heating as enhanced electron temperature reduces the recombination rate resulting in increasing plasma density, which forces the pump wave reflection altitude to descend. This effect has been modeled at EISCAT and will be applied at HAARP to estimate the electron temperature.

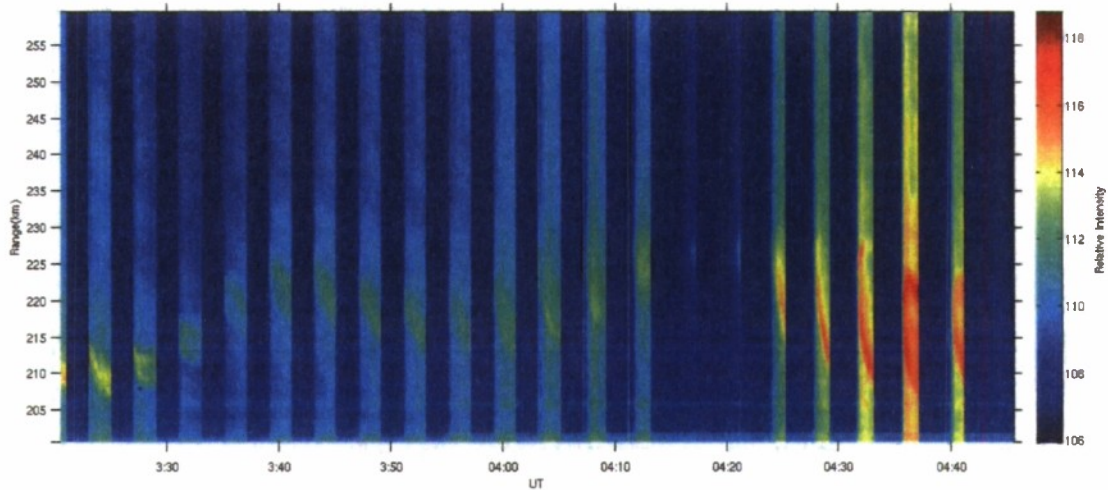


Figure S2. Ion line backscatter observations from the HAARP MUIR UHF radar.

Objective 2: This result depends on having multi-wavelength calibrated optical data available. The different collisional cross-sections for various optical emissions is exploited, e.g. the threshold energy for 630, 557.7, 777.4 and 427.8 nm is about 2, 4, 9 and 19 eV, respectively. The 630 nm photometer data is shown in Figure S3 below. The HAARP-induced optical emissions are clearly seen on top of a descending background of twilight.

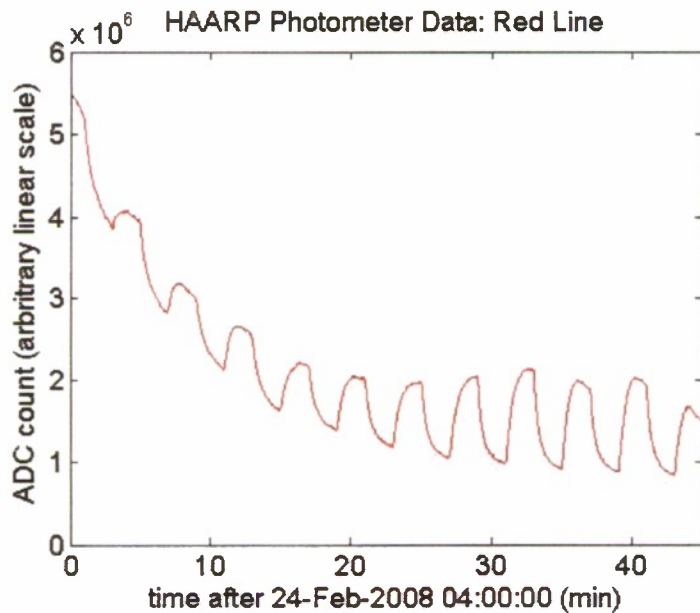


Figure S3. HAARP photometer data at 630 nm.

Objective 3: No VLF signature was found near 8 kHz, which would have corresponded to lower-hybrid waves. As the second gyro-harmonic is a special case, this experiment will be repeated in future for the third or higher gyro-harmonic.

Appendix T

A Coordinated Study of HF-induced Irregularities, Plasma Waves, and Ionospheric Conditions at HAARP

Investigators

J. P. Sheerin, *Eastern Michigan University, Ypsilanti, MI*

B. J. Watkins, W. A. Bristow and Spaleta, *Geophysical Institute, University of Alaska Fairbanks, Fairbanks, AK*

S. I. Oyama, *Solar-Terrestrial Environment Laboratory, Nagoya University, Japan*

T. Leyser, *Swedish Institute of Space Physics, Uppsala, Sweden*

Objective

The full HAARP IRI was operated at low-duty cycle to generate and study Langmuir plasma waves recorded in the MUIR UHF backscatter spectra (the HF-induced plasma line or 'HFPL') for a wide range of HF and UHF pointing angles. High time resolution (3.3 ms) achieved in the MUIR spectra enabled the study of the development of HFPL spectra during each HF pulse. Stimulated electromagnetic emissions (SEE) spectra were recorded for comparison to MUIR radar backscatter from plasma waves.

Observation Technique

The HAARP IRI was operated at full power (3444 kW) in O-mode making use of the higher gain at the temporary frequency allocation granted, 4.1 MHz, while keeping the ionosphere overdense. Based on our previous results, an HF pulse width ('on') of 60 ms in an IPP of 12 sec (for a low-duty cycle of 0.5%), was necessary and sufficient to prevent onset of Artificial Field Aligned Irregularities (AFAI) enabling comparison to theoretical predictions for HFPL spectra. The HF pump pointing was stepped in zenith from vertical to magnetic zenith (14°) in the magnetic meridian. MUIR recorded the upshifted plasma line spectra with 250 kHz bandwidth (sufficient to record expected outshifted plasma line, 'OPL') and 3.3 ms resolution. For each HF pump direction, the MUIR radar was stepped in several pointing directions. The Kodiak SuperDARN HF radar was operated to monitor ionospheric conditions and any development of AFAI. The HAARP ionospheric data instruments (e.g. ionosonde) diagnostics were used for density profile, absorption measurements, and ionospheric conditions.

Preliminary Results and Discussion

For the local afternoon periods on 22 and 23 Feb 2008, the f_oF_2 remained around 5 MHz until 2:30 UT. Favorable ionospheric conditions and the temporary frequency allocation, permitted the first experiments of this type at the higher gain for 4.1 MHz. The Kodiak radar confirmed that the low-duty cycle chosen prevented AFAI. For the HF pump pointed vertically, MUIR recorded both collapse and cascade type spectra (sometimes 'coexistence'). The intensity at these pointings was relatively weak. As predicted, with the IRI beam pointed around the Spitz angle (~ 7°) MUIR recorded very strong cascade lines (Figure T1). There was no evidence of the outshifted plasma line (OPL) as had been recorded in previous HAARP experiments performed at 3.3 MHz.

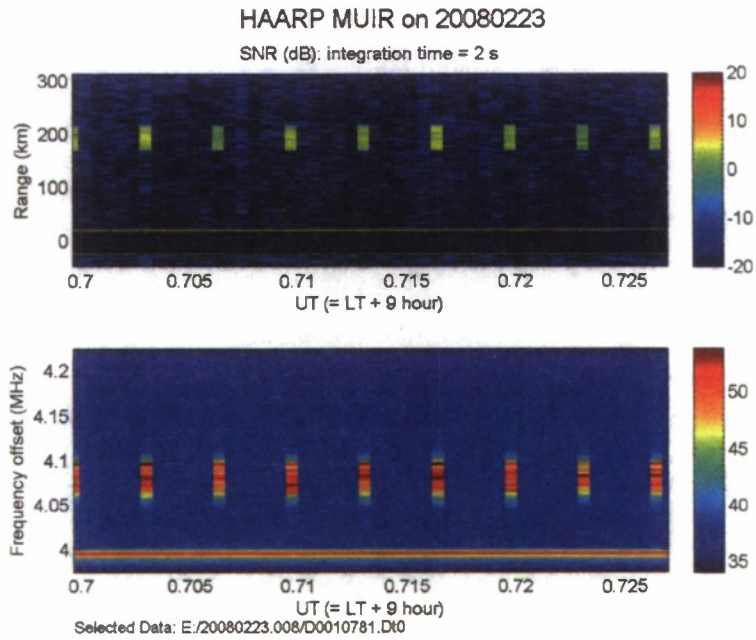


Figure T1. Spectra of HFPL (lower panel) with MUIR at MZ (14°) and HAARP pointed at 7°.

Modeling has suggested a second favorable configuration for detection of HFPL with the HF pointed along magnetic zenith (MZ ~ 14°) and the UHF radar looking along 22°. This prediction was successfully confirmed for the first time in our HAARP experiments during August 2007, performed at 3.3 MHz. Figure T2 shows the strongest cascade lines recorded during all of these experiments at 4.1 MHz, were for this configuration. Analysis of the temporal development of the HFPL spectra and the SEE spectra are in progress.

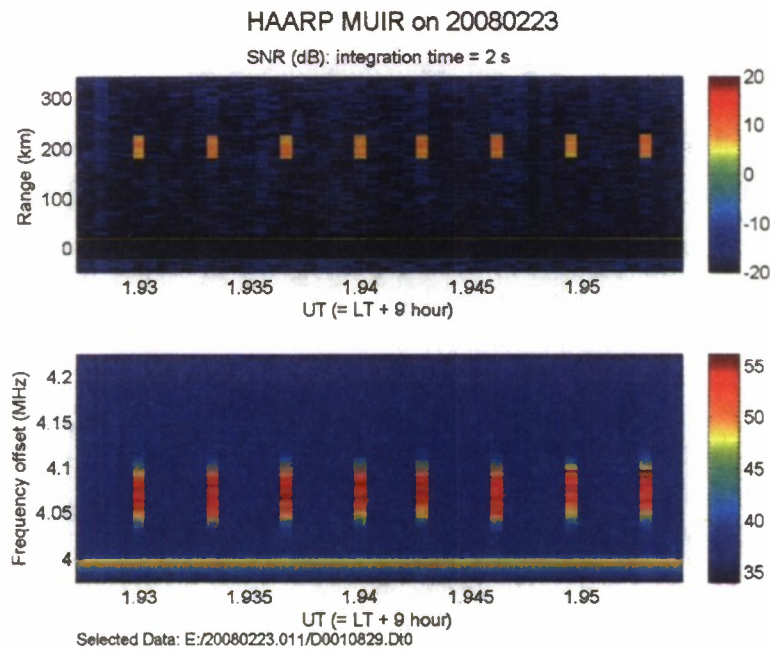


Figure T2. Spectra of HFPL (lower panel) with MUIR at 22° and HAARP pointed at MZ 14°.

Appendix U

Investigation of Large Plasma Sheets, Spatial Distribution of Langmuir Waves, and Whistler Wave Interactions with Ionospheric Plasmas

Investigators

M.C. Lee, R. Pradipta, J.A. Cohen, L.M. Burton, and A. Labno, *Plasma Science and Fusion Center, Massachusetts Institute of Technology, MA*

D. Mabijs, *Department of Electrical and Computer Engineering, Boston University, Boston, MA*

Objective

Our experiments were aimed at investigating (1) generation of large-scale ionospheric plasma sheets [conducted by J.A. Cohen et al.], (2) spatial distribution of Langmuir waves [by M.C. Lee et al.], and (3) electrojet-radiated VLF whistler wave to excite lower hybrid waves and short-scale ionospheric density irregularities [by R. Pradipta et al.], respectively.

Preliminary results

(1) Generation of Large Plasma Sheets

Large plasma sheets generated by O- and X-mode HF heaters are parallel and orthogonal to meridional plane, respectively, as illustrated in Figures U1 and U2.

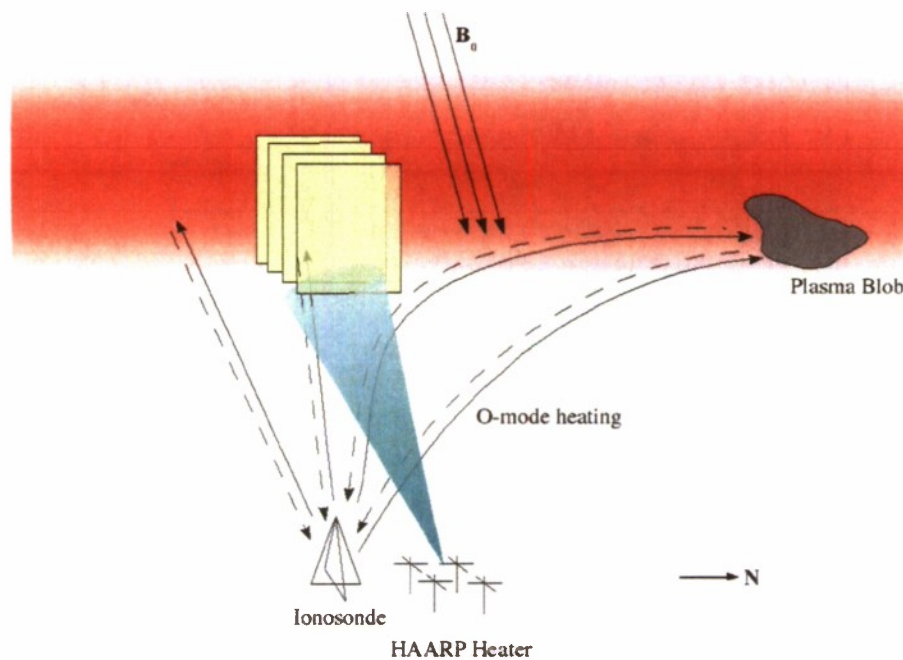


Figure U1. Large plasma sheets are generated by O-mode heater waves within the meridional plane.

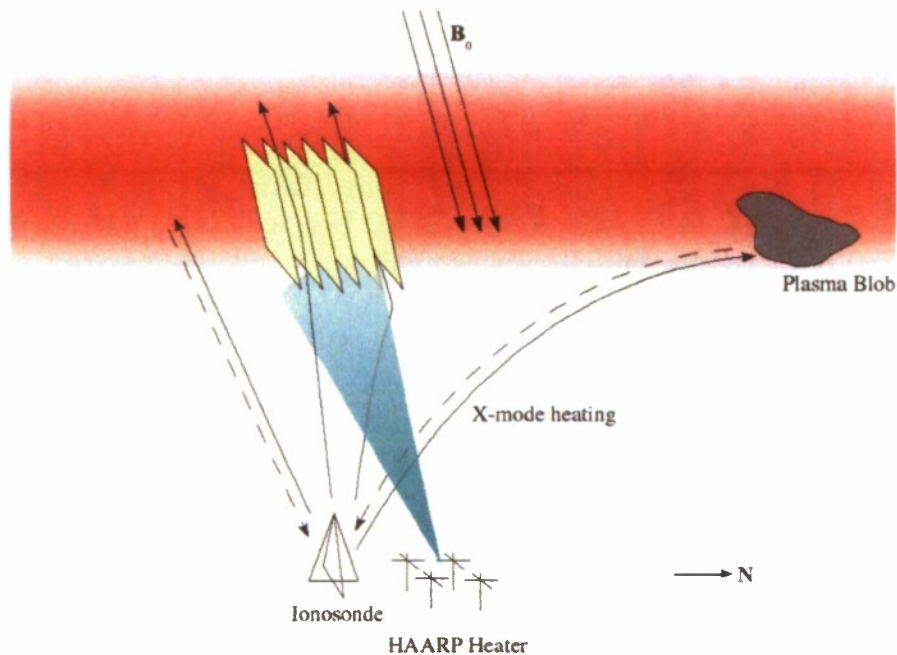


Figure U2. Large plasma sheets generated by X-mode heater waves are orthogonal to the meridional plane. Ionosonde signals transmitted near the zenith will be guided by these plasma sheets to propagate away. Those ionosonde signals transmitted at large angles from the zenith can still be reflected by remote plasma blobs and recorded in ionograms.

Under the $E \times B$ drifts they were detected by Arecibo 430 MHz incoherent scatter radar (ISR) as slanted stripes in the range-time-intensity (RTI) plots (see Figure U3) in our 1997 ionospheric heating experiments [Lee et al., GRL, 1998].

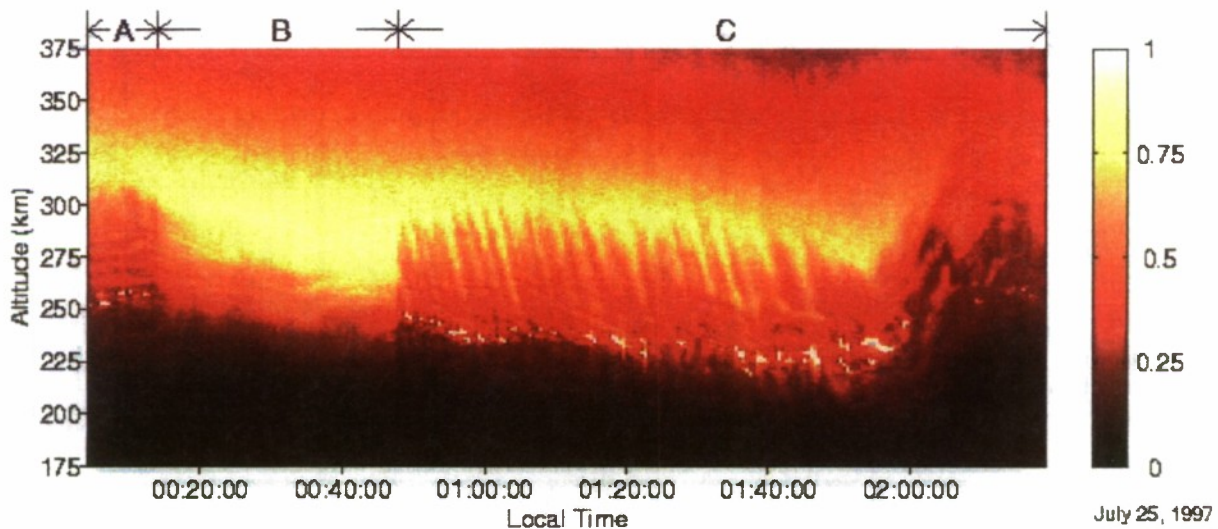


Figure U3. Arecibo radar detection of HF heater-created large plasma sheets seen on RTI plot as slanted stripes, starting from about 00:50 till 00:50 LT on July 25, 1997 [Lee et al., GRL, 1998].

Because of the large magnetic dip angle at Gakona, it would be rather difficult to see the slanted stripes in the ISR-generated range-time-intensity (RTI) plots. However, the RTI plot of

SuperDARN measurements displayed in Figure U4 shows the expected features of these plasma sheets.

The range is about 670 km for the SuperDARN beam to reach the heated ionospheric region above Gakona. During the O-mode heating SuperDARN signals were bounced back by plasma sheets generated within the meridional plane. By contrast, SuperDARN signals were forward-scattered by X-mode generated plasma sheets, which are orthogonal to the meridional plane. These scenarios explain reasonably well why the SuperDARN signals weakened significantly when we changed the heating schemes from O-mode to X-mode.

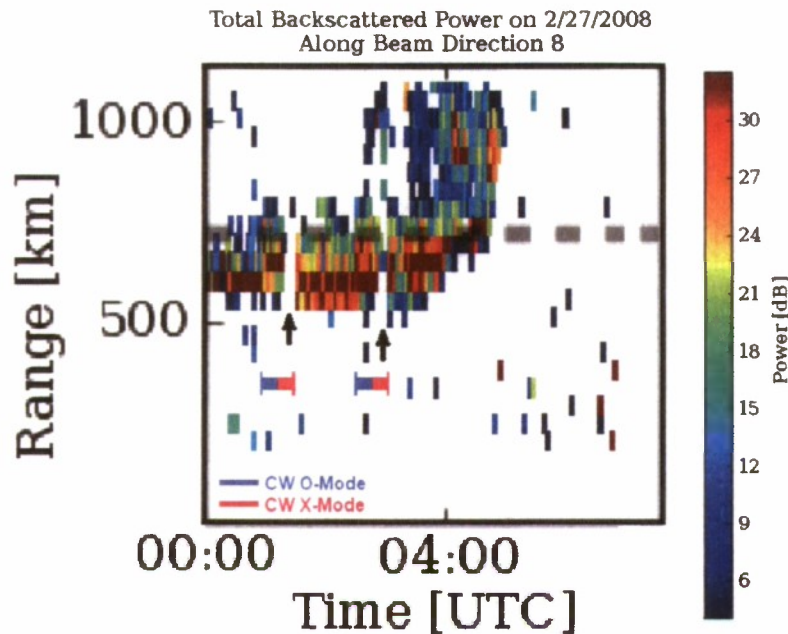


Figure U4. SuperDarn data recorded during CW O-mode and CW X-mode operation of HAARP heater on 2/27/2008 for the investigation of large plasma sheet generation.

This feature is also supported by HAARP Digisonde measurements made in our earlier experiments at PARS Summer School. In brief, as illustrated in Figure U1, digisonde signals had no problem to be totally reflected and appear in ionograms in the presence of O-mode generated plasma sheets. In contrast, because X-mode heater waves induce orthogonal plasma sheets, ionosonde signals transmitted near the zenith will be guided to propagate away, as delineated in Figure U2. They, thus, cannot be reflected to appear in the ionograms. However, when plasma blobs are present, the ionosonde signals transmitted at a large angle may still be bounced back from the remote plasma blobs, as observed in our PARS 2005 summer experiments [Cohen et al., URSI GA Proceedings, 2008; J.A. Cohen, MS Thesis, MIT, 2008].

We are currently analyzing SuperDarn data with Bill Bristow/Jeff Spaleta, scintillation data with Jim Secan, and magnetometer data with Spencer Kuo to understand different aspects of the heater-generated plasma sheets.

(2) Spatial Distribution of Langmuir Waves

Guided by our recent theoretical work [Kuo and Lee, JGR, 2005], we conducted HAARP experiments to investigate the two processes generating spectra of Langmuir waves via resonant

and non-resonant cascading mechanisms. The non-resonant mechanism occurs at the same height where the PDI or OTSI is excited, to generate cascading Langmuir waves under the eigen-frequency mismatch condition. In the resonant process, the PDI or OTSI-excited Langmuir wave will propagate to a lower altitude as a pump wave to excite Langmuir cascades via a parametric instability. The tradeoff is that the Langmuir pump wave experiences propagation attenuation before cascading occurs. The instability thresholds under the frequency mismatch in the former process are found to be significantly greater than those under the propagation loss in the latter. Because of the lower instability thresholds, Kuo and Lee's theory predicts the following for experiments to verify. The resonant cascade process would be the dominating mechanism, which produces cascading spectra of Langmuir waves in several patches at different altitudes during the O-mode overdense heating of ionospheric plasmas. Our earlier Gakona experiment results supporting the theoretical predictions are highlighted below [L.M. Burton et al., BS Thesis, MIT, 2007].

The set of data presented in Figure U5 was acquired by HAARP MUIR radar in our 2006 experiments. The MUIR antenna was directed along the magnetic zenith, transmitting coded-long pulses of 998- μ s length with 10-ms IPP and 1- μ s baud length, thus yielding 150 m range resolution. MUIR detected three cascade lines, as displayed in Figure U5. These results were cross-checked with the predictions from the resonant and non-resonant decay theory. It is found that the non-resonant cascade process requires high thresholds and will not be able to generate three decay lines. The data was fitted by the solid lines, based on the resonant cascade process, with calculated layer separation distances in good agreement with theoretical calculations. We are analyzing plasma line and ion line data recorded in our winter 2008 experiments with Brenton Watkins to get more information on spectral changes of Langmuir and ion acoustic waves with background ionospheric plasma conditions.

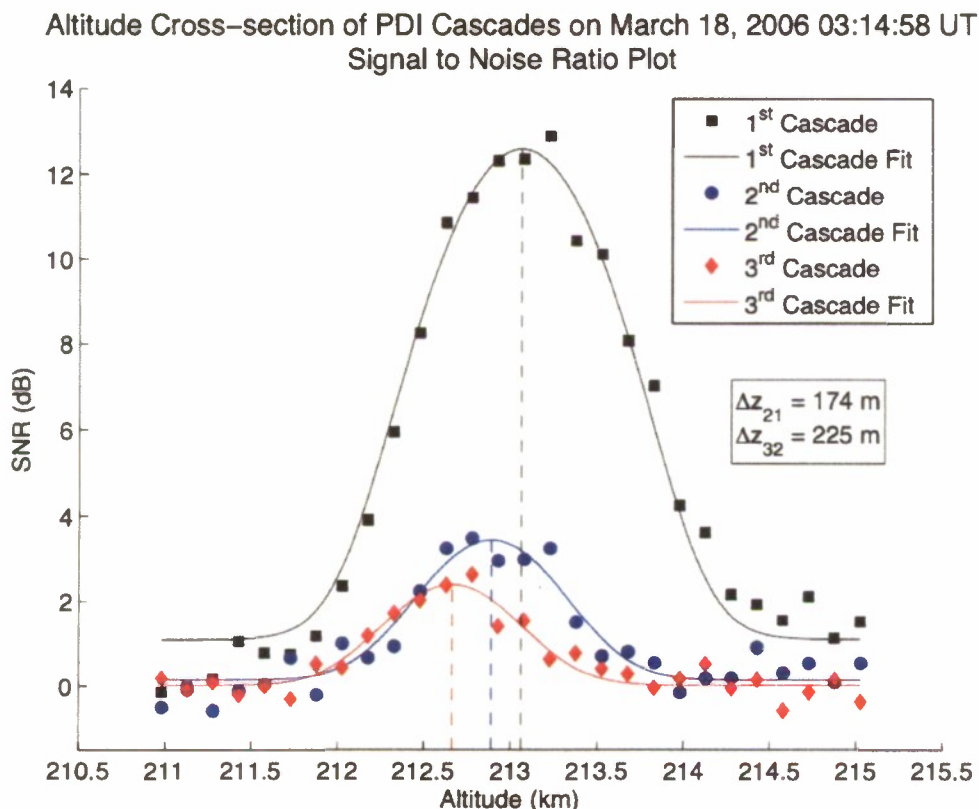


Figure U5. Altitude cross-sections of MUIR data from Winter HAARP Campaign on March 18, 2006.

(3) Whistler Wave Interactions with Ionospheric Plasmas

This work was motivated by our Arecibo experiments to investigate how to diagnose whistler wave interactions with ionospheric plasmas [Labno et al., JGR, 2007] and radiation belts [Pradipta et al., GRL, 2007] at Gakona using MUIR. We started to investigate these processes at the PARS Summer School 2007 by using electrojet-radiated whistler waves to excite lower hybrid waves and short-scale ionospheric density irregularities in the ionosphere. Unfortunately, our winter 2008 experiments (#16) were finally not conducted. However, the preliminary results from our PARS Summer School 2007 experiments (conducted by R. Pradipta et al.) are currently examined by Rezy Pradipta, Joel Cohen, and David Mabijs as part of their graduate thesis research. Experiments to get more data have been planned for PARS Summer School 2008.

References

- Cohen, J.A., L.M. Burton, R. Pradipta, A. Labno, M.C. Lee, S.P. Kuo, B.J. Watkins, S. Oyama, "Ionospheric Ducts and Plasma Waves Induced by HF Heater over Gakona," *Proceedings, URSI GA*, Chicago, U.S.A., 2008.
- Kuo, S.P. and M.C. Lee, Cascade Spectrum of HFPLs Generated in HF Heating Experiments," *J. Geophys. Res.*, **110**, A01309, doi:10.1029/2004JA010674, 2005.
- Labno, A., R. Pradipta, M. C. Lee, M. P. Sulzer, L. M. Burton, J. A. Cohen, S. P. Kuo, and D. L. Rokusek, "Whistler mode wave interactions with ionospheric plasmas over Arecibo", *J. Geophys. Res.*, **112**, A03306, doi:10.1029/2006JA012089, 2007.
- Lee, M.C., R.J. Riddolls, W.J. Burke, M.P. Sulzer, S.P. Kuo, and E.M.C. Klien, "Generation of large sheet-like ionospheric plasma irregularities at Arecibo," *Geophysical Research Letters*, **25**, 3067, 1998.
- Pradipta, R., A. Labno, M. C. Lee, W. J. Burke, M. P. Sulzer, J. A. Cohen, L. M. Burton, S. P. Kuo, and D. L. Rokusek, "Electron precipitation from the inner radiation belt above Arecibo," *Geophys. Res. Lett.*, **34**, L08101, doi:10.1029/2007GL029807, 2007

Appendix V

Artificial ULF Wave Generation at HAARP

Investigators

A. Parent and I.R. Mann, *University of Alberta, Canada*
M. Kosch, *Lancaster University, UK*

Objective

The HAARP HF heater was used to modulate the E region auroral electrojet at ULF frequencies (0.1 to 10 Hz), thereby stimulating the generation of shear Alfvén waves with frequencies matching the ULF modulation rate. Magnetic and optical data were collected in order to characterize the waves and determine if resonance effects due to the presence of the Ionospheric Alfvén Resonator (IAR) above HAARP could be detected.

Observation Technique

Four dual-axis induction coils with a 100 Hz cadence were deployed around the HF array in order to measure the horizontal magnetic field components and characterize ULF waves produced by HAARP (Figure V1).

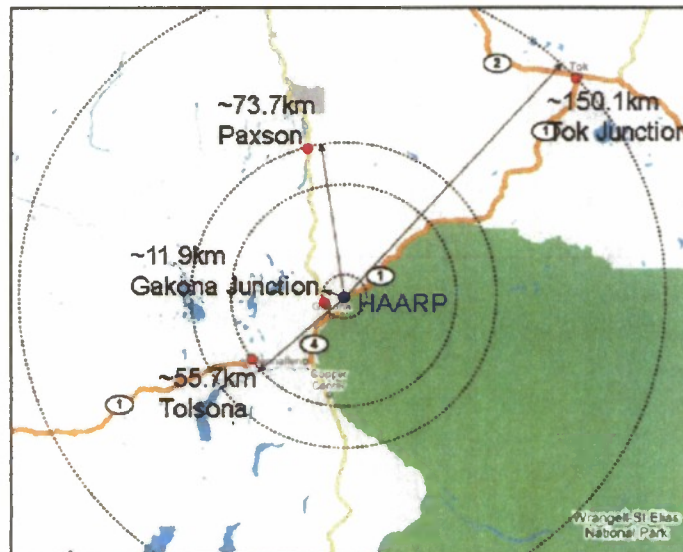


Figure V1. Dual-axis induction coils were deployed at four sites around HAARP.

Three separate ULF heating experiments were performed. In each case, the lowest stable HAARP operating frequency of 2.75 MHz was used to initiate D/E region heating. X-mode transmission was mainly used. Modulation frequencies between 0.1 and 10 Hz were chosen, and the scheme typically involved chirping the frequency in a step-wise manner. This remains a promising technique for the detection of IAR resonance effects on heater-generated ULF waves measured by ground-based magnetometers.

The effect of using different RF beam shapes was investigated during the heating intervals. A broad, north-south fan beam and a regular, ‘pencil-shaped’ beam were utilized (Figure V2).

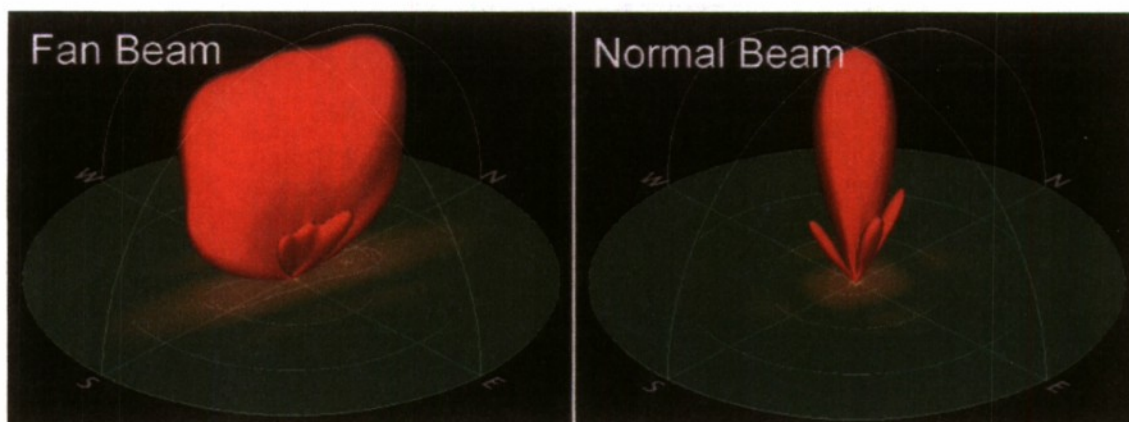


Figure V2. ULF-modulated heating was performed using different beam shapes.(Courtesy of Mike McCarrick)

Preliminary Results

A ‘quick-look’ analysis of the magnetic data shows that ULF wave signals with frequencies matching the heating modulation rate were observed during each of the three ULF experiments. The first heating interval involved a constant 3Hz modulation over 10 minutes, implemented with a fan beam shape. In response, 3Hz heating signatures were observed at all four induction coil locations (e.g., Figure V3, Tok Junction).

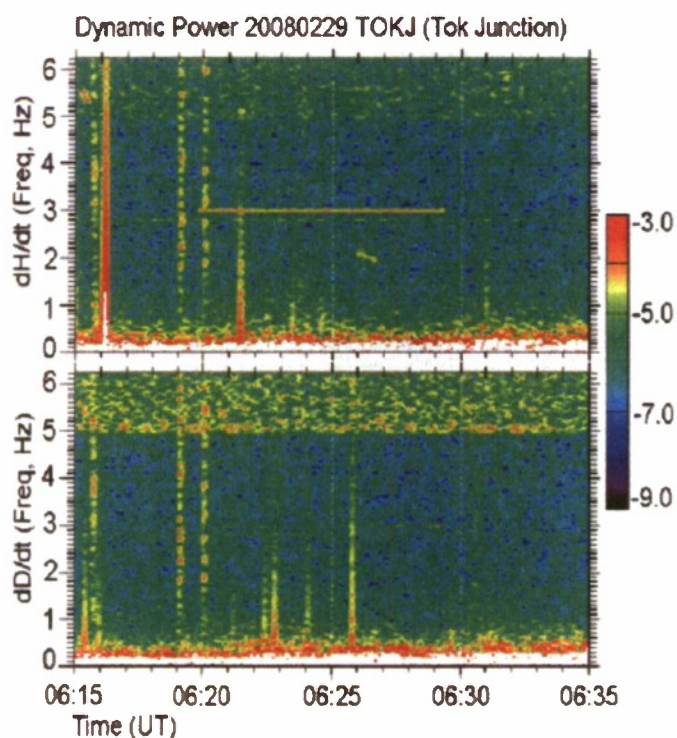


Figure V3. 3Hz heating signature in H and D components recorded by the induction coil at Tok Junction.

A 0.1 to 10 Hz staircase of modulation frequencies was used in the second interval, again with a broad beam shape. Corresponding ULF wave signals were recorded by all four magnetometers once more (e.g., Figure V4, Tok Junction).

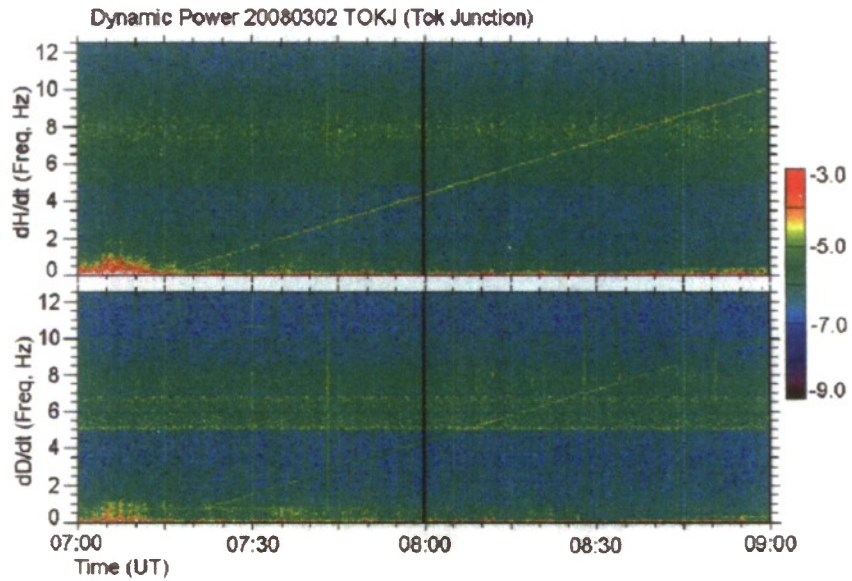


Figure V4. Chirped ULF wave signal recorded by the induction coil at Tok Junction.

The final experiment involved two 0.1 to 5.0 Hz chirped modulation sequences and a normal HAARP beam. Only data from Tok Junction and the Gakona Junction Trailer were available, however both stations recorded signatures (Figure V5). Further analysis is in progress to determine what part experimental parameters, ionospheric conditions and instrument location played in the results. Possible resonance effects of the IAR on the heater-generated ULF waves remain to be examined as well.

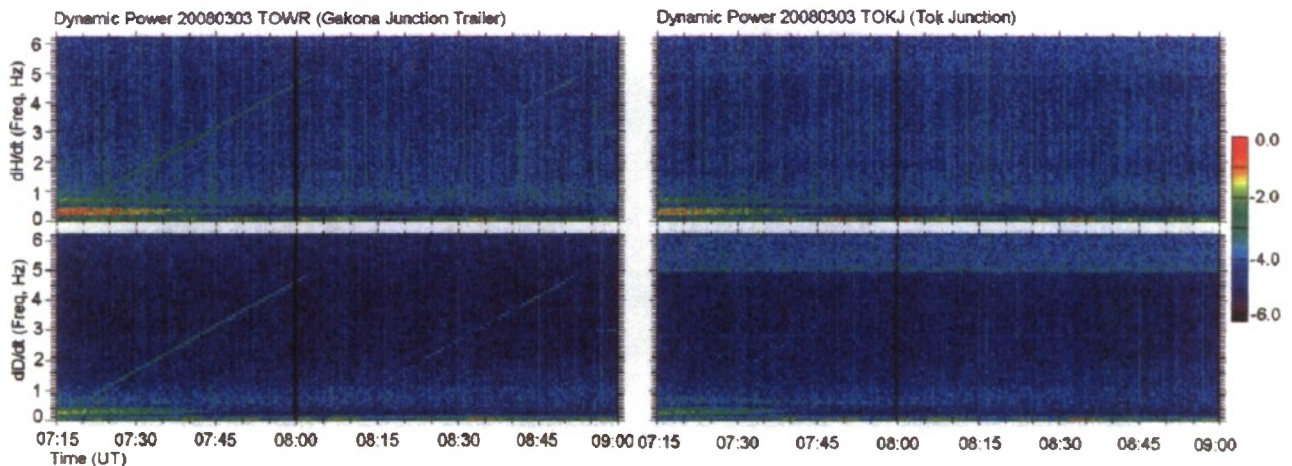


Figure V5. ULF waves at Gakona Junction Trailer (left) and Tok Junction (right).

Appendix W

Investigating the scintillations of discrete cosmic source radiation due to HAARP-stimulated irregularities using the new imaging riometer at Gakona

Investigators

Y. Yampolski, V. Bezrodny, V. Galushko and L. Charkina, *Institute of Radio Astronomy, NAS of Ukraine, Kharkov, Ukraine.*

B. Watkins, *Geophysical Institute, University of Alaska, Fairbanks, AK.*

K. Groves, *Air Force Research Laboratory RVBXI, Hanscom AFB, MA*

Objective

A part of the February'08 heating campaign of HAARP was program #35 of Drs Y. Yampolski and B. Watkins. The main purpose of the experiment was to investigate the possibility of observing scintillations of Discrete Cosmic Source (DCS) radiation owing to HAARP-stimulated ionospheric irregularities.

Observation Technique

The new Imaging Riometer installed at Gakona (Alaska, USA) late in 2007 was used as a receiving facility. The probe signals were radio emissions from two strongest HF Discrete Cosmic Sources (DCS) in the Northern hemisphere which are Cassiopeia A and Cygnus A. The operating intervals of the heater were selected so that the source-riometer line should pass through the HAARP-disturbed region at F-layer altitudes. The heater radiated an O-polarized wave at full power level in the 5 min ON/5 min OFF regime. The total heating time was about 7 hours, including nearly 3.75 hours of beam phasing toward the zenith on February 21 and 3.25 hours of heating along the magnetic zenith on February 22.

Preliminary Results

Shown in Figure W1 are antenna patterns of the 64 beams of the riometer array in the horizontal astronomical coordinates with the center at the zenith above the receiving site, and positions of the disturbed ionospheric regions for the zenith and magnetic zenith orientations of the HAARP antenna. The lines similar to concentric circles show trajectories of four DCS, with points along each trajectory indicating one-hour intervals in the motion of the respective source.

For the given measurement layout, most useful seem to be the observations of Cassiopeia A whose radiation passed through the HAARP-heated region close

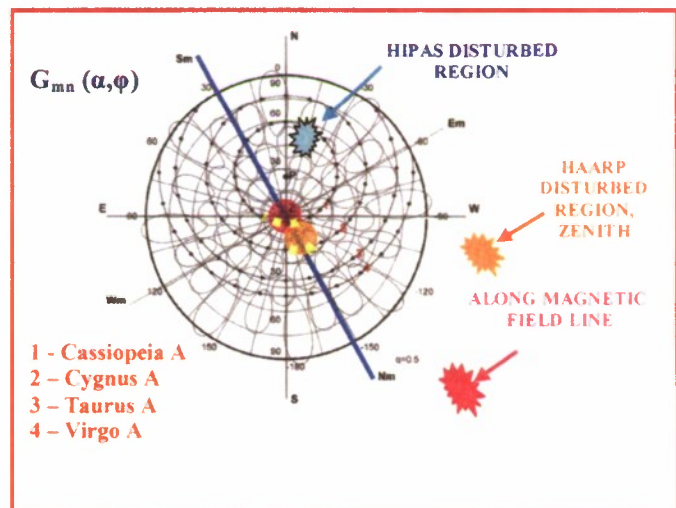


Figure W1. Antenna pattern of the HAARP Imaging riometer showing trajectories of selected DCS and the locations of ionospheric disturbed regions.

to the moment of culmination. Figure W2 shows a two-hour record of the source scintillations (the antenna pattern of the receiving beam has been suppressed). One can clearly see sharp bursts and falls in the scintillation intensity during the ON and OFF intervals, indicated as black and white rectangles, respectively. Analysis of the scintillation spectra for the heater ON and OFF intervals has allowed estimating variations in the scintillation index, and also motion velocities of natural and induced plasma inhomogeneities of the Fresnel scale size (~ 1 km). The knowledge of the specific scale-size and relaxation time of the inhomogeneities may allow suggesting a mechanism of their generation. Synchronous registrations of natural scintillations of the same DCS with another riometer (located at Poker Flat) were used as reference observations to monitor the undisturbed ionosphere. By comparing the data from the two riometers it is possible to quantitatively estimate the contribution of the induced irregularities, and also to analyze the stationarity and spatial homogeneity of natural electron density variations at F-layer altitudes. Also, it seems possible to estimate, in the course of further analysis of the data, the spatial distribution of the induced inhomogeneities along the DCS trajectory inside the disturbed region.

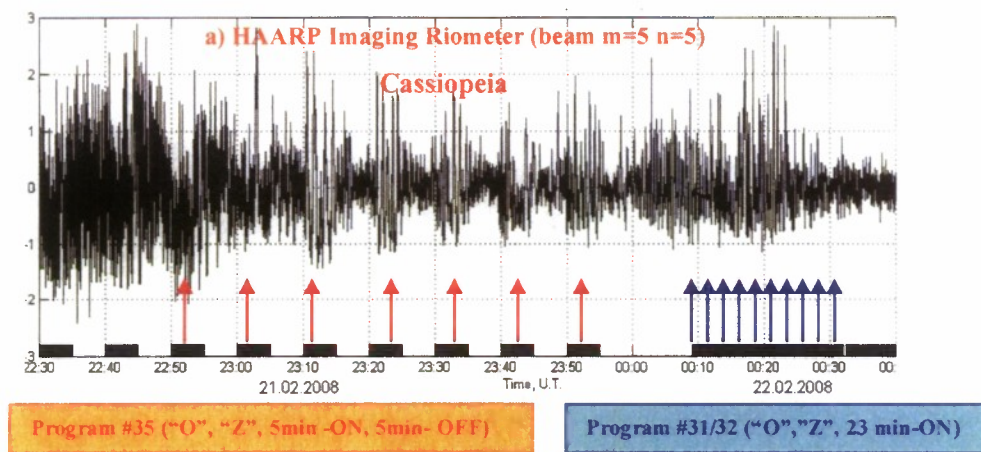


Figure W2. Source scintillations over a two hour period showing the effect of heater ON and OFF intervals.

Our future plans are to compare the space-and-time characteristics of the disturbed ionospheric region that were recovered in the scintillation technique with the data provided by other methods, in particular, with the results of the SuperDARN diagnostics and those of the 30-MHz radar of Cornell University (Dr. Hysell). So, the results of the measurement campaign have shown that imaging riometers can be successfully used not only for monitoring the ionospheric absorption, but also for diagnostics of mid-sized natural and artificial inhomogeneities.

Appendix X

Probing the ELF/VLF Source Region Using Dual-Beam HAARP Experiments

Investigator

Robert C. Moore, *Department of Electrical and Computer Engineering, University of Florida, Gainesville, Florida 32611*

Objective

The HAARP 3600 kW HF transmitter is used in a dual-beam configuration to generate ELF/VLF waves using two different modulation techniques and ten different power settings. The goal of this experiment is to relate the levels of D-region ionospheric absorption at multiple HF frequencies by equating the normalized ELF/VLF field changes observed in each case.

Observation Technique

A broadband (300 Hz–45 kHz) ELF/VLF receiver deployed at Sinona Creek in Chistochina, Alaska is used to detect the ELF/VLF waves generated by HAARP. The system consists of two orthogonal magnetic loop antennas oriented to detect the radial magnetic field at ground level, a preamplifier, a line receiver, and a digitizing computer that samples at 100 kHz with 16-bit resolution. Figure X1 shows a picture of the receiving antennas and preamplifier as deployed

The HAARP HF transmitter is used to modulate the ionospheric conductivity using two different constant modulation depth techniques. The first modulation scheme uses half of the array to generate ELF/VLF waves using square-wave amplitude modulation at 11 different power settings. For each power setting, the difference between the peak power and the minimum power transmitted is kept constant (e.g. at 30% of 1800 kW) while the average HF power is increased in 11 discrete steps. The second method uses the second half of the array to transmit a CW signal (at a different HF frequency) that varies the peak HF power in 11 discrete steps. At the same time as the CW-power-stepping, the first half of the array continually broadcasts with square-wave amplitude modulation at, for instance, 30% HF power, selected to match the modulation depth used in the first method. A cartoon depiction of the two methods can be seen in Figure X2.

From the perspective of total HF power delivered to the ionosphere, the two methods are essentially equivalent. The relative levels of D-region absorption at the two different HF frequencies may then be compared as a function of HF power by equating the normalized ELF/VLF amplitudes observed in each case.

Preliminary Results

Observations of ELF/VLF waves were successfully performed during each of the three allocated one-hour transmission slots. Approximately 15-20 minutes of high (>10 dB) SNR ELF/VLF

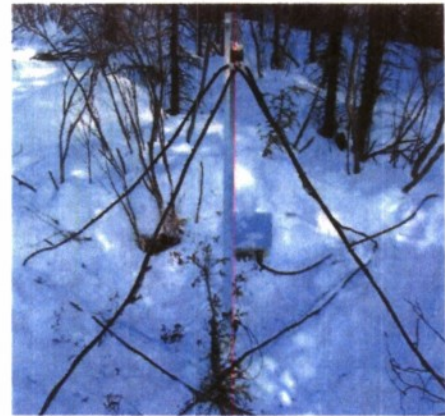


Figure X1. ELF/VLF receiver located at Sinona Creek in Chistochina, Alaska to detect the ELF/VLF signals generated by the HAARP HF heater.

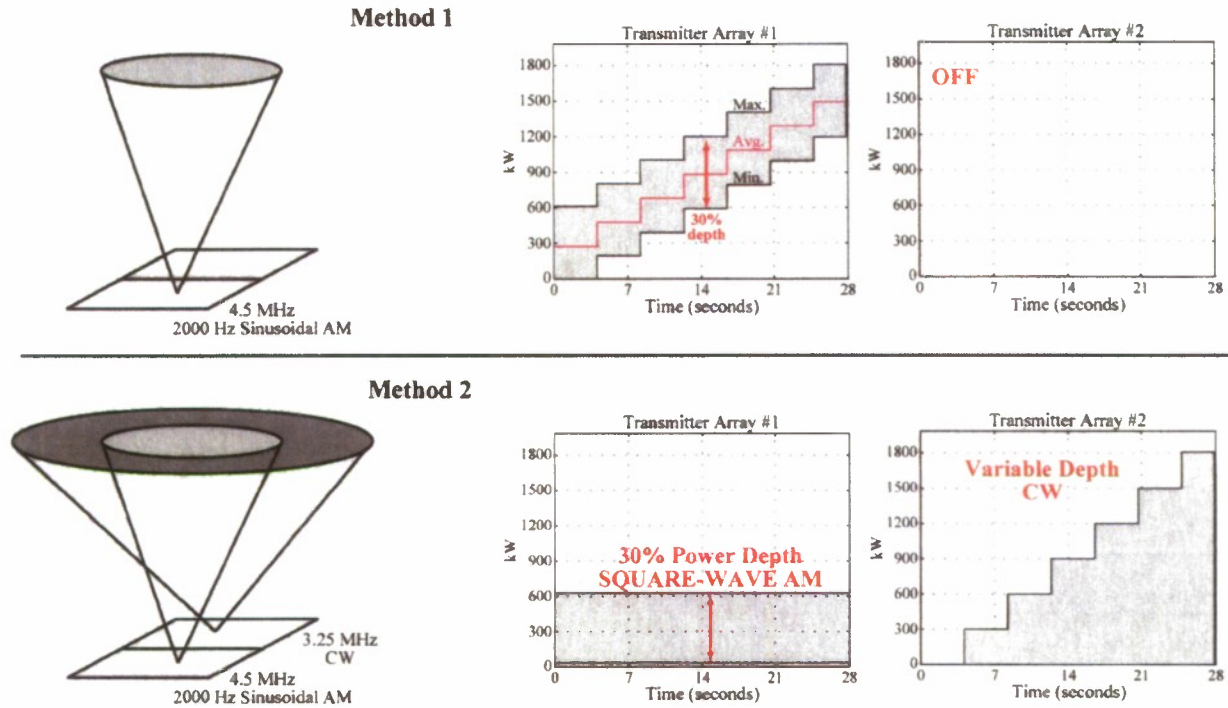


Figure X2. Split-beam HF heating geometry for the experiment. Power-stepped CW heating is coupled with modulated HF heating using a different HF frequency.

signals were observed at Sinona Creek (SC) per hour of transmission. This preliminary analysis will focus on the 2-minute example shown in Figure X3. During the “CW OFF” transmission, the ELF/VLF signal magnitude initially increases and then decreases with increasing average HF power, in agreement with previous observations. During the “CW ON” transmission, the signal magnitude decreases essentially monotonically. The points where the normalized amplitudes are equal indicate the power levels for each HF frequency (in this case 4.5 and 7.9 MHz) for which the ionospheric absorption is the same at the altitude of ELF/VLF wave generation. We are grateful to Umran Inan and the VLF Group at Stanford University for providing additional ELF/VLF coverage (at their flagship Chistochina site (CH)) for this experiment.

ELF/VLF Observations: 2358:00 UT - 2359:30 UT 29 February 2008
4.5 MHz X-mode CW, 7.9 MHz X-mode Square-Wave AM at 2 kHz

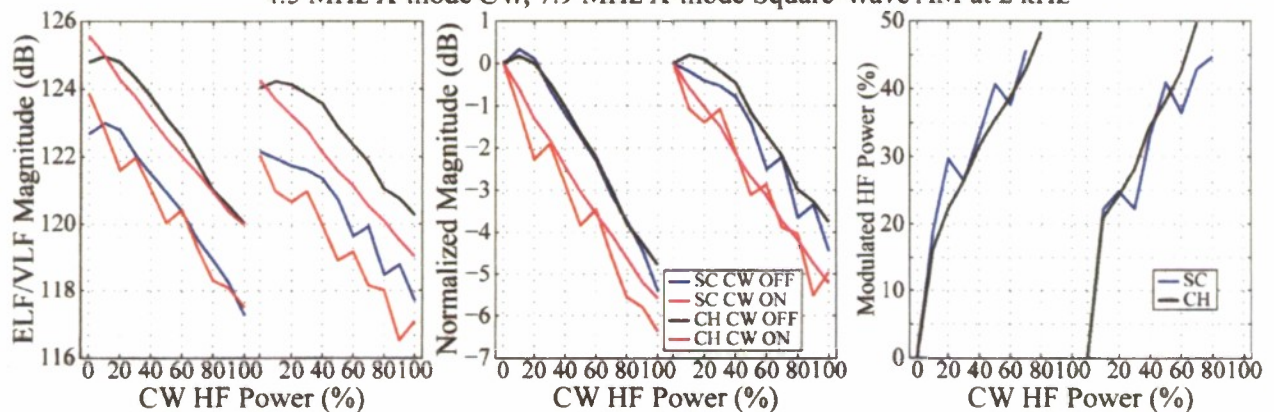


Figure X3. ELF/VLF observations performed at Sinona Creek in Chistochina, AK

Appendix Y

Spectroscopic Observations of Artificially Induced Airglow and Aurora

Investigators

Dr. J. M. Hughes, C. Mutiso, M. Kuss, and Dr. G. G. Sivjee, *Embry-Riddle Aeronautical University, Daytona Beach, FL 32114*

Objective

Observations of heater-induced optical emissions help determine the energy spectrum of accelerated electrons. This is an important variable in understanding the various wave-plasma interactions that occur during high-frequency heating of the ionosphere.

During the 2008 HAARP optics campaign a CCD-equipped grating spectrometer was used to obtain spectra of auroral emissions generated by the HAARP IRI. The primary goal of the experiment was to detect optical emissions from atomic oxygen and molecular nitrogen. A prior experiment led to observations of two previously unreported heater-induced optical emissions: the O+ 732.0-733.0 nm and the OI 799.0 nm. One of the goals of the 2008 campaign was to repeat the experiment with the increased power and better diagnostics now available at HAARP. The repeat detection of these emissions would enable us to better characterize their generation mechanism.

Observation Technique

An optimized grating spectrometer was used to detect sub-visual emissions generated during the heating experiments. This instrument, shown in the photograph in Figure Y1, was pointed along the magnetic field line, in order to take advantage of the maximum optical intensities generated

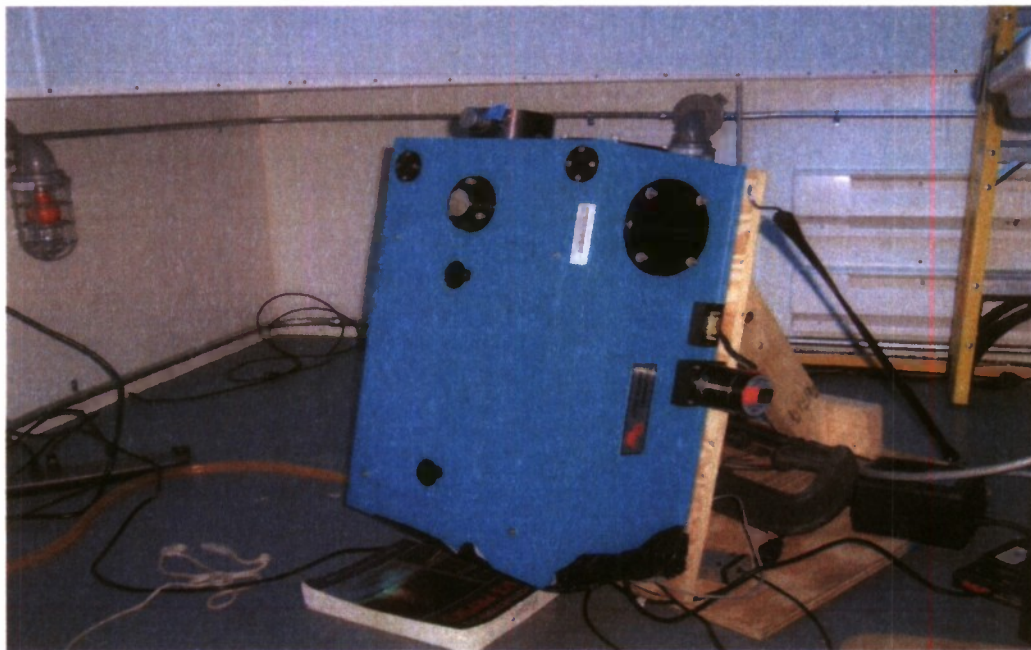


Figure Y1. A CCD-equipped 0.5 m grating spectrometer used to obtain spectra of heater-induced aurora and airglow.

in that direction. Multiple heater transmission modes capable of producing artificial airglow were run, depending on the ionospheric and weather conditions. In general, an O-mode, 2.85 MHz, 2 min on, 2 min off duty cycle was employed.

Preliminary Results

Figure Y2 shows a preliminary determination of artificially induced airglow emissions generated during the 2008 HAARP optics campaign. The top panel shows the spectrum obtained when the heater was ON (red spectrum), and OFF (black spectrum). The bottom panel is a difference spectra (subtraction of the ON and OFF spectra), which will indicate the presence of any heater-induced emissions. Clearly visible in the difference spectra is the atomic oxygen 777.4 nm emission, indicating that electrons are being accelerated to energies of at least 10.74 eV. Also visible in the spectrum is the atomic oxygen emission at 799.0 nm. This marks only the second time that this emission line has been detected during an ionospheric heating experiment.

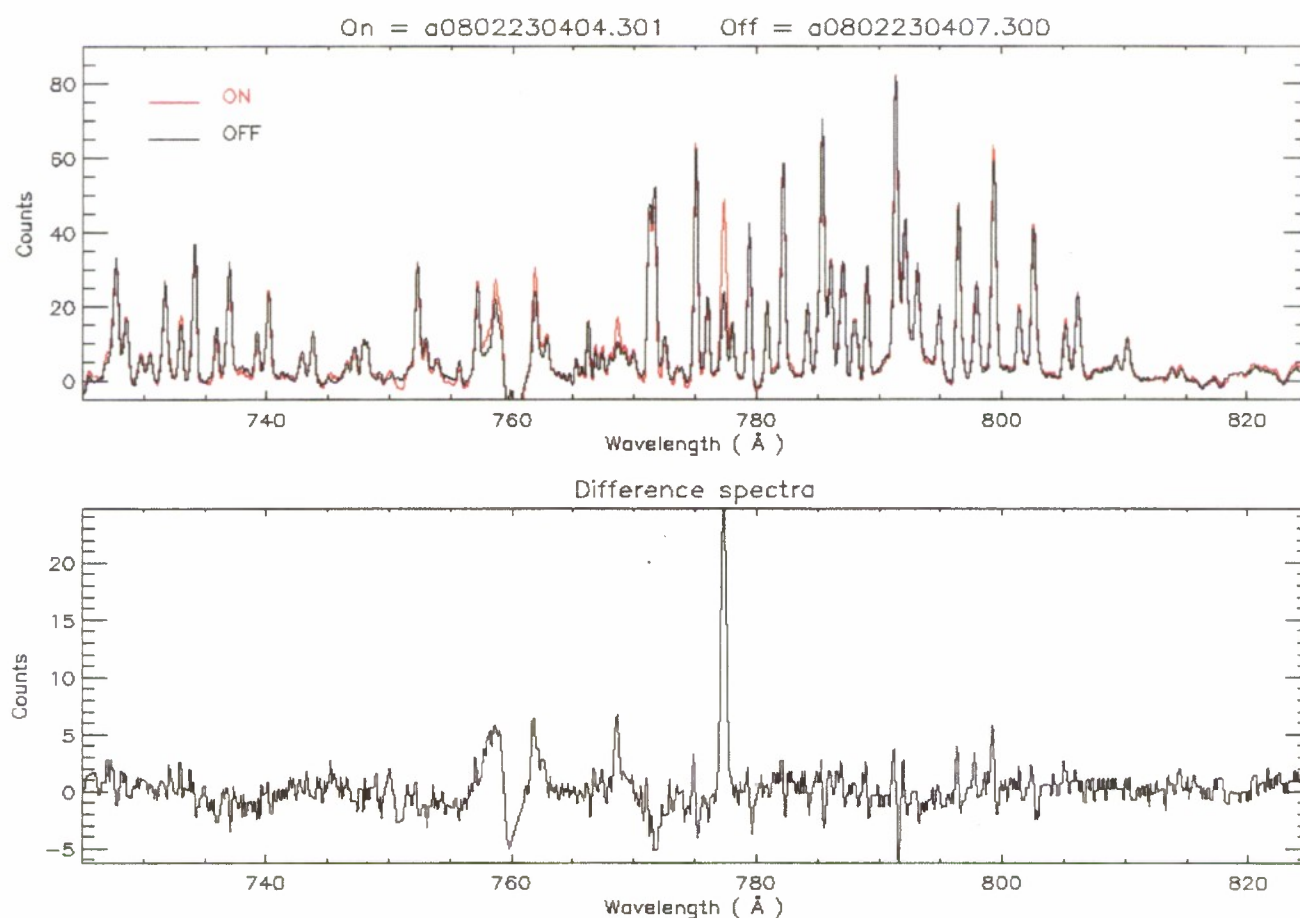


Figure Y2. Sample spectra obtained during the HAARP 2008 optics campaign showing the presence of heater-induced auroral emissions.

In addition to the 777.4 nm and 799.0 nm emissions, there are several other prominent features in the difference spectrum, and in our data from the campaign, which appear to correspond to emissions that have not been previously detected during heating experiments. It is expected that a closer analysis of the data will identify these artificially induced optical emissions.

Appendix Z

High-speed Photometric Imaging of HAARP-induced Artificial Airglow

Investigators

R. A. Marshall, R. T. Newsome and U. S. Inan, *Stanford University, Stanford, CA*

Objective

The objective of this experiment was to make photometric imaging measurements of green-line (557.7 nm) emissions at F-region altitudes due to heating from HAARP (that is, artificial airglow). Recent green-line measurements of such emissions have shown a great amount of spatial structure (e.g., Kosch et al [2007], Figure 4). The best measurements typically occur near the second gyro-harmonic (~2.85 MHz) with CW transmissions. However, these observations were made with 30-second integrations, so the temporal development of the airglow patch could not be resolved.

Observation Technique

We used the Stanford PIPER instrument (Photometric Imaging of Precipitation of Electron Radiation) to make high-speed, high-sensitivity 2D measurements of the airglow signature at 557.7 nm in order to quantify the temporal development of the green-line airglow patch over its development and lifetime. We used the HAARP photometer to make high-speed multi-spectral measurements of the airglow signature at wavelengths of 630 nm, 560 nm, 427.8 nm, 850 nm, and 780 nm, as well as one measurement of all wavelengths longer than 650 nm. To produce the artificial airglow, we used HAARP to transmit in full power at 2.85 MHz in the CW O-mode toward the local magnetic zenith. The transmissions repeated 2 minutes on and 2 minutes off, and the experiment was repeated twice over the course of the campaign. For successful observation, we required clear skies and a strong ionospheric F-layer (parameterized by the ionospheric critical frequency, f_oF_2) well after twilight.

Preliminary Results

The experiment was performed on February 29, 2008 from 0400 to 0530 UTC and on March 3, 2008 from 0400 to 0530 UTC. On the first night, the sky was covered by thick clouds (top row, Figure Z1) and no optical airglow signatures were detected (Figure Z2). On the second night, the sky was overcast earlier in the night but began to clear toward the second half of the 90-minute observation (Figure Z1, bottom row). HAARP photometer data has not yet been analyzed for the second night of observations. PIPER data from both nights has not yet been analyzed.

Bibliography

Kosch, M. J., T. Pedersen, E. Mishin, M. Starks, E. Gerken-Kendall, D. Sentman, S. Oyama, and B. Watkins (2007). *Temporal evolution of pump beam self-focusing at the High-Frequency Active Auroral Research Program*, *J. Geophys. Res.*, 112, A08304, doi:10.1029/2007JA012264.

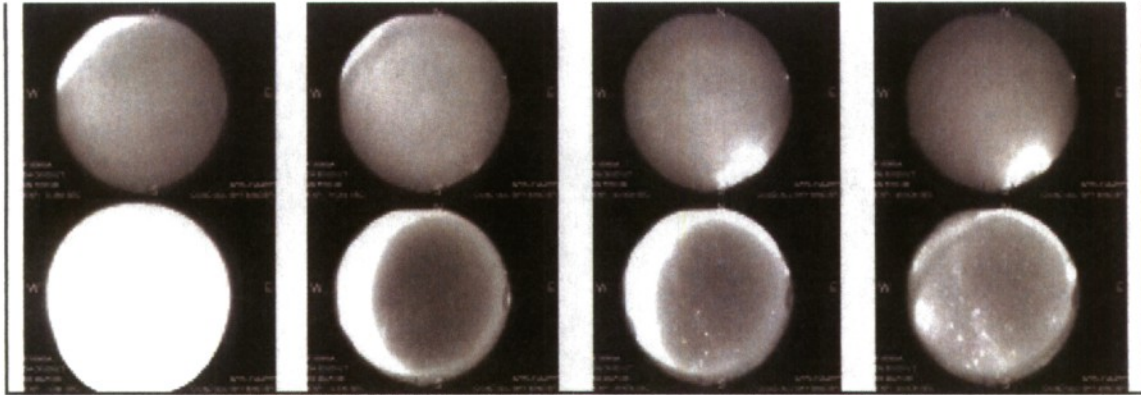


Figure Z1. HAARP All Sky Imager images from (from left column to right column) 0400 UTC, 0430 UTC, 0500 UTC, and 0530 UTC on February 29, 2008 (top row) and March 3, 2008 (bottom row). No stars can be seen in the images in the top row due to overcast skies. In the bottom row, the skies are overcast earlier in the observation period (bottom row, left images) but cleared up (i.e., stars appear in the images) later in the period (bottom row, right images).

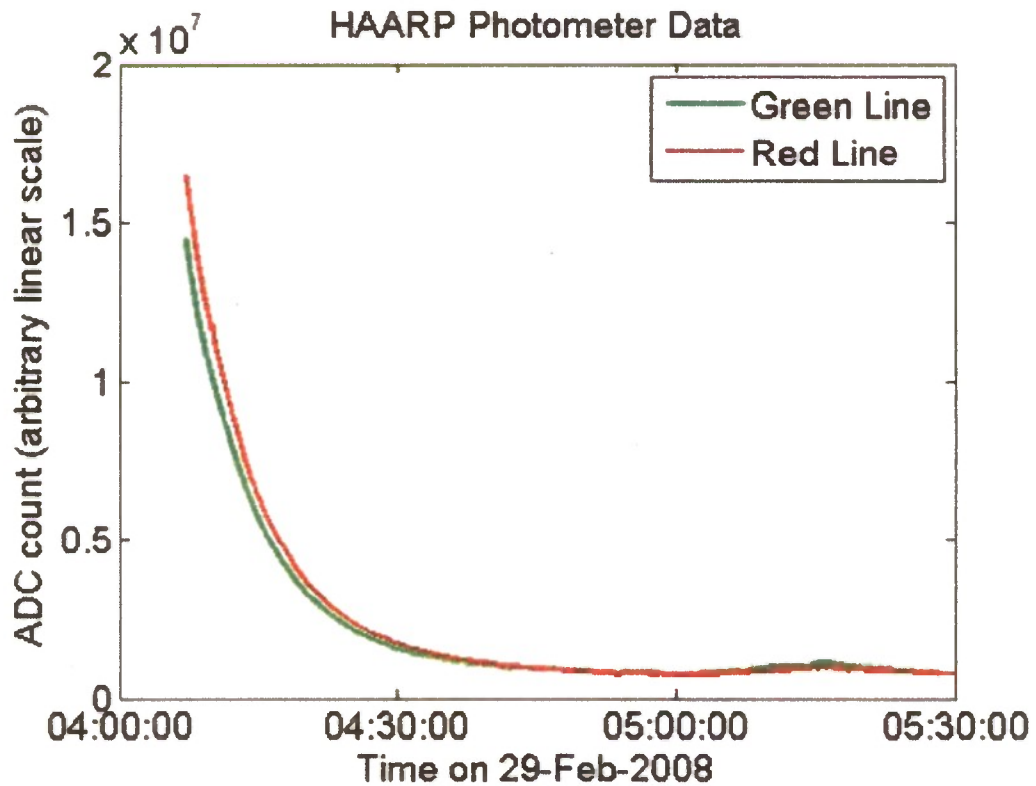


Figure Z2. HAARP photometer data from February 29, 2008 from 0400 to 0530 UTC. Only the red line (630 nm) and green line (560 nm) measurements are shown. The decay brightness during twilight is clearly visible, but no 4-minute periodicities can be seen due to the overcast skies.

Appendix AA

Optical Detection of HAARP-induced Particle Precipitation from the Radiation Belts

Investigators

R. A. Marshall, R. T. Newsome, U. S. Inan, and N. Lehtinen, *Stanford University, Stanford, CA*

Objective

The objective of this experiment was to make optical measurements of HAARP-induced precipitation of electron radiation. This was the second attempt at HAARP to make this measurement (the first being made in March 2007). Such measurements will lead to the quantification of precipitating electrons in terms of their energy distribution.

Observation Technique

We proposed using the Stanford PIPER instrument (Photometric Imaging of Precipitation of Electron Radiation, Figure AA1, left) to make high-speed, high-sensitivity measurements of the precipitation signature at 557.7 nm and at 427.8 nm, two strong lines [Helliwell et al, 1980] with short lifetimes (less than 1 s) which facilitate fast on/off keying of the HAARP beam. We proposed using the HAARP photometer (Figure AA1, right) to make high-speed multi-spectral measurements of the precipitation signature at wavelengths of 630 nm, 560 nm, 427.8 nm, 850 nm, and 780 nm, as well as one measurement of all wavelengths longer than 650 nm.

To produce the electron precipitation, we proposed 5 s on, 5 s off ELF/VLF transmission formats for HAARP involving combinations of transmitter frequencies at 5.8 MHz and 3.2 MHz and ELF/VLF modulation frequencies at 1 kHz and 2 kHz. The ELF/VLF generation was to be monitored in real-time at our VLF AWESOME receiver sites in Chistochina and a variety of other Alaskan locations. These sights also were to serve as monitors for sub-ionospheric VLF perturbations due to electron precipitation.

The pointing of our instruments is based on the fact that HAARP-generated ELF/VLF whistler-mode waves can propagate in either ducted or non-ducted modes. In general, non-ducted propagation is assumed and the instruments are pointed at a pre-defined location south of HAARP where simulation suggests that most of the HAARP-precipitated electrons will be deposited. Should a magnetospheric duct appear, likely along the plasmapause [Inan and Bell, 1977], the instruments will be pointed at the plasmapause location along the magnetic meridian that passes through HAARP. This location is determined from the previous 12 hours of K_p indices using an empirical formula [Carpenter and Anderson, 1992].

For successful optical detections, we required a dark night (no moon), clear skies, strong D-region absorption, and strong ELF/VLF generation.

Preliminary Results

Due to the need for particular environmental criteria to be satisfied for our experiment to be successful (clear skies, strong D-region absorption, and strong ELF/VLF generation), our experiment did not have a set time in the schedule. Instead, it was one of the five floating

experiments that would get priority whenever the right conditions presented themselves. Unfortunately, the block of nights allocated for our experiment were characterized mostly by overcast skies (Figure AA2) and poor D-region absorption. Thus, our experiment was never performed.

Bibliography

Carpenter, D. L., and R. R. Anderson, "An ISEE/whistler model of equatorial electron density in the magnetosphere," *J. Geophys. Res.*, 97, (A2), 1097-1108 (1992).

Helliwell, R. A., S. B. Mende, J. H. Doolittle, W. C. Armstrong, and D. L. Carpenter, "Correlations between 4278-A optical emissions and VLF wave events observed at L~4 in the Antarctic," *J. Geophys. Res.*, 85, (A7), 3376-3386 (1980).

Inan, U. S., and T. F. Bell, "The plasmopause as a VLF wave guide," *J. Geophys. Res.*, 83, (19), 2819 (1977).

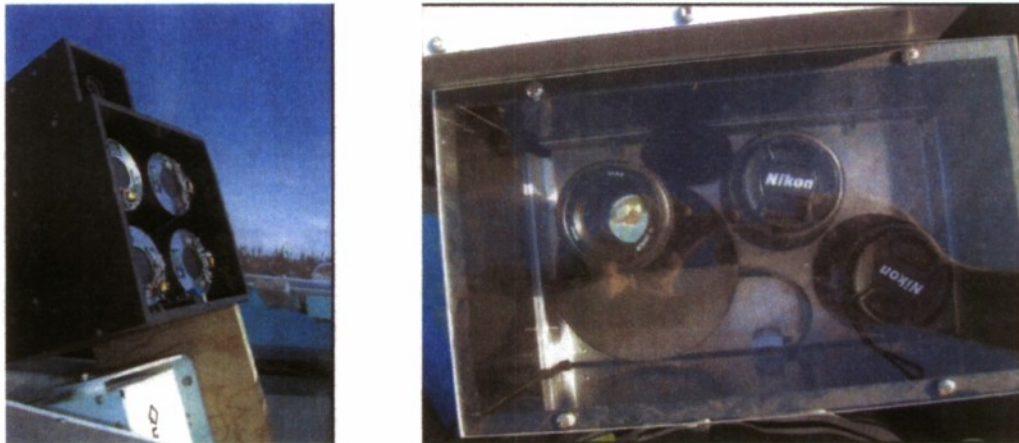


Figure AA1. Pictures of the PIPER instrument (left) and the HAARP photometer (right) as mounted in the optics shelter in Science Pad 3 at HAARP. PIPER is composed of four multi-anode photomultiplier tubes and a field-of-view camera mounted on top. The HAARP photometer is composed of three photometer: two behind fixed-wavelength optical filters and one behind a rotating filter wheel with six different optical filters.

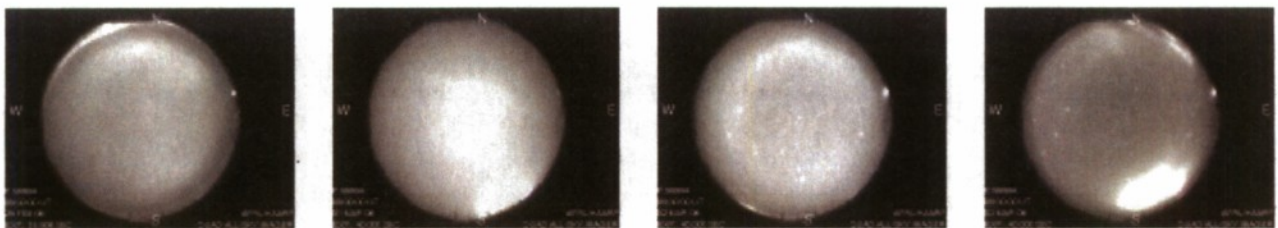


Figure AA2. HAARP All Sky Imager images from 0900 UTC on, left to right, February 29, 2008, March 1, 2008, March 2, 2008, and March 3, 2008. No stars can be seen in the images on the left due to overcast skies. In the images on the right, stars begin to appear due to clearer skies, but these nights saw weak D-region absorption. None of the four nights presented useful observation conditions, and our experiment was not performed.

Appendix AB

Synergistic Auroral Enhancements

Investigators

Brett Isham and Hien Vo, *Interamerican University of Puerto Rico, Bayamon, PR, 00957*

Objective

Observe Langmuir turbulence associated with the aurora and possibly influenced by turbulence stimulated by the HAARP HF pump. Previous work has been done in Norway where these phenomena were observed. This proposal is in part to validate the possibilities that MUIR has for continuing this type of investigation and in particular to search for auroral events occurring in combination with HF radio wave pumping, which has led to potentially interesting results in the Norwegian experiments.

Observational Technique

The primary diagnostic is the MUIR radar observing ion-acoustic and Langmuir waves enhanced by natural particle precipitation and artificial radio wave pumping. No special HAARP operations were requested, only MUIR radar operation during times when MUIR was otherwise not in use, both with and without HAARP HF transmission. Times when auroral activity was anticipated were especially interesting, as were dark times when optical imaging was also available. MUIR should be pointed along the geomagnetic field, nominally aligned with potentially precipitating particles and auroral arcs. Any mode of HF transmission is suitable, in order to search for unexpected effects. No HF transmission is also suitable, to search for auroral enhancements with no HF pumping effects.

Preliminary Results

There are as yet no results to report. The observations were performed in absentia and the data have not yet been obtained by the PIs.

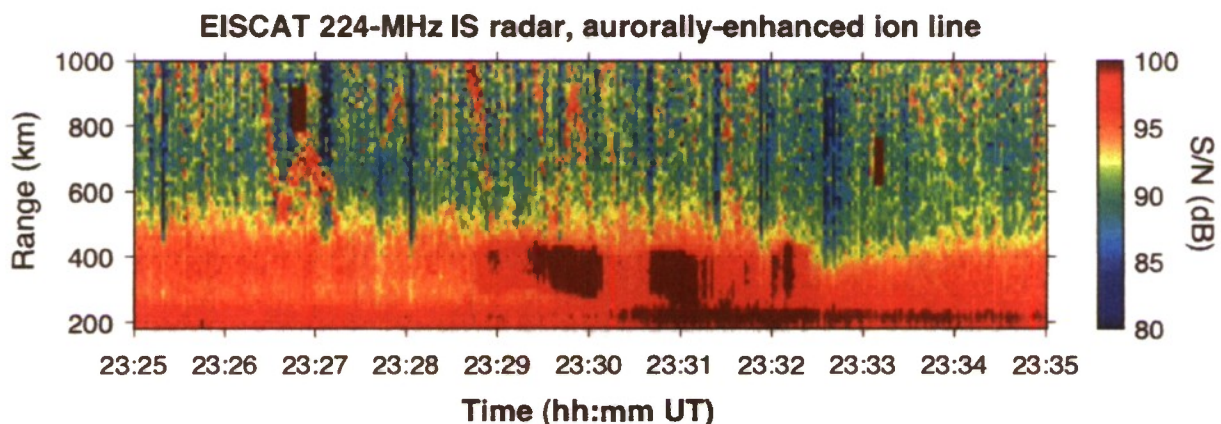


Figure AB1. An example of the type of data sought from the MUIR observations. This example was recorded by the EISCAT VHF radar and shows aurorally-enhanced ion lines between 200 and 500 km altitude and between 23:28 and 23:33 UT. Collaborators: Brett Isham, Vasily Beley, and Mike Rietveld.

Acknowledgements

Thanks to Brent Watkins and Mike McCarrick for assisting in the observations.

Appendix AC

Topside Turbulence

Investigators

Brett Isham and Hien Vo, *Interamerican University of Puerto Rico, Bayamon, PR, 00957*

Objective

Measure the dependence of bottomside and topside Langmuir turbulence on angle with respect to the magnetic field. Past work on this topic has been done in Norway, and similar observations were briefly attempted during PARS in summer 2007.

Observational Technique

Higher maximum ionospheric frequencies (f_oF_2) are preferred for this observation. Full-power HF pulses are optimal, at an HF tx frequency just below critical. The primary diagnostic is the MUIR radar. The MUIR radar is pointed at angles from vertical out to beyond the B-field angle, both along the N-S meridian and at an offset to it, using steps as small as 1 deg. Especially interesting is the region between field-aligned (15 deg from vertical) and Spitze (7 deg from vertical). It is of interest to try a variety of transmitter frequencies, especially 5 MHz and above. It is also interesting to operate on several different days in order to explore the effect of geophysical conditions. The HF transmission is O mode.

Preliminary Results

There are as yet no results to report. The observations were performed in absentia and the data have not yet been obtained by the PIs.

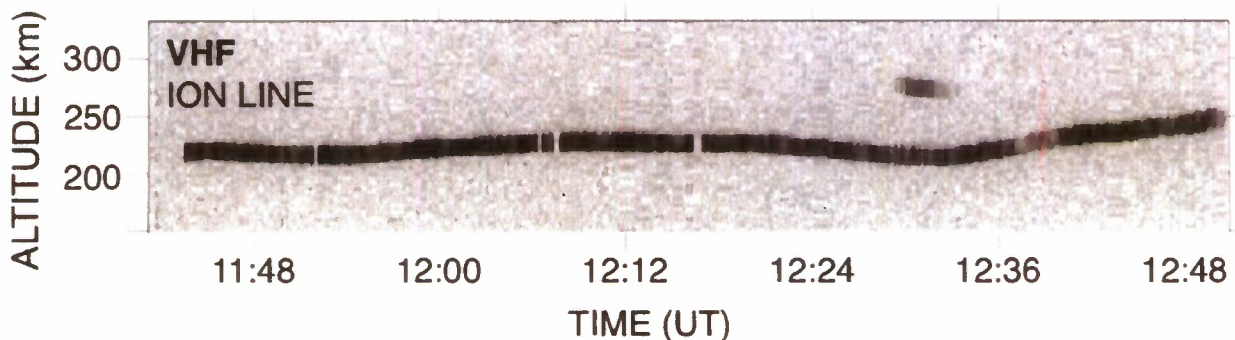


Figure AC1. An example of the type of data sought from the MUIR observations. This example was recorded with the EISCAT VHF radar showing HF-excited topside ion lines between about 12:30 and 12:33 UT. Reference: Isham et al., 1999, Aspect angle dependence of HF-enhanced incoherent backscatter, *Adv. Space Res.*, 24(8), 1003-1006.

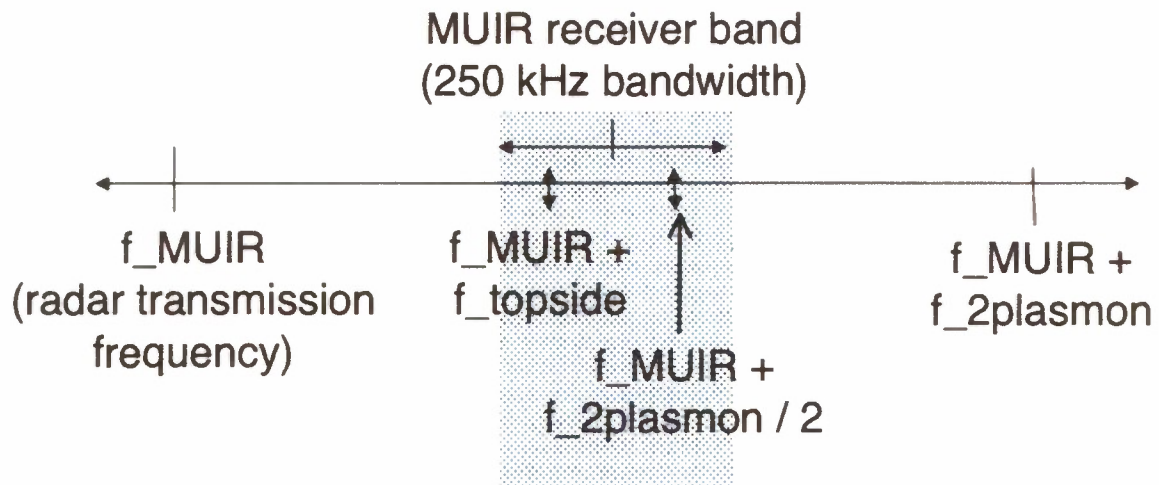


Figure AC2. Diagram showing the relationship between the MUIR receiver band and the HAARP HF pump frequency used for this observation (exp. 8) and for the two-plasmon observation (exp. 9).

Acknowledgements

Thanks to Brent Watkins and Mike McCarrick for assisting in the observations.

Appendix AD

Two-Plasmon Decay

Investigators

Brett Isham and Hien Vo, *Interamerican University of Puerto Rico, Bayamon, PR, 00957*

Objective

Attempt observations of enhancements occurring at half the HF pump frequency (quarter-critical electron density) at a variety of angles with respect to the magnetic field. Past attempts have been carried out in Norway at lower HF pump power, and similar observations were briefly attempted during PARS in July 2007 at 6.9-MHz HF pump frequency, which for the HAARP HF antenna has about half the theoretical power density as compared to 10 MHz.

Observational Technique

Observations made when the maximum ionospheric frequency (f_oF_2) is 5 MHz or more theoretically allow the highest HF ERP, which is important for this attempt. The primary diagnostic is the MUIR radar. Both the HF pump and the radar are pointed at several angles between vertical and the geomagnetic field angle. It is interesting to operate on several different days in this mode in order to explore the effect of geophysical conditions. The HF transmission is O mode.

Preliminary Results

There are as yet no results to report. The observations were performed in absentia and the data have not yet been obtained by the PIs.

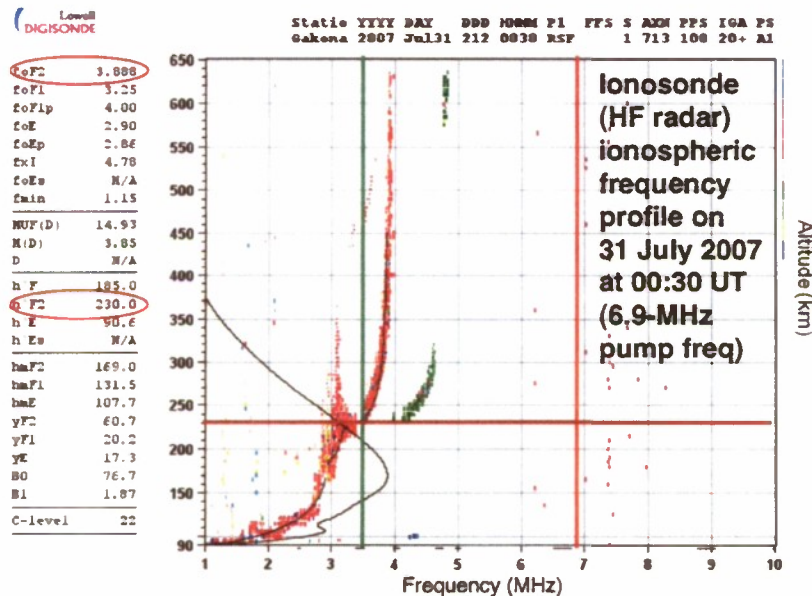


Figure AD1. Standard ionosonde (HF radar) ionospheric frequency profile recorded on 31 July 2007 at 00:30 UT showing 6.9-MHz pump frequency (vertical red line) and 3.45-MHz observation frequency (vertical green line), along with height of anticipated enhancement (horizontal red line). Collaborators: Darlene Maldonado-Nieves, Noel Robles-Arce, Brent Watkins, and Brett Isham.

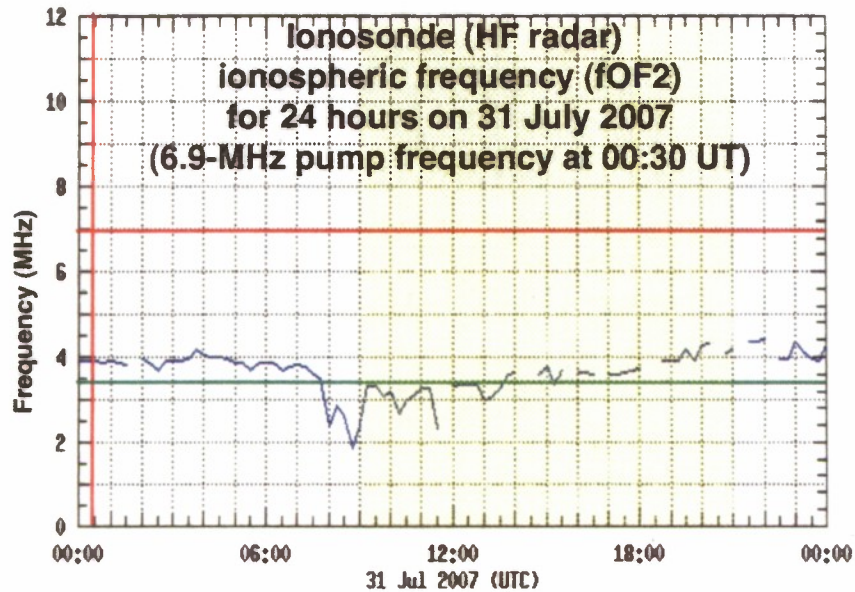


Figure AD2. Maximum ionospheric frequency (f_oF_2) for 24 hours on 31 July 2007 as measured by ionosonde (HF radar). The 6.9-MHz pump frequency (horizontal red line) and 3.45-MHz observation frequency (horizontal green line) are shown, as utilized at 00:30 UT (vertical red line). Collaborators: Darlene Maldonado-Nieves, Noel Robles-Arce, Brent Watkins, and Brett Isham.

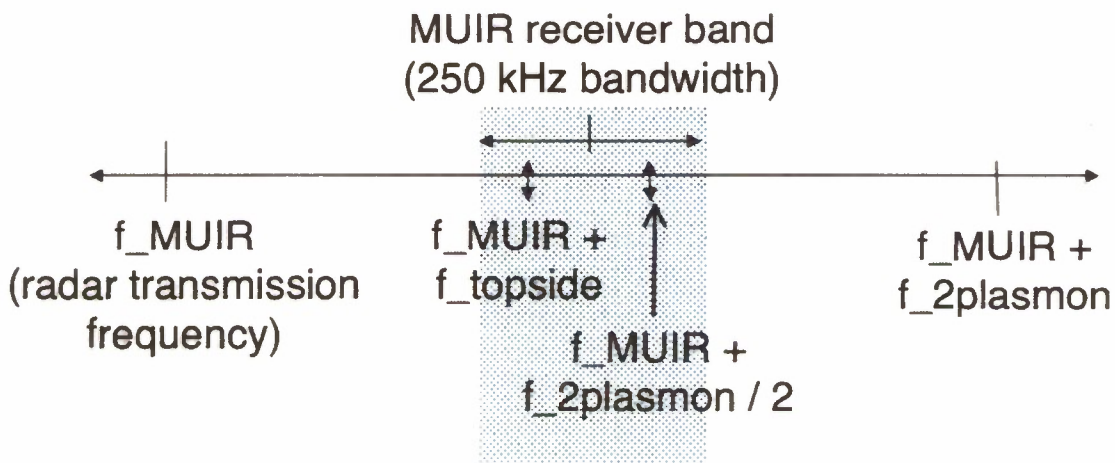


Figure AD3. Diagram showing the relationship between the MUIR receiver band and the HAARP HF pump frequency used for this observation (exp. 9) and for the topside turbulence observation (exp. 8).

Acknowledgements

Thanks to Brent Watkins and Mike McCarrick for assisting in the observations.

List of Symbols, Abbreviations, and Acronyms

AFRL	Air Force Research Laboratory
AMISR	Advanced Modular Incoherent Scatter Radar
DARPA	Defense Advanced Research Programs Agency
ELF	Extremely Low Frequency
eV	Electron volt
FAI	Field-Aligned Irregularities
f_oF_2	Critical frequency (O-mode) of the F ₂ layer (MHz)
GIOS	NWRA GPS Ionospheric Observing System software
GPS	Global Positioning System
EISCAT	European Incoherent Scatter Scientific Association
ELF	Extremely Low Frequency (Frequencies in the range 3-30 Hz)
HAARP	High-frequency Active Auroral Research Program
HF	High Frequency (Frequencies in the range 3-30 MHz)
IPP	Ionospheric Penetration Point or Inter-Pulse Period
IRI	Ionospheric Research Instrument
ITS	Ionospheric Tomography System
K	Kelvin (degrees)
kHz	Kilohertz (10^3 cycles/seconds)
kW	Kilowatt (10^3 watts)
L-band	Radio frequency band covering 1.0 GHz to 2.0 GHz (nominal)
MHz	Megahertz (10^6 cycles/seconds)
MUIR	Modular UHF Ionospheric RADAR
NIMS	Navy Ionospheric Monitoring System
NRL	Naval Research Laboratory
NWRA	NorthWest Research Associates
ONR	Office of Naval Research
PARS	Polar Aeronomy and Radio Science
PCA	Polar Cap Absorption
PRN	Pseudo-Random Noise (GPS identification signature)
rms, RMS	root mean square
S ₄	Ionospheric intensity scintillation index (non-dimensional)
S-band	Radio frequency band covering 2.0 GHz to 4.0 GHz (nominal)
SEE	Stimulated Electromagnetic Emission

sps	samples per second
SRII	SRI International
SuperDARN	Super Dual Auroral Radar Network
TEC	Total Electron Content (el/m ²)
UHF	Ultra High Frequency radio band (300 MHz – 3 GHz)
UML	University of Massachusetts at Lowell
UMLCAR	University of Mass Lowell, Center for Atmospheric Research
UPS	Uninterruptible Power Source
VHF	Very High Frequency radio band (30 MHz – 300 MHz)
VLF	Very Low Frequency radio band (3 kHz – 30 kHz)
VTEC	Vertical (or equivalent vertical) TEC (el/m ²)